DYNAMIC AND CATALYTIC PROPERTIES OF SOME METALLIC NANOPARTICLES

A Thesis

Presented to

The Academic Faculty

By

David Jackson Hathcock

In Partial Fulfillment

Of the Requirements for the Degree

Doctor of Philosophy in the School of Chemistry

Georgia Institute of Technology

February 2004

DYNAMIC AND CATALYTIC PROPERTIES OF SOME METALLIC NANOPARTICLES

Approved:

L. Andrew Lyon

Robert L. Whetten

Zhong L. Wang

Z. John Zhang

Mostafa A. El-Sayed, Committee Chair

Date Approved: February 6, 2004

Georgia Institute of Technology

2004

Dedicated To My Family

ACKNOWLEDGEMENTS

First, I would like to thank Prof. Mostafa El-Sayed for his support and encouragement throughout the course of my graduate studies. His patience and guidance during the course of this work has allowed me to grow both as a scientist and a person. Without this support this thesis would not exist. I would also like to thank Dr. Stephan Link for the many hours he spent teaching me the ins and outs of ultrafast spectroscopy and the many discussions we had. A great deal of thanks also goes to the members of the Laser Dynamics Laboratory, particularly Dr. Christy Landes, from whose friendship and discussions I learned a great deal. I would like to express special thanks to all of my friends in the Department of Chemistry who made my time in and out of lab greatly enjoyable and enriched my life.

Lastly, I would like to express my sincere thanks to my parents. Their love and unwavering support has always been the bedrock upon which every worthwhile achievement in my life has been built. Through every hardship or triumph they have been behind me every step of the way and this work is a direct result.

TABLE OF CONTENTS

LIST OF TABLES

LIST OF FIGURES

SUMMARY

Using a variety of techniques including femtosecond transient absorption spectroscopy, optical absorption, atomic force microscopy, the hot electron cooling dynamics of lithographically prepared gold nanoarrays, the effect of the surrounding environment, and the phonon oscillations of gold and silver nano-arrays were investigated. The cooling dynamics of gold nanoarrays on a glass substrate were found to be different from those of either colloidal nanodots in colloidal solution or films on glass substrate. The electron-phonon component of the electronic relaxation in the arrays was found to be longer than that in the dots or the films. The spatially isolated nanoarray particles experience a significantly different environment than the gold nanodots in solution, thus the long phonon-phonon component resulting from the coupling of particles to the medium, is not observed. This also limits the energy dissipation pathways of the electrons in the array particles and leads to higher electronic temperatures and longer electron-phonon relaxation times. The excitation and high electronic temperatures also lead to impulsive excitation of the particle lattice. The hot electrons couple to the lattice phonons and lead to an expansion and contraction of the particle volume. This causes a change in the surface electron density and therefore a shift in the surface plasmon absorption band. As the volume of the particle oscillates, the surface plasmon band shifts to the red and to the blue leading to an oscillation on the picosecond transient negative absorption (bleach)

signal during its decay following its femtosecond pulsed excitation. Both the gold and silver nanoarrays were found to have phonon oscillations present that were very similar to the impulse oscillations seen in particles embedded in a glass matrix.

The catalytic effectiveness of platinum nanoparticles for the hydrogenation of propene was investigated. The system with platinum particles was found to have a slightly lower activation energy than other systems in the literature. The effect of encapsulating the platinum particles in alumina was also investigated and it was found that the activation energy for the reaction was even lower. This is due to the protective environment provided by the alumina and the interaction of the alumina matrix with the particles.

The effect of adding platinum, palladium, and rhodium particles to the proton exchange membrane of polymer electrolyte fuel cells, on the output power of the cells was also investigated. The effects of pH and precursor salt concentration, and particle composition were also investigated. The addition of the catalytic particles increased the observed output power of the cells when compared to cells using unmodified membranes.

CHAPTER I

INTRODUCTION

This chapter is aimed at giving background materials needed for the different studies described in the following chapters. Thus Section 1 gives background material to the work described in Chapter II. Section 2 and 3 present the necessary background material concerning the studies covered in Chapters III and IV. The background for the studies detailed in Chapters V and VI are given in Section 4a. Finally, the background for Chapter VII is given in detail in Section 4b. At the end of each section below, the topic of study or the reason for each study is given.

1. Optical Properties of Noble Metal Nanoparticles

The unique optical properties of metal nanoparticles can be observed in relics from Rome and China. In fact, the vibrant wine-red color associated with the stained glass of many cathedrals throughout Europe is the result of a process that embedded gold nanoparticles in the glass. This color is a product of the unique properties associated with the decreasing size of the particles as compared to those of the bulk metal. Faraday[1] was the first to recognize in the 1800s, that the color of gold sols was derived from particles of gold in the solution.

As previously mentioned, the intense color of noble metal colloids has aroused interest since Faraday explored its nature[1] Mie, using Maxwell's equations, has shown that this strong color is caused by the collective excitation of the free electrons in the conduction band of the metal from one surface to the other. This coherent excitation is called a surface plasmon resonance (Figure 1-1) is slightly dependent on size, as it is not due to quantum confinement effects as is seen in semiconductor nanoparticles, but is a consequence of the change in the polarizability of the particle. In his treatment, Mie assumes the spheres will have the same frequency dependent dielectric constant as the bulk metal and also takes into account the contribution of the medium surrounding the particle. The derived equations expressions are for calculating the scattering and extinction cross sections of the particles. In the realm of small particles, where the diameter of the particle is much less than the wavelength of light, the expression can be approximated using only the dipole oscillation. This approximation can accurately model features of the absorption spectrum of small particles. Mie Theory also assumes that the particles do not interact and are effectively separated. These unique properties make the study of noble metal nanoparticles by optical methods highly inviting. These studies are necessary to understand the relaxation dynamic properties of the particles as well as determine what effects changing the synthetic and environmental parameters has on the surface plasmon absorption.

To that end, these particles have been under investigation for several years for their uses in solar energy conversion, opto-electronics, and catalytic applications[2-8].

Gold nanoparticles have demonstrated themselves to be particularly well adapted to a variety of applications. They have been used in scattering studies[9], Raman enhancement studies[10,11], and in biological marking systems[12]. The versatility of these particles in spectroscopic applications is in large part due to the plasmon band. This absorption is extremely strong and somewhat tunable with the size, shape, and composition of the particles [13,14].

2. Nonradiative Relaxation of the Plasmon Electrons

Understanding the dynamics of the excited electrons responsible for the surface plasmon absorption band is tremendously important to future applications. Previous [13,14,15-24] studies of the dynamics of the plasmon band of colloidal gold particles have found a fast initial electron-electron (on the femtosecond time scale) , electron-phonon (on the order of a few picosecond time scale) relaxation followed by a longer phonon-phonon decay. The coupling of the electrons to the phonons of the particle lattice and to the phonon sea of the surrounding medium are integral to the equilibration of the non-Fermi distribution of the initial non-thermalized state. The electron-electron and ballistic electron scattering components occur on the few femtosecond time-scale and are difficult to resolve in the initial decay component, primarily because they are on the same scale as the 100 femtosecond laser pulse[13,14].

The excitation of the electron gas and coupling to the lattice can be described using the two temperature model (TTM)[25]. In the TTM, the heat capacities of the

lattice and the electron gas are described by a set of coupled differential equations shown below.

$$C_e(T_e)\frac{\partial T_e}{\partial t} = -g\cdot(T_e - T_l) + \nabla(\kappa'\nabla T_e) + LP(z,t) \quad (1)$$

$$C_l\frac{\partial T_l}{\partial t} = g\cdot(T_e - T_l) \quad (2)$$

where T_l is the lattice temperature, T_e is the electron temperature, κ' is the electronic thermal conductivity, g is the coupling constant, and LP(z,t) is the spatial and temporal evolution of the laser pulse.

The equations describe the heat capacity of the electron gas as small which means that the incoming pulse energy quickly raises the electronic temperature of the electron gas creating a non-Fermi distribution. The hot electrons then dissipate their energy via electron scattering events, and couple to the lattice. The electron gas also couples a portion of the energy to the lattice of the particle. The larger heat capacity of the lattice means that this temperature is much less than that of the initial electron temperature of the electron gas since the heat capacity of the lattice is much larger than that of the electrons[25]. The hot lattice can then also couple with the surrounding phonon sea. This can be affected by the composition of the particle as well as the dielectric constant of the surrounding material[26-30]. The thermalization and relaxation can be visualized in Figure 1-2. In Chapter II, we describe our study on the hot electron cooling dynamics of gold nanoarray particles on glass substrate and compare the behavior with that of

colloidal gold nanodots and gold films on a glass substrate. We found that the electron-phonon relaxation time for the nanoarrays is much longer than that of either the films or the colloidal dots.

3. Coherent Lattice Vibrations

The hot electron gas couples to the surface phonon modes via the acoustic or capillary modes. As Hodak et al point out, the interaction with the acoustic mode leads to an oscillatory change in the volume of the particles[16] which induces a corresponding oscillation in the absorption spectrum of the particles. In their investigations of colloidal particles they found the frequency of oscillation is linearly dependent on 1/R where R is the particle radius. In their samples the frequency varied from 1.0 cm^{-1} for 120 nm particles to 11.6 cm^{-1} for 8.3 nm particles. They found this to be consistent with the spherical vibrational breathing modes of the particles and calculate an $\eta = 2.95 \pm 0.06$ from their experimental results, where η represents the eigenvalue of the radial mode (in this case the lowest radial mode) . Whereas $\eta = 2.93$ for the lowest radial mode, showing good agreement between the experimental and theoretical values. They also attribute, as others do, the oscillation of the plasmon band to the coherent breathing of the particle. The breathing of the particle changes the electron density and thus causes the plasmon band to shift to the blue and red side of the equilibrium absorption. The physical explanation offered is that the heating of the lattice is caused by the electron gas energy dissipation. According to Hodak, for particles smaller than 8 nm, the heating occurs more rapidly than the frequency of the breathing mode leading to an impulse[16]. When

studied as a function of power, as expected the particles show a decrease in the magnitude of the oscillations when compared to the bleach signal.

Hartland et al have also explored the effect of using nanorods instead of nanospheres. Gold rods were synthesized electrochemically [32,33] with aspect ratios between 2 and 4.9 [34]. The transverse plasmon band was centered at 520 nm and the longitudinal band varied from 600 nm and 840 nm. In the case of the nanorods, as is seen by Hartland and others in spheres, an initial large magnitude signal is seen followed by an oscillation overlaid on the phonon-phonon decay component. When probed on the blue and red sides of the plasmon the rod signal is out of phase, though not completely out of phase as has been seen in sphere investigations, where the behavior is attributed to a periodic shift of the plasmon band as the lattice expands and contracts [31]. The rods also show several oscillations in contrast to the single "impulse" oscillation seen by Perner et al.[35] and shown Figure 1-3. When shown side-by-side with the data from the silver arrays, the similarities are undeniable. However, Hartland et al did not perform the polarization experiments that displayed the unique traces seen in the work of Perner though the experiments from the rods were followed up by a theoretical treatment. Hu [36] determined that the heating causes excitation of not only the breathing mode of the rods but also the mode that is responsible for extension of the rod itself. The calculations show that there are in fact two different contributions to the observed dynamics. The lower frequency oscillations with a period of between 40 and 120 ps for aspect ration 2 and 6 ps are the result of the extension mode. The shorter period oscillations (~11 ps) are

assigned to the breathing mode. They propose that the extension mode dominate the observed dynamics because of the finite time scale that the heating occurs on.

The intense heating of the nanoparticles caused by the laser pulse poses the question: Does the heating cause particle melting or deformation? Results from the work of Link et al, [37] have shown that indeed femtosecond laser pulses can be used to photothermally reshape gold nanorods. Hartland [31]et al have investigated the effects of femtosecond heating on the symmetric breathing mode of colloidal gold nanoparticles. They found that the period of the oscillation is dependent on the pump power , increasing as the power is increased up to the melting point of gold. The particles are thought to not completely melt but to only partially melt and form a liquid shell on the particles. For example, the period of 50 nm particles is observed to increase from ~16.6 ps to ~17.5 ps as the laser power is increased from 0 to 1.5 μJ [31]. The partially molten nature of the particle and thus the different speed of sound in the solid and liquid portions of the particles, which varies with pump power, leads to the damping of the oscillations.

Hodak et al[15] also investigated the dynamics of core-shell particles composed of gold and lead. Gold was used as the core with variable thicknesses of lead as the shell. The gold core was kept a constant 47 nm and the thickness of the lead varied. It was found that the period of the oscillation increased as the number of atomic layers of lead increased. The plasmon of the particle was primarily gold in character but was shifted because of the lead and is center around 500 nm with the lead present. They propose that the two layers act together during the oscillation when the lead layer is thin, but as the

layer thickness increases the lead acts as a restraining force, like stiffening the spring in an oscillator, to retard the oscillations. They present a qualitative picture of the data.

Voisin et al [23,24,30,38] focused on silver nanoparticles and investigated the coherent vibrational dynamics using femtosecond pump probe spectroscopy. The oscillation dynamics of the silver particles follow the same theoretical underpinnings as the gold oscillations. The heating of the electron gas transfers energy to the lattice which then oscillates in response to the cooling. However, the silver particles were grown and investigate in a glass matrix and prepared via heat treatment. The particles oscillate just as in the colloidal case , however the oscillations decay much faster (<10ps). Other work by Voisin[41] has investigated the effect of the environment on the oscillation. Using essentially the same experiment as before, they were able to determine that the interaction between the particles and matrix drastically effect the relaxation of the oscillations. This is of particular importance when applied to the array particles since they are unique in the interaction with both air and the glass substrate. This substrate may act by damping the oscillations just as the lead overlayers used by Hodak do.

When the electron gas is heated by the laser pulse, the impulse of the heat imparted to the lattice causes an expansion of the lattice coinciding with the lattice breathing mode. The expansion and contraction of the lattice changes the electron density of the particle and thus causes a shift in the plasmon band. The plasmon shifts to the blue and red of the equilibrium value with the oscillation of the particle. Thus if the dynamics of the particle are measured on the blue and red side of the equilibrium plasmon value,

the oscillations will be π out of phase with each other due to the periodic oscillation of the plasmon absorption band [31]. This oscillatory behavior has been studied for both gold and silver particles in colloidal solution and embedded in a glass matrix.

In order to be able to detect the oscillation phenomenon the particle size dispersity must be extremely small. Otherwise the oscillatory behavior is averaged out by the different breathing mode periods of the different size particles. Since the observation of this behavior is dependent on the size distribution of the sample. In order to achieve the highly monodisperse particle solutions necessary for work in colloidal solution, Hodak et al and others [15-17,31] , have used gamma irradiation to initiate the particle growth. The monodispersity of the solution makes the lattice oscillations easier to detect since almost all of the particles will have the same oscillation frequency. The nanosphere lithography method developed by Van Duyne et al.[38-40] offers an effective means to produce highly monodisperse samples on substrate. The unique geometry of the particles, truncated octahedral in contrast to the spherical shape of the previously studied particles, also provides an interesting comparison to that of the previously studied particles. The study of this system is given in Chapter III. The effect of the glass substrate is also discussed.

4. Transistion Metal Nanoparticles

a) Catalytic Properties

In contrast to the strong optical absorption of the noble metal nanoparticles, the plasmon band of transition metal such as platinum , palladium, and rhodium is quite weak.

However, since the primary interest in these materials is their catalytic properties this is of little consequence. In relation to catalysis, the difference between nano-scale and bulk was noted very early and has been the subject of early studies.[2,4) The specific properties of nano-sized metal particles in catalysis are usually associated with a change in their electronic properties relative to the bulk samples. This change is a result of size effects giving rise to an increase in the surface energy and a characteristic high surface-to-volume ratio. These lead to an enhancement of their catalytic properties [3] as large fractions of the active metal atoms are on the surface and thus are accessible to reactant molecules and available for catalysis [4]. For these reasons, many workers have synthesized platinum nanoparticles deposited on inorganic materials as used in heterogeneous catalysis for use in various reactions [5-8]. These catalysts are typically prepared without capping materials by impregnation/ion-exchange methods using various Pt precursors such as H_2PtCl_6 [5], $Pt(NH_3)_4(NO_3)_2$ [6], $Pt(AcAc)_2$ [6], $Pt(NH_3)_4Cl_2$ [7], $Pt(NH_3)_4(OH)_2$ [15] and $Pt(allyl)_2$ [8] which, give mainly amorphous (no shaped) nanoparticles.

Generally, the particle sizes and the dispersion states of metal nanoparticles are important factors in explaining their catalytic property. A relationship between the size of copper nanoparticles and the catalytic activity evaluated by hydrogenation of unsaturated nitriles was reported by Hirai et al. [41]. They attributed the increase in the catalytic activity to an increase in the surface area of the nanoparticles due to the decrease of the particle size. However, the opposite result was also reported [27]. An enhancement of

both the specific activity and the turnover-frequency on the large silver particles in the hydrogenation of crotonaldehyde was observed compared with the small silver particles. In addition, the selectivity to the unsaturated alcohol is found to increase with increasing silver particle size [27]. This catalyst gave a higher selectivity to crotyl alcohol (53 %) than the ultradispersed small silver particles that produced crotyl alcohol with a selectivity of only 28 %. These results indicate that the rate-determining step depends critically not on the surface areas and dispersion states but on the silver particle size and surface structure. As described by these workers [27], the activity and selectivity of some reactions depend on the nature of the surface sites on the nanoparticles. Factors which determine the coordination of surface metal atoms depend on size, shape, exposed facets and surface roughness [28].

The dependence of the selectivity and activity on the substrate surface has been well known for many years. A variety of different surface reactions have shown a large dependence not only on the surface roughness of the catalyst but also on the crystal lattice. This has been shown for single crystal platinum samples under UHV conditions by a variety of groups and in several early works for dispersions of colloidal transition metals.

The use of nanoparticles in colloidal solution requires that a capping material (e.g. polymer) is added to the suspension in order to prevent coagulation and precipitation of the metal nanoparticles. A part of the added polymer exhibits a protective function by the adsorption of the polymer onto the metal nanoparticles and the other part of the polymer

dissolves freely in the suspension of the metal nanoparticles. Both the amount of the polymer adsorbed on metal nanoparticles and the concentration of free polymer are important for the application of the metal nanoparticles. However, there have been no reports on correlation of the catalytic activity with either the amount of the polymer adsorbed on metal nanoparticles or the concentration of free polymer in catalysts. This polymer capping material can diminish the catalytic effectiveness of the particles by blocking access to the steps and kinks of the surface. Even though the polymer may be removed by heating the sample, this has been shown to leave deposits on the surface of single crystals in UHV conditions. In the single crystal experiments Somorjai found that a carbonaceous layer was actually mobile on the surface and blocked access to catalytically active sites on the crystal.

Though the study of single crystals under ultra-high vacuum [42] has done much to elucidate the catalytic process, since the early 1940s the potential use of transition metal nanoparticles in catalysis have attracted a great deal of interest[43]. These particles have been the subject of study in solution [42,44], in polymers [45], and immobilized on supports [43,46,47]. The wide variety of media in which these particles can exist have facilitated their use in exploring their catalytic properties in a wide variety of reactions including, but not limited to, hydrogenation [48], CO oxidation[43], Suzuki coupling reactions [48], and isomerization [43].

Particles within this size range exhibit interesting properties that are unique to their small size. As the number of atoms in the particle decreases, the fraction of the

number of atoms on the surface to the total increases. This increases the surface to volume ratio of the particles and thus increases the number of atoms per gram that can be involved in the catalysis process. Furthermore, as the size of the particle decreases, the chemical activity of the surface atoms is expected to change due to an increase in the surface tension of the particle with decreasing size and increasing curvature.

Rampino et al[42] studied the effect of size on rate of hydrogenation using platinum and palladium particles capped with polyvinyl alcohol, methyl methacrylate , and polyacrylic acid methyl ester. They compared the rates of hydrogen uptake of the Pd-PVA catalyst with the uptake rates of several commercially available catalysts of known activity. Their test shows that the uptake rate of the Pd-PVA catalyst is almost 5 times larger than the uptake of the Pd-C catalyst. These early results set the context for investigations of metallic nanoparticle catalysis showing the much greater efficiency of the nanoparticles over standard catalysts.

More recently, groundbreaking work by Schmid[43,46] and Bonnemann[43,47,49] has shown the effect and uses of nanoparticles in heterogeneous catalysis process such as hydrogenation and hydroformylation reactions. In Schmid's early work he found that, in order for the catalyst to survive the reaction and maintain its effectiveness, it was necessary to support the particles on substrates such as TiO_2 or Al_2O_3 [58]. In these studies the ability of small rhodium and palladium particles to catalyze the hydroformylation of ethene was explored. These particles were supported on

TiO_2 and a Na-Y zeolite. These catalysts are produced by chemisorption of the particles onto the support surface via addition of the support to a solution containing the particles. This results in loading of 5% and 1.5 % by weight for the zeolite and the TiO_2 respectively. The catalytic effect of the particles was tested heterogeneously on the hydroformylation reaction of ethene, however the deactivation of the surface due to by-products formation led to the study of these species using an aqueous suspension of the particles. The limited solubility of the by-products in the aqueous media decreases the chances of catalyst deactivation. The studies of ethene hydroformylation, using 1 % loading , achieved a turnover frequency of 140 mol mol^{-1} min^{-1} while similar studies using propene led to turnover frequencies of 400-600 mol mol^{-1} min^{-1}. These turnover frequencies are much higher than those found using homogeneous catalysts, but show decreased selectivity.

The hydrogenation of 1-hexene[46] was investigated using small Pd particles on TiO2. In these studies the difference in effectiveness between the supported particles and commercially available catalysts is truly remarkable, with 100% conversion to the alkane by the supported particles and only 29.7% conversion by the commercial catalyst. Similarly impressive results are achieved with diverse compounds such as dicyclopentadiene (100%), 1-hexyne (97.5%), and crotonaldehyde (95.1%). These catalysts not only show an increased effectiveness over traditional catalysts, but in contrast to the rhodium particles, show no deactivation even after many cycles.

Studies by Bonnemann[47] using rhodium nanoparticles have also shown vastly increased activities. The hydrogenation of butyronitrile was performed using a commercially available 5% Rh on charcoal catalyst and a 5% Rh on charcoal nanoparticle catalyst. The difference in activity is astounding, with the nanoparticle catalyst having essentially double the activity of the commercially available catalyst at the same loading. The colloidal Pd nanoparticle catalyst also shows an increased lifetime over conventional catalysts, lasting approximately 2.5 times longer than the conventional catalyst. These studies eloquently show the enhanced activity of transition metal colloid based catalysts in relation to the activity of comparable commercially available catalysts.

Ahmadi et al have shown in a Science report [51] that polymer stabilized platinum and palladium nanoparticles of different shapes can be synthesized using a hydrogen gas reduction in an aqueous solution[51]. This relatively simple method allows us to produce nanoparticles of tetrahedral, cubic, and truncated octahedral shapes. Each shape has its own characteristic crystal facets that can catalyze surface reactions. It has been shown from work on single crystals that certain reactions are sensitive to the surface structure of the crystal. This sensitivity can take the form of enantioselective reactions, and or simple selectivity towards product formation only using a certain facet[52]. In the case of our particles different shapes have different facets. The cubes only have (100) facets, while the tetrahedral have only (111) facets. Recent work by our group has already shown that these catalysts are effective in the catalytic hydrogenation of propylene[53]. Others have also shown that platinum/gold alloys can be used to catalyze

the reaction of H_2 and O_2 up to 50 times the normal rate[54]. This opens the possibility of greatly increasing the output of traditional PEM (polymer electrolyte membrane) fuel cells.

B. Fuel Cells

Fuel cells have long been of interest as an alternative energy source in a wide variety of applications ranging from the space program[55] to more terrestrial concerns such as a replacement for the aging internal combustion engine[55]. While some applications have been realized, such as the use of fuel cells in some bus systems and cellular phone batteries, there are still many areas that could benefit from the use of fuel cells as an energy source. The auto industry is one of the most promising sectors for growth, primarily because of the higher efficiency and lower emissions of a fuel cell system relative to the conventional internal combustion energy. While conventional combustion engines reach only ~30% efficiency, low temperature fuel cells could routinely reach efficiencies of 40% - 50% with emissions of only water vapor. Using such technology in only a fraction of the cars produced in the next decade could significantly reduce the amount of greenhouse gases for which the US is responsible, as well as increase energy security by reducing the dependence of the US on oil imports.

Larger scale fuel cells using a variety of different fuels also hold promise as a cleaner replacement for present day fossil fuel based power plants[55]. Running on renewable resources and emitting almost no waste gases, these plants generate power not

only by conversion in the fuel cell but also by utilizing the waste heat for power generation increasing the efficiency of the process further.

Many previous studies[57-68] and patents[48, 57-71] have focused on enhancing the porous carbon electrode or the catalyst layer using supported catalysts. Theses methods vary from sputtering a thin layer of Pt on to the gas diffusion electrode [57] to reduction of organometallic precursors onto supports for use in the catalyst layer [47,49]. The effect of sputtering Pt on to the carbon electrodes on the oxygen reduction reaction kinetics was recently studied by Mukerjee et. al [57]. The sputtered layer electrodes had Pt nanocrystallite with an average size of 25-30 Å on the surface. The loading of the catalyst layer was held constant at 20% Pt/C in the carbon cloth catalyst layer. They found that the addition of the small Pt nanocrystallites caused a 4-fold improvement in the oxygen reduction reaction at 0.9V and a 3.6-fold improvement in the exchange current densities. This study illustrates how the accessibility of the oxygen to the Pt nanocrystallites vastly increases the efficacy of the process.

Recent work by Bonnemann et al[49] has explored the idea of using a bimetallic colloidal precursor on polymer electrolyte fuel cell anode to improve the CO tolerance. Pure platinum catalysts suffer from poisoning problem resulting from CO adsorption on the surface. However, this problem has been addressed by the development of alloy catalysts that are much more resistant to poisoning than the pure metals. Bonnemann et al seek to take advantage of not only the increase in activity shown with nanoparticles, but also the CO resistance introduced by alloying with other metals. The platinum precursor

colloids were produced by coreduction of platinum and ruthenium chloride using tetractylammonium-triethylhydroborate in THF. The platinum-ruthenium and platinum-tin particles are produced via a multi-step borate reduction mechanism. The platinum-ruthenium particles are also synthesized via a trialkylaluminum reduction. The particles were then deposited on a Vulcan XC72 substrate. The capping layer was then removed by reactively annealing at 300^{o}C in a 10% O_2 in N_2 atmosphere and then at 300^{o}C in pure H_2. The particles were then deposited onto a glassy carbon electrode and then fixed with Nafion solution. These catalysts show a slightly higher activity towards the reduction of H_2 than commercial catalysts as well as having essentially the same activity even when 2% CO is added to the reaction mixture.

Obviously, to realize these goals much more basic research needs to be done to increase the amount of energy the cells can produce so that one day they may become as ubiquitous as standard flashlight batteries. One method by which this can achieved is by increasing the efficiency of the conversion of the cell. The most interesting way to achieve this is to use the advantages afforded by novel nanomaterials, specifically, transition metal nanoparticles.

Our primary interest is in the polymer electrolyte fuel cell, and more specifically in the proton conducting membrane sandwiched between the electrodes. In the polymer electrolyte fuel cell, a feed stream of hydrogen is fed to the anode and there split into individual protons giving up two electrons. The electrode often has a thin layer of platinum either on it or adjacent to it in a carbon support matrix. The electrons travel

through the external circuit, while the protons are conducted through the polymer electrolyte to the cathode where the oxygen is reduced and combines with hydrogen to give of water and energy as shown here[55]:

$$\text{Anode: } 2H_2 \rightarrow 4H^+ + 4e^-$$

$$\text{Cathode: } O_2 + 4H^+ + 4e^- \rightarrow 2H_2O$$

$$\text{Overall: } 2H_2 + O_2 \rightarrow 2H_2O + \text{energy}$$

These cells hold the advantage of their low operating temperature (<80 ^oC) and their relatively high efficiencies of ~ 50%. Unfortunately, the catalyst is very sensitive to the purity of the feed gases and thus easily poisoned. Our proposed research focuses on the modification of the polymer membrane with the addition of shape controlled Pt nanoparticles. We shall use our hydrogen reduction technique[51] to synthesize shape controlled alloy nanoparticles designed for poisoning resistance and to increase catalytic activity. Watanabe and co-workers have recently reported data [56] on the incorporation of platinum nanoparticles into the membranes of polymer electrolyte fuel cells. They used membranes containing Pt, TiO_2, and Pt-TiO_2 particles. The primary focus of their work was the suppression of gas crossover and to introduce a method to control self-humidification of the membranes. The platinum particles were produced by soaking the membranes in a precursor solution consisting of $[Pt(NH_3)_4]Cl_2$ overnight. The ions were reduced to the metal by reacting with excess neutral hydrazine overnight. TEM

images of the particles confirmed the size range of 1-2 nm. The terminal voltage and power density measurements show a substantial increase in the performance of the modified membranes versus the unmodified ones. While they conclude that many of these effects are due to the better water distribution achieved with their particles, they make no mention of the catalytic enhancement of the oxidation of the hydrogen or reduction of the oxygen. The effects of adding transition metal nanoparticles to the proton exchange membrane are studied in Chapter V.

Thesis Outline

This thesis is structured as follows. The electron cooling dynamics of periodic gold arrays are examined in Chapter I. The power dependence of the arrays is compared to those of colloidal gold nanaoparticles, films, and literature values. The dynamics are discussed in terms of the contrast in environmental coupling between the different systems. In Chapter II , evidence for the existence of phonon oscillations in gold and silver nano-arrays is presented. These oscillations are the result of heat imparted to the lattice via the plasmon electrons heated coherently by use of femtosecond laser pulses. This data is discussed within the context of this theory and compared to work previously done with gold and silver systems in solution and glass matrices and discussed in Section 2 of this this introduction. The medium effects on the relaxation of gold arrays are elucidated in Chapter III. This is done by comparing the dynamics in air, pyridine, and water and their respective thermal properties.

In the second half of this thesis, the catalysis by transition metal nanoparticles is investigated. The catalytic effects of platinum, palladium, rhodium, and Pt/Pd alloy nanoparticles on the power output of polymer electrolyte membrane fuel cells is discussed in Chapter V. In Chapter VI, the heterogeneous catalysis of the hydrogenation of propene over truncated octahedral platinum nanoparticles on alumina is investigated. In Chapter VII, the efficiency of the catalytic action of platinum nanoparticles encapsulated in alumina on the hydrogenation of propene is examined

References

1) Faraday, M., *Phil. Trans. Royal Soc.* **1857**, *147*, 145

2) Schmid, G. *Clusters & Colloids: From Theory to Application*; VCH: Weinheim, 1994.

3) Kamat, P. V.; Meisel, D. *Studies in Surface Science and Catalysis, Vol. 103, Semiconductor Nanoclusters - Physical, Chemical, and Catalytic Aspects*; Elsevier: Amsterdam, 1997.

4) Edelstein, A. S.; Cammarata, R. C. *Nanoparticles: Synthesis, Properties and Applications*; Institute of Physics Publishing: Bristol, 1996.

5) Graetzel M. In *Electrochemistry in Colloids and Dispersions*; Mackay, R. A.; Texter, J., Eds.; VCH: Weinheim, 1992.

6) Ahmadi, T. S.; Wang, Z. L.; Green, T. C.; El-Sayed, M. A. *Science* **1996**, *272*, 1924.

7) Henglein, A. *J. Phys. Chem.* **1993**, *97*, 8457

8) Mulvaney, P. *Langmuir* **1996**, *12*, 788.

9) Yguerabide, J.; Yguerabide, E *Anal. Biochem*. **1998**, *262*, 157

10) Nikoobakht, B.; El-Sayed, M. A. *Chem.of Mat*. **2003**, *15*, 1957

11) Nikoobakht, B.; Wang, J.; El-Sayed, M. A. Chem. Phys. Lett. **2002**, *366*, 17

12) Storhoff, J. J.; Mirkin, C. A. *Chem. Rev.* **1999**, *99*, 1849.

13) Link, S.; El-Sayed, M. A. *International Reviews in Physical Chemistry* **2000**, *19*, 409

14) Link, S.; El-Sayed, M. A. *J. Phys. Chem. B* **1999**,*103*, 8410

15) Hodak, J. K.; Henglein, A.; Hartland, G. V. *J. Phys. Chem. B.* **2000**, *104*, 5053

16) Hodak, J. K.; Henglein, A.; Hartland, G. V. *J. Phys. Chem. B.* **2000**, *104*, 9954.

17) Hodak, J. K.; Martini, I.; Hartland, G. V. *J. Phys. Chem. B* **1998**, *102*, 6958.

18) Sun, C.-K.; Vallee, F.; Acioli, L. H.; Ippen, E. P. Fujimoto, J. G. *Phys. Rev. B* **1993**, *48*, 12365

19) Sun, C.-K.; Vallee, F.; Acioli, L. H.; Ippen, E. P.; Fujimoto, J. G. *Phys. Rev. B* **1994**, *50*, 15337

20) Del Fatti, N.; Voisin, C.; Christofilos, D.; Vallee, F.; Flyzantis, C.; *J. Phys. Chem.* A **2000**, *104*, 4321

21) Voisin, C.; Del Fatti, N.; Christofilos, D.; Vallee, F. *J. Phys. Chem. B* **2001**, *105*, 2264

22) Portales, H.; Saviot, L.; Duval, E.; Fujii, M.; Hayashi, S.; Del Fatti, N.; Vallee, F.; *J. Chem. Phys* **2001**, *115*, 3444

23) Voisin, C.; Christofilos, D.; Del Fatti, N.; Vallee, F. *Physica B* **2002**, *316*, 89.

24) Voisin, C.; Christofilos, D.; Del Fatti, N.; Vallee, F. *App. Surf. Sci.* **2000** *164*, 131

25) Anisimov, L.; Kapeliovich, B. L.; Perel'man, T. L. *Sov. Phys. JETP* **1975**, *39*, 375.

26) Maxwell-Garnett, J. C. *Philos. Trans. R. Soc. London* **1904**, *203*, 385.

27) Kerker, M. *The Scattering of Light and Other Electromagnetic Radiation*; Academic Press: New York, 1969.

28) Bohren, C. F.; Huffman, D. R. *Absorption and Scattering of Light by Small Particles*; Wiley: New York, 1983.

29) Roberti, T. W.; Smith, B. A.; Zhang, J. Z. *J. Chem. Phys.* **1995**, *102*, 3860.

30) Ashcroft, N. W.; Mermin, N. D. *Solid State Physics*; Saunders College: Philadelphia, 1976.

31) Hartland, G.; Hu, M.; Sader, J. *J. Phys. Chem. B* **2003**, *107*, 7472

32) Yu, Y.; Chang, S.; Lee, C.; Wang, C. *J. Phys. Chem B* **1997**, *101*, 6661

33) Chang, S.; Shih, C.; Chen, C.; Lai, W.; Wang, C. *Langmuir* **1999**, *15*, 701

34) Hartland, G.; Hu, M.; Wilson, O.; Mulvaney, P.; Sader, J. *J. Phys. Chem* **2002**, *106*, 743

35) Perner, M.; Gresillon, S.; Marz, J.; von Plesson, G.; Feldmann, J.; Porstendorfer, J.; Berg, K.-J.; Berg, G *Phys. Rev. Lett.* **2000**, *85*, 792.

36) Hu, M.; Wang, X.; Hartland, G.; Mulvaney, P.; Juste, J.; Sader, J. *J. Amer. Chem. Soc*. **2003**, *125*, 14925

37) Link, S.; Burda, C.; Nikoobakht, B.; El-Sayed, M. A. *Jf Phys. Chem. B* **2000**, *104*(26), 6152

38) Hulteen, J.C.; Treichel, D.A.; Smith, M.T.; Duval, M.L.; Jensen, T.R.; Van Duyne, R.P. *J. Phys. Chem. B* **1999**, *103*, 3854-3863.

39) Hulteen, J.C.;Van Duyne, R.P. *J. Vac. Sci. Technol. A.* **1995**, *13* **,** 1553-1558.

40) Jensen, T.R.; Schatz, G.C.; Van Duyne, R.P. *J. Phys Chem. B* **1999**, *103*, 2394-2401.

41) Tas, G.; Maris, H.J. *Phys. Rev. B* **1994**, *49*, 15046

42) Rampino, L.D., Nord, F.F. *J. Am. Chem. Soc*., **1942**, *63*, 2745

43) Aiken III, J.D., Finke, R.G.; *J. Mol. Catalysis A: Chemical*, **1999**, *145*, 1 and references therein

44) Li, Y., Petroski, J., El-Sayed, M.; *J. Phys. Chem*., **2000**, *104*, 10956.

45) Li, Y., Hong, X., Collard, D., El-Sayed, M.; *Organic Le*tters, **2000**, *2*, 2385.

46) Scmid, G. ; *Chem. Rev*. **1992**, *92*, 1709 and therein

47) Bonnemann, H., Braun, G., Brijouz, W., Brinkmann, R., Schulze Tilling, A., Seevogel, K., Siepen, K.; *J. Organometallic Chem.* **1996**,*520*, 143

48) U.S. Patent #5767036

49) Bonnemann, H. Brinkmann, R., Britz, P., Endruschat, U., Mortel, R., Paulus, U.A., Feldmeyer, G.J., Schmidt, T.J., Gasteiger, H.A., Behm, R.J.; *J. New Mat. Electrochem.*

Systems, **2000**, *3*, 199

50) Bonnemann, H., Brinkmann, R., Britz, P., Endruschat, U., Mortel, R., Paulus, U.A., Feldmeyer, G.J., Schmidt, T.J., Gasteiger, H.A., Behm, R.J., *J. New Mat. Electrochem. Systems*, **2000**, *3*, 199

51) Ahmadi, T.S., Wang, Z.L., Green, T.C., Henglein, A., El-Sayed, M.A. *Science*, **1996**, *272*, 1924

52) Somorjai, G. Introduction to Surface Chemistry and Catalysis **1994**, John Wiley & Sons; New York

53) J.W. Yoo, D.J. Hathcock, M.A. El-Sayed J. Catalysis, **2003**,*1*,214

54) Lam, Y.L., Criado, J., Boudart, M.; *Nouv. J. Chem*., **1977**, *1*, 461

55) www.fuelcelltoday.com

56) Watanabe, M., Uchida, H., Emori, M.; *J. Phys. Chem. B*, **1998**, *102*, 3129

57) Mukerjee, S.,Srinivasan, S., Appleby, A.J.; *Electrochimica Acta*, **1993**, *38*, 1661

58) Steigerwalt, E.S., Deluga, G., Cliffel, D., Lukehart, C., *J. Phys. Chem. B*, **2001**, *105*, 8097

59) Lasch, K., Jorissen, L., Garche, J., *Journal of Power Sources*, **1999**, *84*, 225

60) Starz, K., Auer, E., Lehmann, Th., Zuber, R., *Journal of Power Sources*, **1999**, *84*, 167

61) Rohlans, B., Plzak, V., *Journal of Power Sources*, **1999**, *84*, 183

62) Gupta, S., Tryk, D., Zecevik, S., Aldred, W., Guo, D., Savinell, R.F., *J.Appl. Electrochem*., **1998**, *28*, 673

63))Ticianelli, E.A., Derouin, C.R., Srinivasan, S.; *J. Electroanal. Chem.*, **1988**, *251*, 275

64) Dalmia, A., Linken, C.L., Savinelli, R.F.; *J. Coll. Interface Sci*. , **1998**, *205*, 535

65) Gottesfeld, S., Wilson, M.S.; *J. Appl. Electrochem*, **1992**, *22*, 1

66) Gottesfeld, S., Wilson, M.S.; *J. Electrochem Soc*. , **1992**, *139*, L28

67) Taylor, E.J., Anderson, E.G., Vilambi, N.R.K.; *J. Electrochem. Soc.* **1992**, *139*, L45

68) Faubert, G., Guay, D.,Dodelet, J.P.; *J. Electrochem. Soc.* **1998**, *145*, 2985

69) U.S. Patent #5489563

70) U.S. Patent #6287717

71) U.S. Patent #5861222

72) Petroski, J.M. Green, T.C., El-Sayed, M.A. *J. Phys. Chem. A* **2001**, *105*, 5542

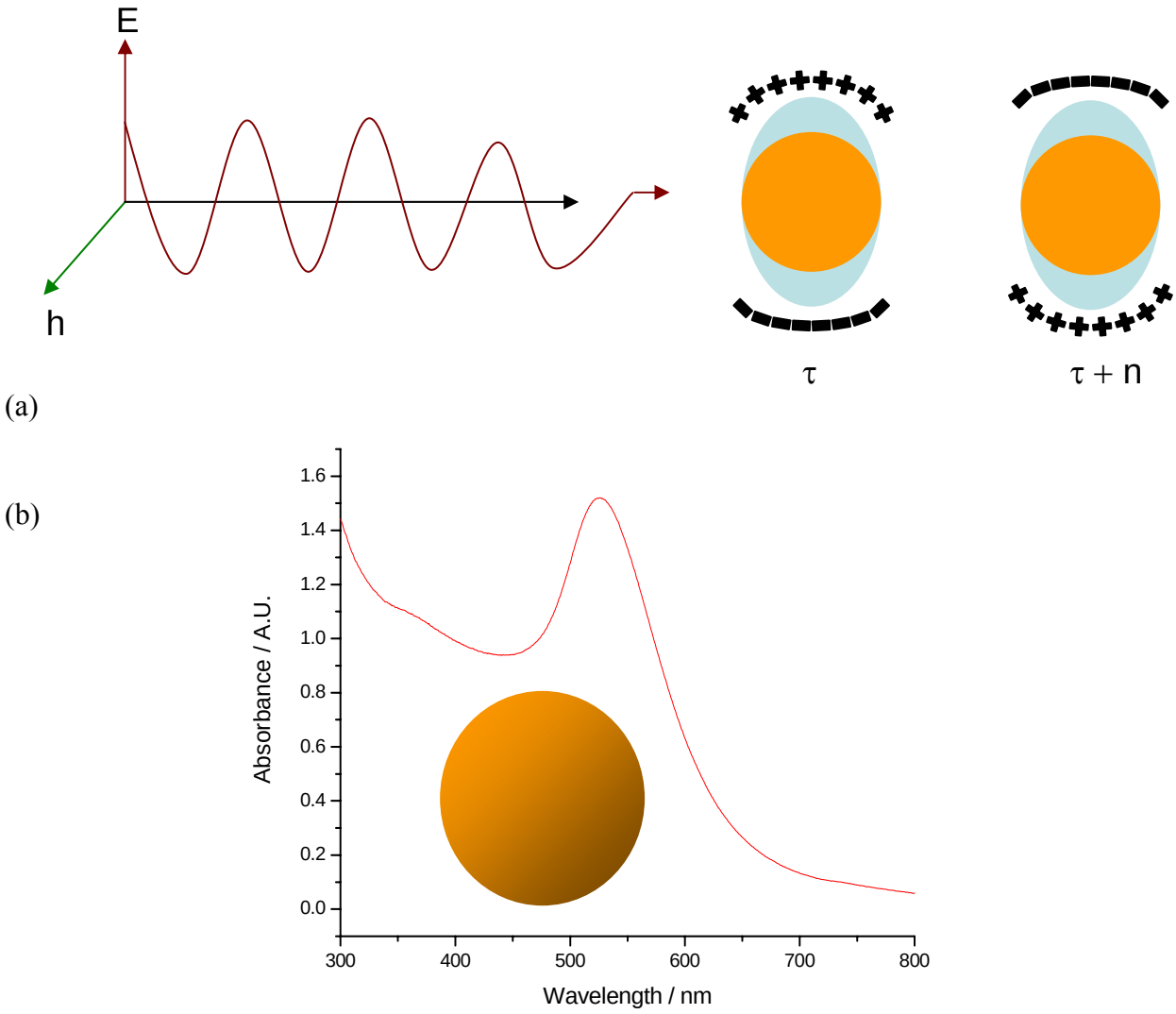

Figure 1-1 Schematic (a) of the surface plasmon phenomenon showing the interaction of light with the free electrons of the particle. This creates a coherent bulk oscillation of the electrons leading to the surface plasmon absorption (b).

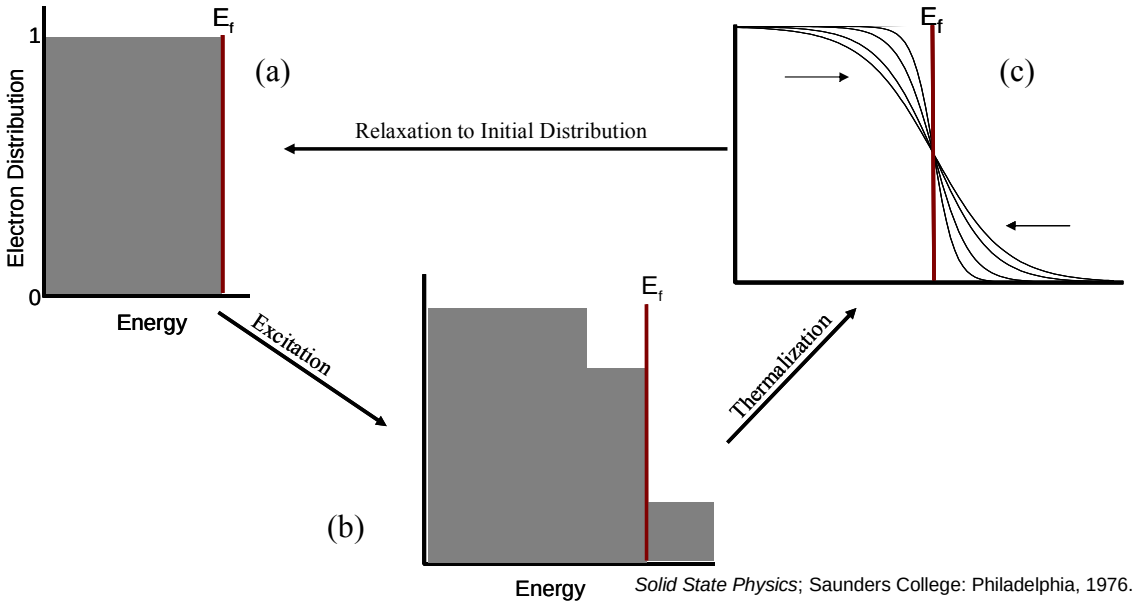

Figure 1-2 Representation of the electron distribution before (a) , during (b) , and after (c) thermalization. Before laser excitation (a) the system occupies levels below the Fermi energy. When the system is excited, the energy causes a non-thermal distribution above the Fermi energy. The system then begins to quickly thermalize via electron-electron, electron-phonon, and phonon-phonon interactions. The system then relaxes down to the initial distribution.

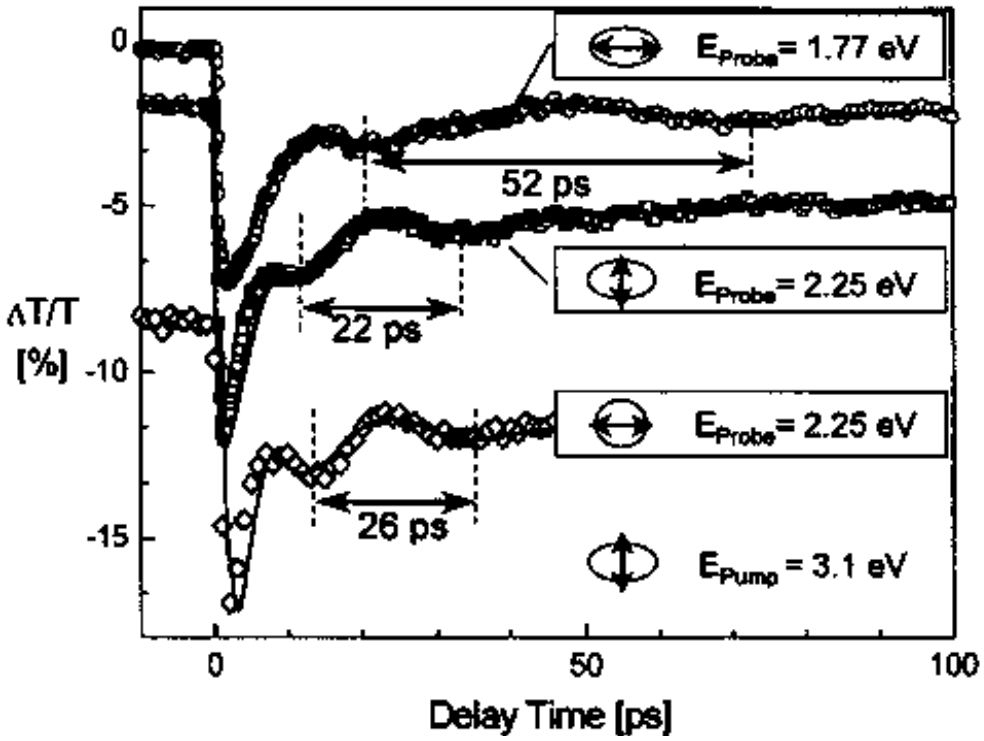

Figure 1-3 Data from Perner et al showing oscillations detected in the plasmon of silver nanorods in a glass matrix. (Perner, M et al. *Phys. Rev. Lett.* **2000**, *85*, 792.)

CHAPTER II

HOT ELECTRON COOLING DYNAMICS OF LITHOGRAPHICALLY PREPARED AU NANOARRAYS

Abstract

The relaxation dynamics of Au arrays prepared via nanosphere lithography were investigated using femtosecond pump-probe spectroscopy. The hot electron relaxation dynamics in arrays of truncated tetrahedra shaped 90 nm gold nanoparticles on glass, 50nm thick gold film, and gold nanodots in solution are compared. The initial relaxation (due to the electron-phonon relaxation) of the Au array is longer (2.9 ps) than the relaxation of the Au thin film (1.5 ps). The thin film system exhibited single component decay, while the nanodot in solution displayed an additional longer decay due to the phonon-phonon relaxation or heat dissipation which is in the 80-100 ps range. This is explained in the context of the differences in the relative rate of heat dissipation compared to the rate of electron-phonon relaxation in the different systems. In the gold film, the rapid transport of heat away in the continuous film allows faster relaxation of the system and the observation of only one component in the overall relaxation. In this system the rate of heat dissipation is comparable to the electron-phonon relaxation rate. In the arrays, the electron-phonon relaxation time is longer than in the films as a result of the amount of surface that is exposed to the less thermally conductive air. In the nanodot

system in solution, the rate of heat dissipation is in-between that in the films and the arrays as it involves the gold phonon relaxation to the micellar capping material and to the solution phonons, giving rise to the slow component.

Introduction

The dynamics noble metal nanoparticles have been the subject of intense interest in recent years. The effect of the surrounding media on the relaxation of the hot electrons is also of intense interest. Theses have been studied in solution, particle films, membranes, powders and glasses. However, the method of nanosphere lithography developed by Van Duyne[1-3], allows the production of very monodisperse particles with no capping material, on a variety of substrates, in a variety of sizes. These particles may be composed of any material such as metals, polymers, or semiconductors that is thermally evaporated through the lithographic mask on to the substrate. The work by Van Duyne *et al* [1-3] has shown that these particles may be readily prepared of silver or gold and show very discrete surface plasmons, which could be probed by femtosecond transient absorption spectroscopy. This offers the ability to use nanolithographically prepared nanoparticles, which are spatially isolated, uncapped, and surrounded only by an air matrix as a method to study the differences in the relaxation times of the hot electrons in these nanoparticles versus noble metal nanoparticles dissolved in solution.

The work of Sun *et al*[6] has helped elucidate the mechanism of electron thermalization in gold films, showing that the hot electrons quickly relax by dissipating energy via electron-phonon and phonon-phonon interactions. This is supported by the work of Bigot *et al* [15] who showed that the relaxation time of silver nanoparticles imbedded in a glass matrix becomes shorter when then matrix is changed to more thermally conductive alumina. The differences in the hot electron relaxation times between films, nanoparticles in solution, and spatially isolated arrays then gives a clearer picture of how these vastly different environments influence the relaxation dynamics of noble metal nanoparticles.

Experimental

Regular arrays of gold nanoparticles were prepared using nanosphere lithography.[1-3] In short, an ordered layer of polystyrene nanospheres (Polysciences) was prepared on a glass coverslip (Fisher Scientific) as shown in Figure 1. The coverslips were then mounted in a Denton DV-502A Thermal Evaporator to deposit gold in the spaces between the spheres. This gives rise to the triangular shape of the particles in the arrays. The height of the particles is determined by the mass thickness of material deposited and can thus be easily controlled. The thickness of the evaporated gold was monitored by a quartz crystal thickness monitor (Inficon). After evaporation the mask was removed from the substrate by sonicating for 30s in methylene chloride. The arrays were then allowed to dry overnight to allow any residual liquid to evaporate. The size of

the particles was then determined using a Quesant Q-SCOPE atomic force microscope (AFM). The average size of the particles was calculated to be approximately 90 nm wide using the geometric relations determined by Van Duyne *et al* [1] and 50 nm in height when 356 nm polystyrene spheres were used as the mask material. The AFM images are raw images uncorrected for tip convolution effects, and thus the particles appear larger than the calculated value. As shown in Figure 2, after removal of the nanosphere mask hexagonal arrays of nanoparticles were present on the coverslip, but did have some defect sites. The 50 nm gold films were prepared by simply evaporating gold onto clean coverslips. The absorption spectra of the arrays and the films were then recorded using a Shimadzu UV-3101-PC spectrophotometer in standard transmission geometry.

The dynamics of the arrays and the films were studied by using femtosecond pump-probe spectroscopy. The setup consisted of regeneratively amplified Ti:Sapphire laser system (Clark-MXR CPA 1000) pumped by the doubled frequency of a Nd:Vanadate laser (Coherent Verdi). The system repition rate was 1 kHz and produced 100 fs (FWHM) duration pulses with energy of 1 mJ centered at 800 nm. A portion of the output beam was split off and focused on a 1 mm thick sapphire plate to generate a white light continuum for use as a probe beam. The remainder of the beam was then doubled by second harmonic generation to produce 400nm light for use as a pump beam.

The pump beam was then sent to a computer controlled variable delay line and then passed through a chopper to modulate the beam at 500 Hz with the same phase. It was then focused onto the sample. The continuum beam was split into probe and reference beams. The probe beam was focused onto the sample and overlapped with the pump beam, and then collected and focused onto a fiber optic cable coupled to a monochromator. The reference beam was focused onto a fiber optic cable that was coupled to the same monochromator. The kinetics measurements were made by monitoring the probe and reference beam signals using two photodiodes at the exit slit of the monochromator. The voltage from the photodiodes was then amplified and fed into a sample and hold system.

Results and Discussion

The gold array nanoparticles have a UV-Vis spectrum as shown in Figure 3. The different peaks at 700 nm are all from the same sample. The substrate was simply shifted such that the sample beam impinged on different portions of the sample. The spectra show that the position of the peak remains relatively constant, with only the value of the absorbance varying with the number of particles in the beam area. Since the beam must inevitably include some defect sites this also serves to bolster the idea that these defects have little effect on the spectral shape of the absorption band, only on the absorbed intensity. The absorbance is in roughly the same position as the longitudinal absorbance of the gold nanorods having an aspect ratio of 3:1 but, as expected, does not

display the transverse band. The work of Martin[26] et al. and van Blaaderen[23-25] et. al. using gold nanorods embedded in an alumina and polymer matrices has shown that the angle of incidence for the probe beam, as wells as the aspect ration of the rods, can have a significant effect on the features of the spectra. By changing the orientation of the particles it is possible to selectively excite the transverse and longitudinal modes. This could explain the appearance of only one band for the array nanoparticles since they are excited in the direction perpendicular to the substrate. This would lead to the observation of the absorbance along the long axis , and not the short axis of the base in correspondence to the longitudinal mode of the nanorods. For a triangular shape this would correspond to the in plane absorption while the transverse band would transverse band would be perpendicular to the plane.

The interband transitions appear in the 350 nm – 500 nm region [4,5,8,14,19] but the absorption of the glass substrate interferes with further characterization below that region. The maximum absorbance of the system is also relatively small (<.1 OD) due to the relatively large spacing of the particles as concluded by comparing the particles to a gold film with a thickness of 50 nm. Unfortunately, the extremely low OD of the particles in the 400 nm range makes it difficult to excite the particles with the second harmonic of the Ti:Sapphire laser. The particles were probed at 520 nm in accordance with the absorption of the gold nanospheres [9,14]. It should be noted that this is on the blue side of the plasmon absorbance.

The electron cooling dynamics of the gold array nanoparticles and a 50 nm gold thin film were studied at several different excitation powers. Representative kinetic traces are shown in Figure 4 and Figure 5, respectively. The relaxation time of both the film and the arrays showed an increase with increasing pump energy. As shown in Figure 4, the relaxation time of the gold array nanoparticles increases from 2.83 ps at 7926 K to 9.17 ps at 14322 K, the highest electronic temperature change. The 50 nm gold films were also investigated and showed a definite increase in relaxation time from 1.06 ps at 3381 K to 6.94 ps at 18094 K. However, the relatively low optical density of the array samples (.0148 at 400 nm), in comparison to the films(>1.2 at 400nm), leads to only a very small fraction of the incident energy being absorbed. Unlike the gold nanodots in aqueous solution, shown in Figure 6, no long component was detected at any of the powers investigated for the film or the arrays.

The observed relaxation time for the film, even at the lowest excitation power , is found to be shorter than the relaxation time of the array particles. The difference in the relaxation rate in the two systems can be explained by two factors: the difference in the temperature dependence of the heat capacity of the electron gas and the heat transfer characteristics of the two systems. It is well known that the heat capacity of the electron gas is temperature dependent and thus varies with the excitation power.[16-18] Also, at higher excitation powers the hot electrons must dissipate a larger amount of absorbed

energy. Depending on the cooling mechanism of the nanoparticles to the surroundings, the measured relaxation time might be affected.

Both the film and array systems are on a glass substrate, which has a significantly higher thermal conductivity than the aqueous solution in which the nanodots are dissolved. The high thermal conductivity of the medium plays an important role in the relaxation of the hot gold arrays and film.[7,20,21] In a previous work from our lab, it has been asserted that the relaxation components may be separated into components responsible for the heat transfer to the surroundings and then the conduction of the heat away.[20,21] The previous work from our lab detailing the electron relaxation dynamics of gold nanodots in a $MgSO_4$ solid matrix [20] using diffuse reflectance spectroscopy has shown the dependence of the relaxation times on the surrounding medium. Using $MgSO_4$, THF, and air as different matrices, Link and co-workers [20] found a definite link between the short component of the relaxation of the gold nanodots embedded in different matrices and the nature of the matrix. The particles in the $MgSO_4$/air matrix showed that the fast component was twice as long as the same particles in a $MgSO_4$/THF matrix. The heat is therefore transferred to the surrounding media in the $MgSO_4$/THF faster than in the case of $MgSO_4$/air, and the fast component of the plasmon band bleach recovery has been assigned to electron-phonon coupling within the particles as well as a partial heat transfer to the surrounding medium. However, the long component is found to be comparable in the two systems. These results might suggest that the electron-phonon coupling involves interfacial phonons, which are dependent on the particle environment.

The phonon-phonon relaxation (the long component) could involve the same phonons or different phonons with different coupling constant and phonon densities as to give similar relaxation rates in the two different environments.

In the case of the gold film, the electron gas in the excitation volume is heated and because a continuous film is used, the heat transfer is extremely fast between the hot electrons and the surrounding area of the film.[6,10-13] The hot electrons quickly transfer the excitation energy to the essentially infinite lattice of the film via diffuse motion and ballistic transport, thus producing an extremely short electron-phonon component to the relaxation. The energy is then quickly conducted away by the rest of the gold lattice. The conduction is also aided by the substrate. The glass substrate is in intimate contact with the entire film and acts as another sink for the conduction of the heat away from the excitation area. The conduction component of the long portion of the relaxation is therefore greatly enhanced , decreasing its relaxation time to become comparable to the electron-phonon relaxation time at the powers investigated. This contention is supported by the work of Bigot *et al*.[15] in which they studied the dynamics of silver nanoparticles in glass and alumina. They found that the relaxation time decreased markedly when the particles were embedded in the more conductive alumina.

The significantly longer (2.5 ps) short component decay time of the arrays measured under similar excitation conditions points to a difference in the rate of heat transport from the array particle to the environment. In contrast to the film system, the array system is much more spatially isolated and therefore cannot conduct heat away

from the excitation volume as efficiently as the gold film. The hot array particles could cool by transferring heat to the surrounding environment, which in this case is air and the glass substrate. The rate of heat conduction through air is very small. Thus this partial spatial isolation of the particles limits the overall rate of heat transfer and conduction channels that are available to dissipate the heat resulting form the electron-phonon relaxation . The array particles do not have a continuous high thermal conductivity film to quickly conduct this heat away from the excitation area. The isolation of the particles also limits the amount of energy that can be dissipated by ballistic electron motion. As a result the apparent electron-phonon relaxation time (the short component) becomes longer (2.5 ps). Within the continuous gold film it is relatively easy to transfer the system heat to the rest of the film and then have it conducted away. The arrays however, are only able to transfer and conduct to the air surrounding the particle on three sides and the glass substrate to which the particles are attached on one side. The surrounding air has a much lower thermal conductivity than the gold metal of the films and the glass substrate is not as good a heat conductor as the gold metal film. Therefore, the conduction of the array particles should be much slower than conduction in the gold film. The contribution of the glass substrate must also be less in the arrays than in the film case since contact is continuous in the film while the arrays have only one face in contact with the substrate. The transfer is thus hindered because of the small amount of surface area in contact with the substrate in relation to the volume of the particle on account of the slow phonon

relaxation in the array (compared to that in the film), one can understand its relatively longer electron-phonon relaxation time (the short component)

The differences between the decay components of the nanodots, arrays, and films may now be explained by the differences in heat transfer and conduction properties. The gold nanodots have an electron-phonon relaxation time in-between those in the film and the array particles. The nanodot in solution also has a phonon-phonon relaxation time (on the order of 90 ps) which is in between the film and the arrays.. The thermal conductivity for water is the largest for a liquid, but while it is faster than air, it is much smaller than that for either gold (in the thin film) or the glass substrate (in the arrays).

These contentions are further supported by the different relationships of the relaxation time of the short component in each system to the electron temperature, as shown in Figure 6. These temperatures were calculated using the equation (1), a derivation of the two-temperature model for each point in the power dependence series.

$$T_e(x) = \left(T_i^2 + \frac{2U_L}{\gamma} \right)^{1/2} \qquad (1)$$

Where U_L is the absorbed laser energy density, γ is heat capacity of gold, and T_i is the temperature of the electron gas before excitation (i.e. room temperature). Thus knowing the spot size of the impinging beam, one can calculate the electron temperature of the aqueous particles, array particles, and films. One can then compare the relaxation times across various particle environments.

The aqueous particles show a rise in relaxation time as the power is increased, until the short component levels off at an electron gas temperature of ~15 000 K. This short component has been shown to be a combination of the electron-electron scattering and the electron-phonon relaxations. This relaxation bottlenecks as the energy is dissipated to the lattice phonons and then must be transferred to the phonons of the surrounding media. In the case of the nanodots , the surrounding media is water. The thermal conductivity of the water allows for the transfer of energy away from the lattice phonons to the media, but not instantaneously. As shown in Figure 7 , at high ΔT_e ,the electron-phonon relaxation time levels off and remains relatively constant even at relatively high values such as ~18 300 K. However, in Figure 6, one can see that the contribution of the long phonon-phonon component is increasing with increasing pump power. Since the electron-phonon relaxation times stay relatively constant at the higher electronic temperatures, while the magnitude of the phonon-phonon contribution increases, it is well known that the coupling to the surrounding media can play an important role in the cooling dynamics, one can conclude that the energy is bottlenecked at point where the phonons of the gold lattice transfer energy to the surroundings. In this case limited by the transfer from the nanoparticle to the aqueous solution.

In the case of the film, the relaxation time is seen to increase linearly with the increased ΔT_e. The films, as discussed earlier, can rapidly dissipate the excitation energy through electron-electron, electron-phonon, and phonon-phonon paths with the rest of the film. The thermal conductivity of the gold (3.17 W/cm K @300 K) is much higher than

that of the water (.006071 W/cm K @ 298 K) surrounding the aqueous particles and the air (26.2 mW/m K) surrounding the array particles. Thus the energy can be dissipated into the virtually infinite sea of phonons surrounding the excitation spot. This fast thermalization is well known in thin films and has been characterized for thin gold films in particular by Sun et al[6].

The arrays are the most insulated system studied, since they are surrounded on three sides by air and one side by the glass substrate. Several studies[9,10,19] have shown the dependence of the relaxation on the external medium, as mentioned earlier. The steep slope of the array data, when compared to the aqueous particle and thin film data, can be explained in terms of the difference in the environment. The arrays represent a system where the particles are isolated from each other, and not surrounded by a conductive medium like water as in the dots. While the air is thermally conductive, its thermal conductivity is orders of magnitude smaller than the gold of the thin films, or the water of the aqueous gold dot particles. The efficient coupling of the energy of the thermalized electrons out of the particles into the surroundings is therefore hindered. As shown in Figure 7, the relaxation time increases quickly with ΔT_e over the same temperature range as the film and particle systems. This can be attributed to the isolation of the array particles, which does a great deal to limit the phonon-phonon relaxation channel. The temperature of the array particles is thus rapidly increased with respect to that of the particles in solution and the films since the phonon-phonon relaxation channel

to the surrounding media is greatly hindered. The measured relaxation time thus becomes longer with the increased laser fluence.

In summary, the relaxation of hot electrons in gold nanoparticle arrays, thin films, and gold nanodots has been shown to depend strongly on the degree of coupling to surrounding medium of the material. It has been proposed that the thermal conductivity and heat capacity of the surrounding media are responsible for the observed cooling dynamics in each of the different systems. By comparing the results of thin films, nanoparticle arrays created using nanosphere lithography, and gold nanodots in solution, we have supported this proposal by showing the effects of different environments on the observed relaxation dynamics.

Acknowledgements. We gratefully acknowledge Dr. L.A. Lyon and Dr. R.M Dickson and their students C.Jones and L.Peyser for the use of, and their assistance with, the thermal evaporator and AFM instruments respectively. We would also like to thank the National Science Foundation (Grant #CHE-9727633) for their financial support.

References:

1) Hulteen, J.C.;Van Duyne, R.P. *J. Vac. Sci. Technol. A.* **1995**, *13* **,** 1553-1558.

2) Hulteen, J.C.; Treichel, D.A.; Smith, M.T.; Duval, M.L.; Jensen, T.R.; Van Duyne, R.P. *J. Phys. Chem. B* **1999**, *103*, 3854-3863.

3) Jensen, T.R.; Schatz, G.C.; Van Duyne, R.P. *J. Phys Chem. B* **1999**, *103*, 2394-2401.

4) Mulvaney, P. *Langmuir* **1996**, *12*, 788-800.

5) Henglein, A. *Israel J. Chem* **1993**, *33*, 77-88.

6) Sun, C.-K.; Vallee, F.; Acioli, L.H.; Ippen, E.P.; Fujimoto, J.G. *Phys. Rev. B* **1994**, *50*, 15337-15348.

7) Perner, M.; Bost, P.; Lemmer, U.; von Plessen, G.; Feldman, J.; Becker, U.; Mennig, M.; Schmitt, M.; Schmidt, H. *Phys. Rev. Lett*. **1997**, *78*, 2192-2195.

8) Creighton, J.A.; Eadon, D.G. *J. Chem. Soc Faraday Trans*. **1991**, *87*, 3881-3891.

9) Hodak, J.; Martini, I.; Hartland, G.V. *Chem. Phys. Lett.* **1998**, *284*, 135-141.

10) Sun, C.-K.; Vallee, F.; Acioli, L.; Ippen, E.P.; Fujimoto, J.G. *Phys. Rev. B* **1993**, *48*, 12365-12368.

11) Juhasz, T.; Elsayed-Ali, H.E.; Smith, G.O.; Suarez, C.; Bron, W.E. *Phys. Rev. B* **1993**, *48*, 15488-15491

12) Suarez, C.; Bron, W.E.; Juhasz, T. *Phys. Rev. Lett*. **1995**, *75*, 4536-4539

13) Fann, W.S.; Storz, R.; Tom, H.W.K.; Bokor, *J. Phys. Rev. Lett*. **1992**, *68*, 2834-2837.

14) Link, S.; El-Sayed, M.A. *J. Phys. Chem. B* **1999**, *103*, 4212-4217

15) Halte, V.; Guille, J.; Merle, J.-C.; Perakis, I.; Bigot, J.-Y. *Phys. Rev. B* **1999**, *60*, 11738-11746

16) Kanavin, A.P.; Smetanin, I.V.; Isakov, A.; Afanasiev, Y.V.; Chichkov, B.N.; Wellegehausen, B.; Nolte, S.; Momma, C.; Tunnermann, A. *Phys. Rev. B.* **1998**, *57*, 14698-14703

17) Fatti, N.D.; Voisin, C.; Achermann, M.; Tzortakis, S.; Christofilos, D.; Vallee, F. *Phys. Rev. B* **2000**, *61*, 16956-16965

18) Bonn, M; Denzler, D.N.; Funk, S.; Wolf, M.; Wellershoff, S.-S.; Hohlfield, J. *Phys. Rev. B* **2000**, *61*, 1101-1105

19) Hodak, J.; Martini, I.; Hartland, G.V. *J. Phys. Chem*. **1998**, *102*, 6958-6967

20) Link, S.;Furube, A.; Mohamed, M.B.; Masuhara, H.; and El-Sayed, M.A. *J. Chem. Phys.*, (Submitted)

21) Mohamed, M.B.; Ahmadi, T.S.; Link, S.; Braun, M.; El-Sayed, M.A. (Submitted)

22) Hornyak, G.L.; Patrissi, C.J.; Martin, C.R. *J. Phys. Chem. B* **1997**, *101*, 1548-1555

23) Foss, C.A.; Hornyak, G.L.; Stockert, J.A.; Martin, C.R. *J. Phys. Chem*. **1994**, *98*, 2963-2971

24) Hulteen, J.C.; Martin, C.R. *J. Mater. Chem*. **1997**, *7*, 1075-1087

25) Kunkel, D.L.; Hornyak, G.L.; Martin, C.R. *Abstr. Pap. Amer. Chem. Soc*. **1995**, *209*

26) van der Zande, B.M.L.; Pages, L.; Hikmet, R.A.M.; van Blaaderen A. *J. Phys. Chem. B* **1999**, *103*, 5761-5767

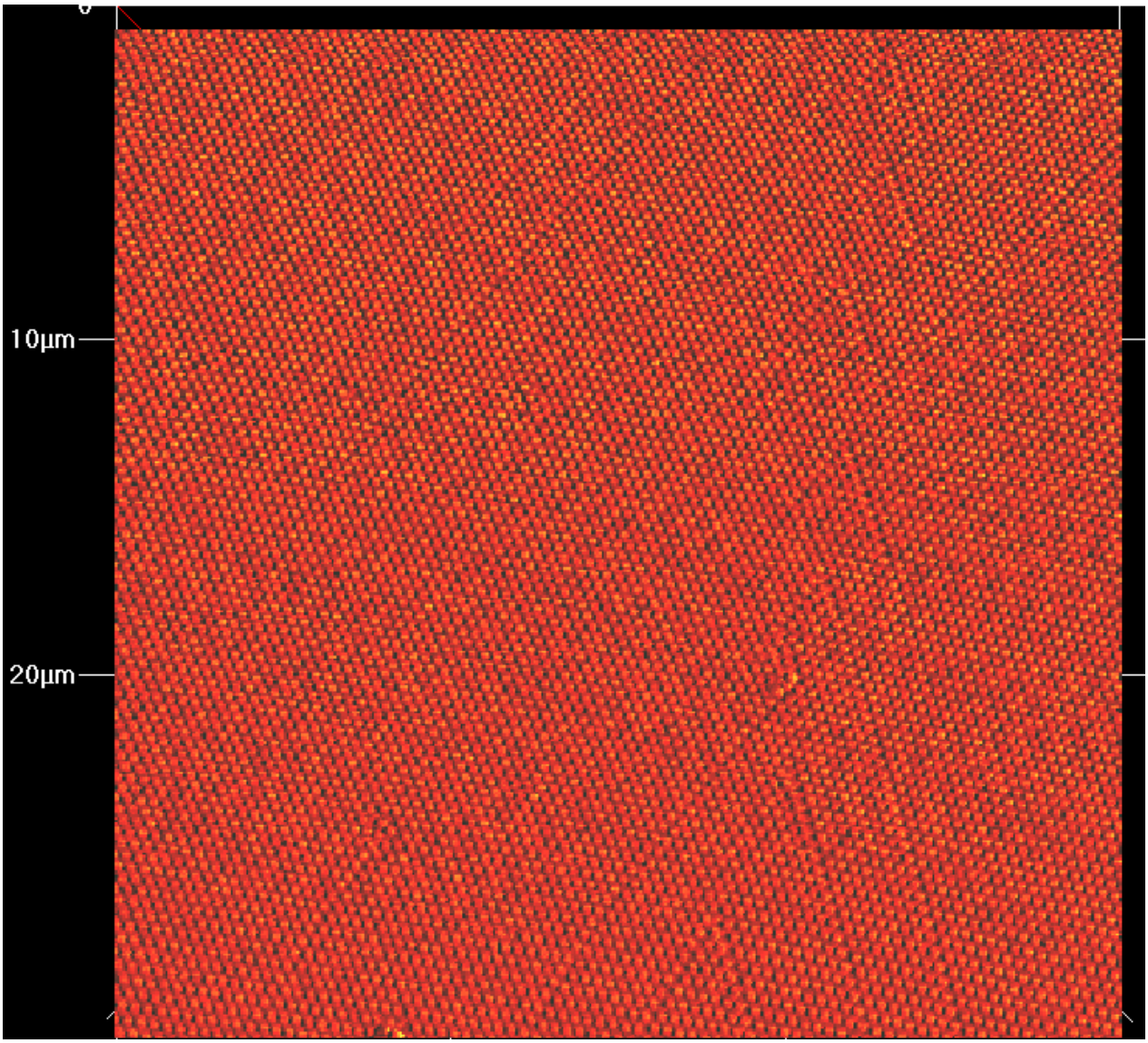

Figure 2-1 30 µm X 30 µm AFM image of polystyrene spheres on coverslip surface.

mask is one monolayer thick and can be seen to diffract light.

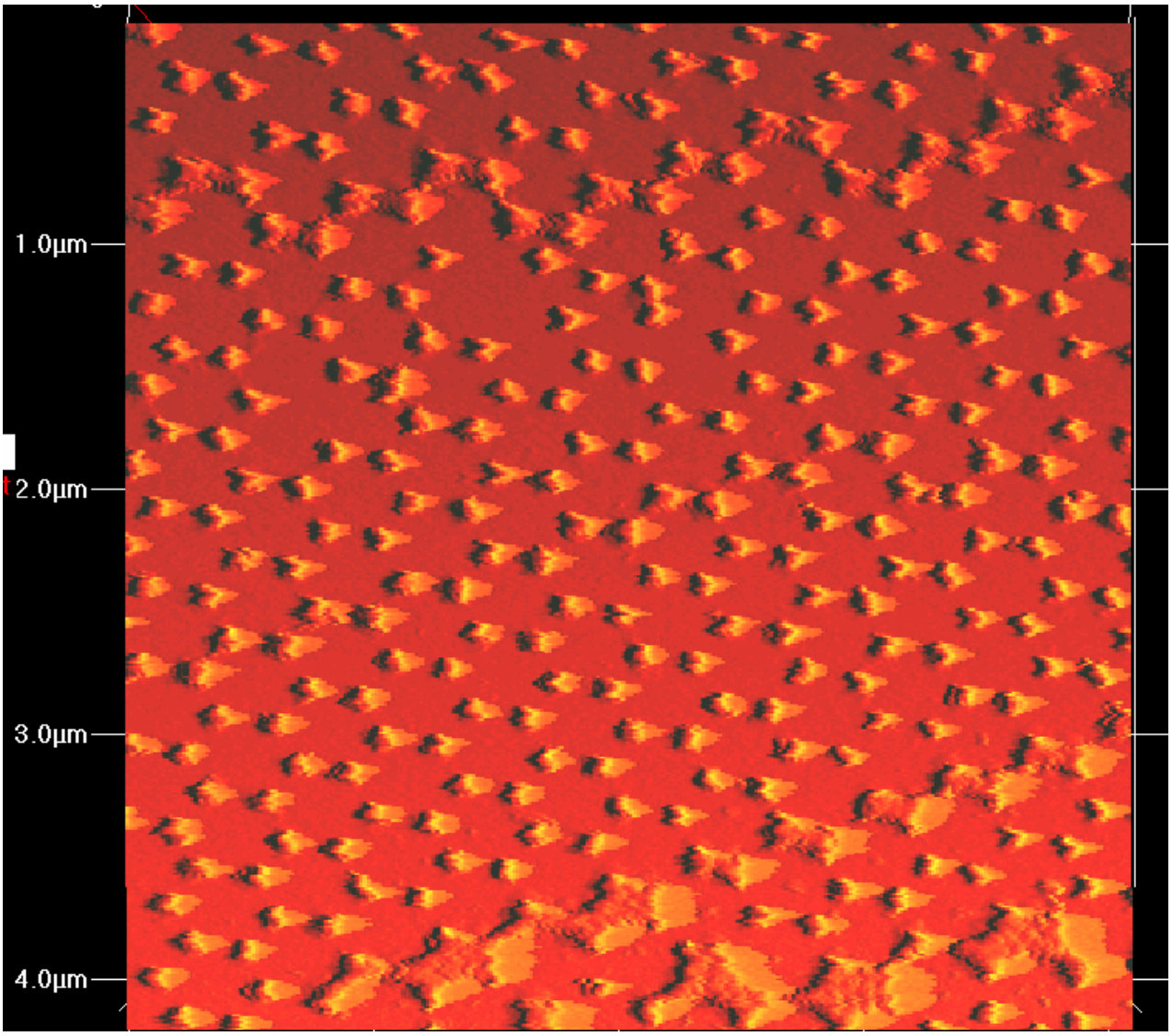

Figure 2-2 AFM image of 4µm X 4 µm area of nanolithographically prepared gold particle arrays. Particles are 50 nm in height and approximately 90 nm in width at the base.

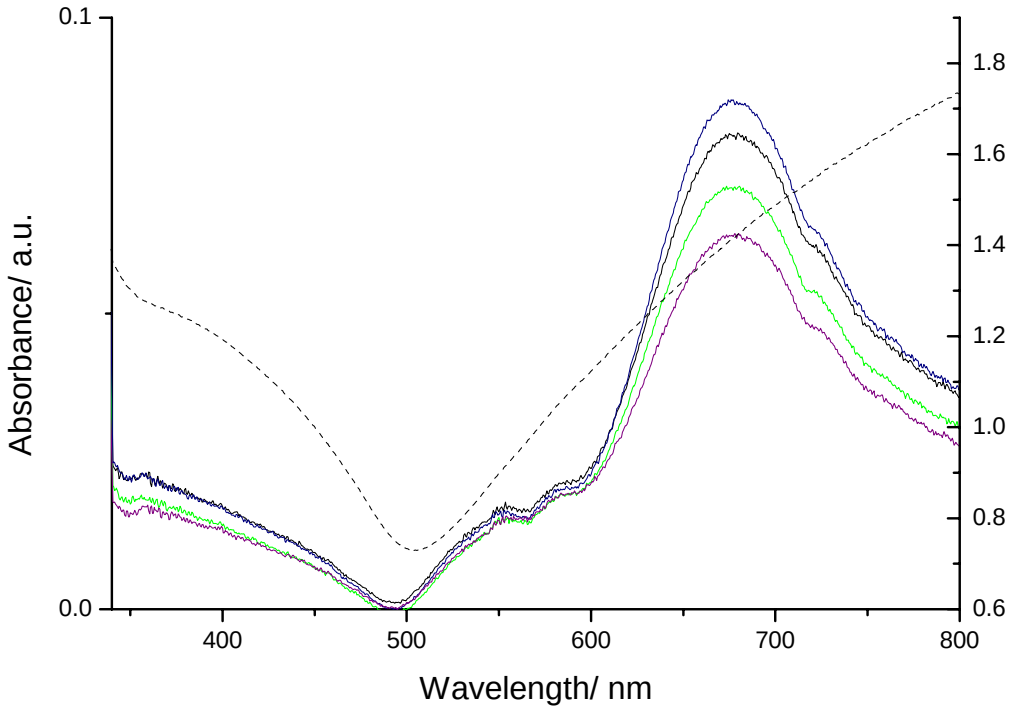

Figure 2-3- Steady-state absorption spectra of 50 nm thin film (---), and Au nanoparticle array (—) taken on glass coverslip, in transmission geometry. The different spectra of the arrays represent spectra taken at different spots on the glass substrate.

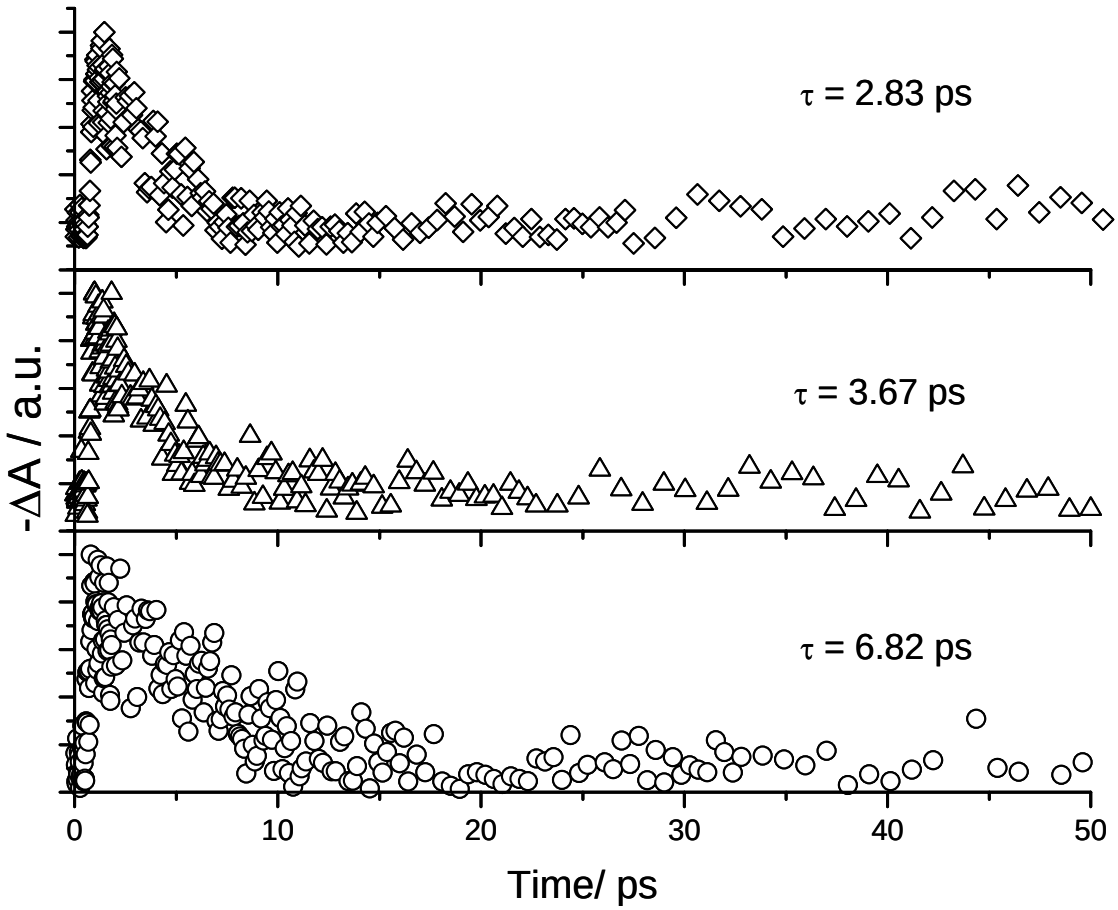

Figure 2-4- Electron cooling dynamics (followed by the bleach , -ΔA, decay) of Au nanoparticle arrays as a function of pump power. As pump power is increased, it becomes more and more difficult to effectively dissipate the heat of the particles. Note that the bleach does not completely decay to zero amplitude due to the very long component.

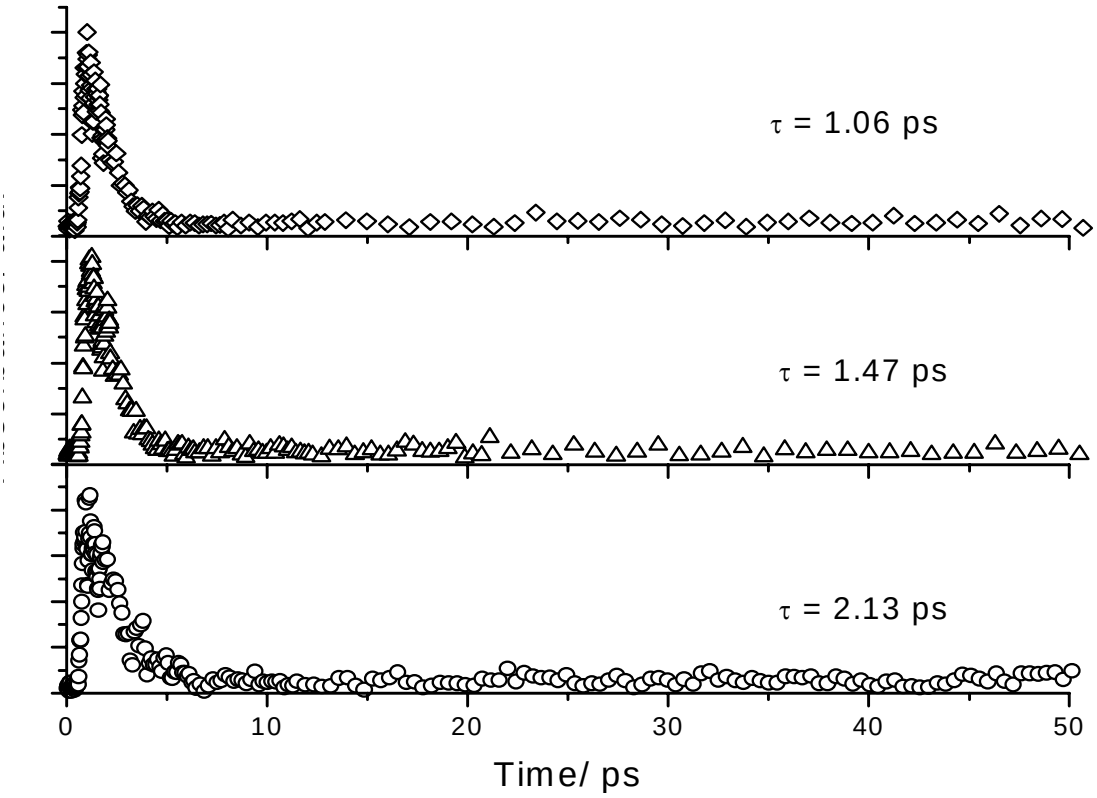

Figure 2-5 Electron cooling dynamics of 50 nm Au thin film as a function of pump power. The times are relatively short because of increased efficiency of heat transport through the film as opposed to the isolation of the array particles.

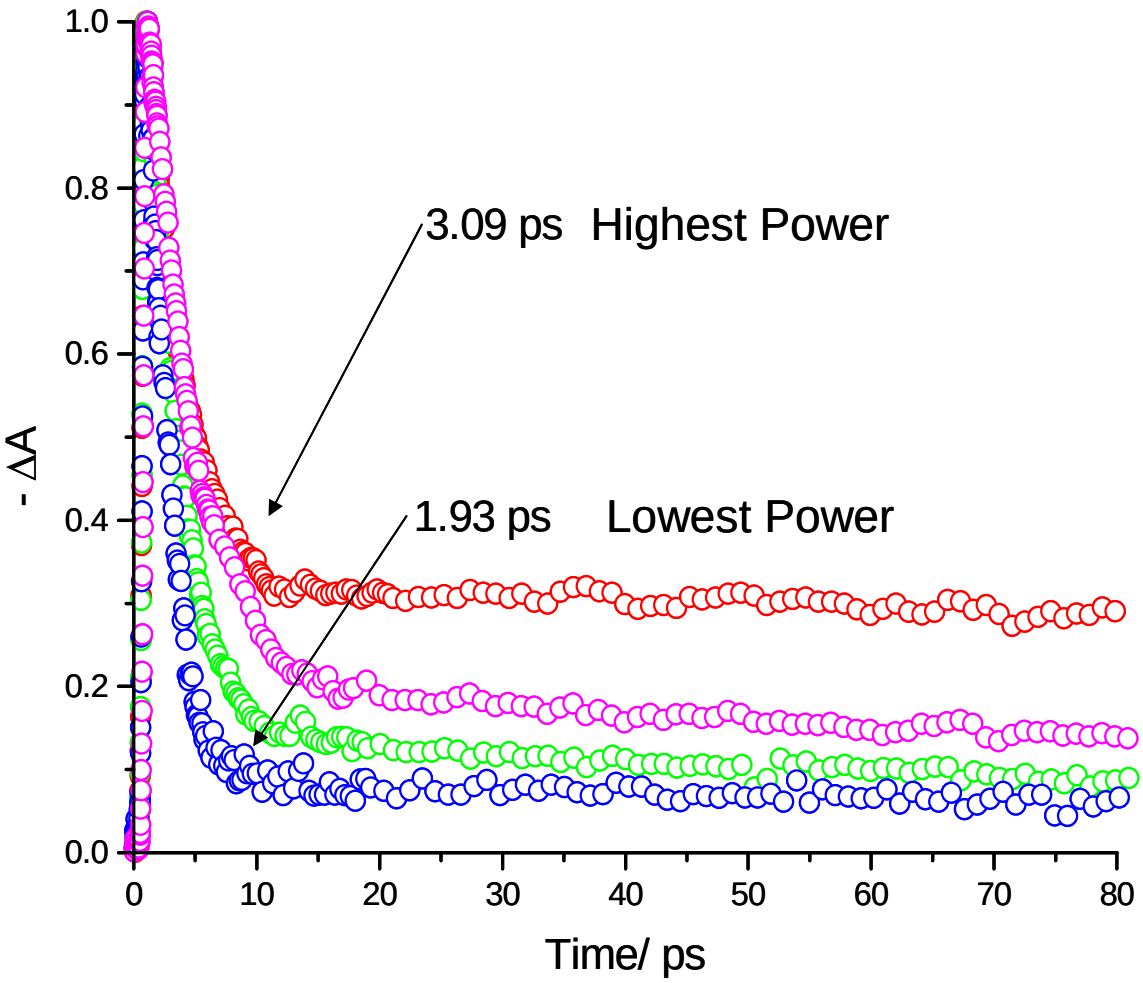

Figure 2-6 Dynamics of gold nanodots in aqueous media. Note the presence of the long time component linked to heat conduction and transfer to the media.

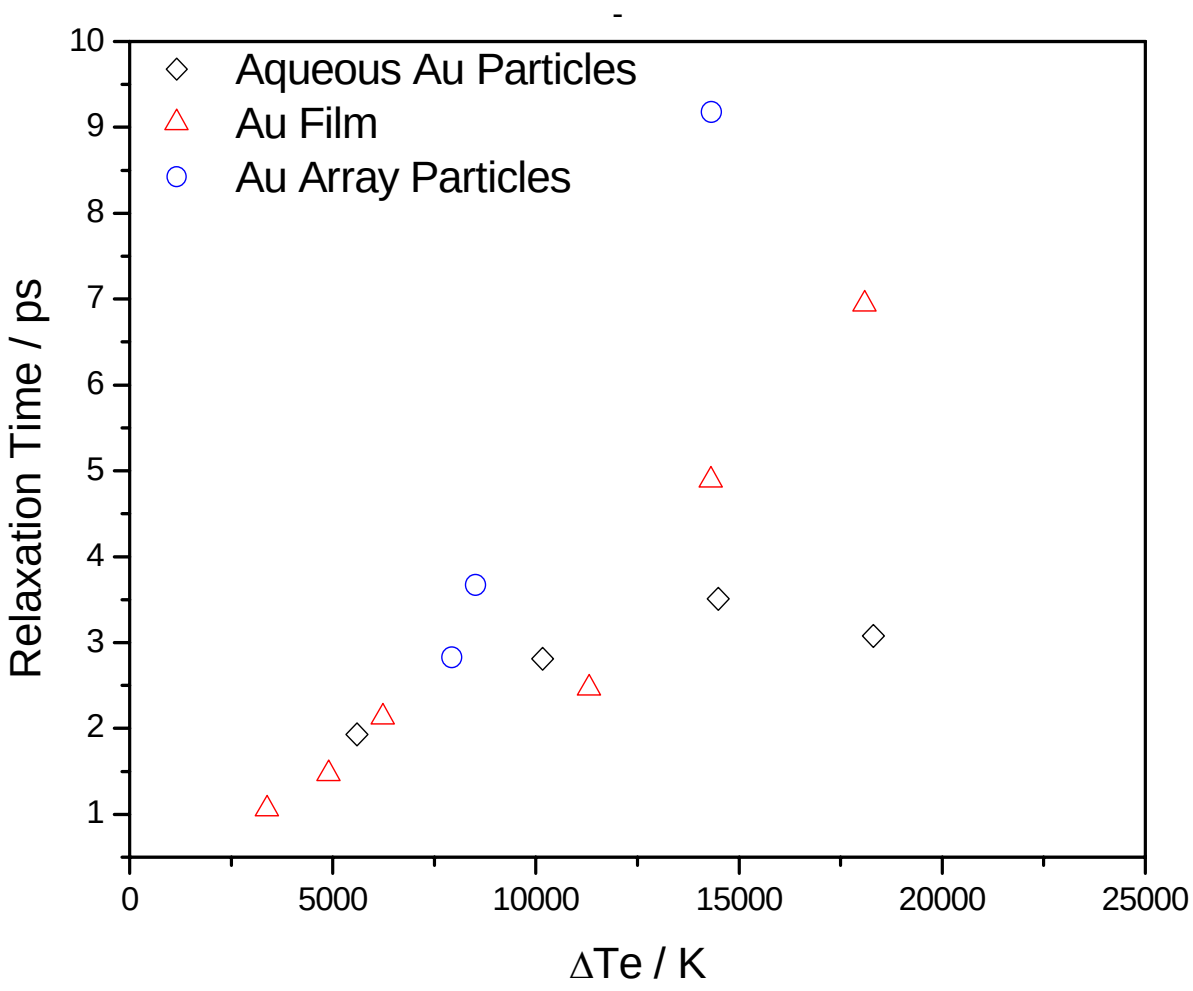

Figure 2-7 Plot of relaxation time vs electronic temperature for the arrays (○), thin-film(▲), and nanodots(◊). Note the difference in line slope which is indicative of the effect of the increased temperature on the electron-phonon relaxation time and the coupling to the surroundings.

CHAPTER III

Phonon Oscillations in Silver and Gold Nanoarrays

Abstract

Evidence for phonon oscillations in lithographically prepared gold and silver nanoarray particles. The oscillations are the result of the rapid rise in electronic temperature induced by femtosecond laser pulses. The hot electron gas couples to the acoustic surface phonons and results in an expansion and contraction of the particle lattice. This expansion and contraction changes the electron density over the particle and thus causes the surface plasmon absorption band to shift to the red and to the blue of the center wavelength respectively. The results are discussed in the context of previous work concerning the coherent vibrations seen with particles in both colloidal solution and embedded in glass matrices. Here we offer evidence for the coherent vibrations of gold and silver array particles.

Introduction

Nanoparticles have been under investigation for several years for their uses in solar energy conversion, opto-electronics, and catalytic applications[1-7]. Gold nanoparticles have demonstrated themselves to be particularly well adapted to a variety of applications. They have been used in scattering studies[8], Raman enhancement studies[9,10], and in biological marking systems[11]. The versatility of these particles in spectroscopic situations is in large part due to the plasmon band. This absorption is extremely strong and tunable with the size, shape, and composition of the particles [12,13]. Understanding of dynamics of the excited electrons in this band is tremendously important to future applications. Previous studies of the dynamics of the plasmon band of colloidal gold particles have found a fast initial electron-electron/electron-phonon (on the order of a few picoseconds) relaxation followed by a longer phonon-phonon decay[12-23]. The coupling of the electrons to the phonons of the particle lattice and to the phonon sea of the surrounding medium are integral the equilibration of the non-Fermi distribution to the initial non-thermalized state. The electron-electron and ballistic electron scattering components occur on the few femtosecond time-scale and are difficult to distinguish in the initial decay component, primarily because they are on the same scale as the laser pulse[12,13].

The excitation of the electron gas and coupling to the lattice can be described using the two temperature model (TTM)[24]. In the TTM, the heat capacities of the

lattice and the electron gas are described by a set of coupled differential equations shown below.

$$C_e(T_e)\frac{\partial T_e}{\partial t} = -g\cdot(T_e - T_l) + \nabla(\kappa'\nabla T_e) + LP(z,t) \quad (1)$$

$$C_l\frac{\partial T_l}{\partial t} = g\cdot(T_e - T_l) \quad (2)$$

where T_l is the lattice temperature, T_e is the electron temperature, κ' is the electronic thermal conductivity, g is the coupling constant, and LP(z,t) is the spatial and temporal evolution of the laser pulse.

The equations describe the heat capacity of the electron gas as small which means that the incoming pulse of energy quickly raises the electronic temperature of the electron gas creating a non-Fermi distribution. The thermalized electrons then dissipate their energy via electron scattering events, and couple to the lattice. The electron gas also couples a portion of the energy to the lattice of the particle. The larger heat capacity of the lattice compared to the electron(s) means the lattice temperature is much less than that of the initial thermalization of the electron gas [24]. The heated particle lattice can then also couple with the surrounding phonon sea. This can be affected by the composition of the particle as well as the dielectric constant of the surrounding material[25-29].

The hot electron gas couples to the surface phonon modes via the acoustic or capillary modes. As Hodak et al [14-15,30] point out, the interaction with the acoustic mode leads to a change in the volume of the particles. In their investigations of colloidal

particles they found the frequency of oscillation is linearly dependent on 1/R where R is the particle radius. In their samples the frequency varied from 1.0 cm^{-1} for 120 nm particles to 11.6 cm^{-1} for 8.3 nm particles. They find this is consistent with the spherical vibrational breathing modes of the particles and calculate an $\eta = 2.95 \pm 0.06$ from their experimental results, where η is the an eigenvalue describing the breathing mode which in this case is the lowest radial mode. Whereas $\eta = 2.93$ for the lowest radial mode, showing good agreement between the experimental and theoretical values. They also attribute, as others do, the oscillation of the plasmon band to the coherent breathing of the particle. The breathing of the particle changes the electron density and thus causes the plasmon band to shift to the blue and red side of the equilibrium absorption. The physical explanation offered is that the heating of the lattice is caused by the electron gas energy dissipation. According to Hodak, for particles smaller than 8 nm, the heating occurs more rapidly than the frequency of the breathing mode leading to an impulse[15]. When studied as a function of power, as expected the particles show a decrease in the magnitude of the oscillations when compared to the bleach signal. Most importantly the cause for the decay of the oscillations is investigated and determined to be controlled by the polydispersity of the samples.

Hartland et al have also explored the effect of using nanorods instead of nanospheres. Gold rods were synthesized electrochemically synthesized[31,32] with aspect ratios between 2 and 4.9 [33]. The transverse plasmon band was centered at 520 nm and the longitudinal band varied from 600 nm and 840 nm. In the case of the

nanorods, as is seen by Hartland and others in spheres, an initial large magnitude signal is seen followed by an oscillation overlaid on the phonon-phonon decay component. When probed on the blue and red sides of the plasmon the rod signal is out of phase, though not completely out of phase as has been seen in sphere investigations. The rods also show several oscillations in contrast to the single "impulse" oscillation seen by Perner et al.[34]. However, Hartland et al did not perform the polarization experiments that displayed the unique traces seen in the work of Perner though the experiments from the rods were followed up by a theoretical treatment. Hu [35] determined that the heating causes excitation of not only the breathing mode of the rods but also the mode that is responsible for extension of the rod itself. The calculations show that there are in fact two different contributions to the observed dynamics. The lower frequency oscillations with a period of between 40 and 120 ps for aspect ration 2 and 6 ps are the result of the extension mode. The shorter period oscillations (~11 ps) are assigned to the breathing mode. They propose that the extension mode dominate the observed dynamics because of the finite time scale that the heating occurs on.

The intense heating of the nanoparticles caused by the laser pulse poses the question: Does the heating cause particle melting or deformation? Results from our lab have shown that indeed femtosecond laser pulses can be used to photothermally reshape gold nanorods. Hartland [30]et al have investigated the effects of femtosecond heating on the symmetric breathing mode of colloidal gold nanoparticles. They found that the period of the oscillation is dependent on the pump power , increasing as the power is increased

up to the melting point of gold. The particles are thought to not completely melt but to only partially melt and form a liquid shell on the particles. For example, the period of 50 nm particles is observed to increase from ~16.6 ps to ~17.5 ps as the laser power is increased from 0 to 1.5 μJ [30]. The partially molten nature of the particle and thus the different speed of sound in the solid and liquid portions of the particles, which varies with pump power, leads to the damping of the oscillations.

Hodak et al[14] also investigated the dynamics of core-shell particles composed of gold and lead. Gold was used as the core with variable thicknesses of lead as the shell. The gold core was kept a constant 47 nm and the thickness of the lead varied. It was found that the period of the oscillation increased as the number of atomic layers of lead increased. The plasmon of the particle was primarily gold in character but was shifted because of the lead and is center around 500 nm with the lead present. They propose that the two layers act together during the oscillation when the lead layer is thin, but as the layer thickness increases the lead acts as a restraining force, like stiffening the spring in an oscillator, to retard the oscillations. They present a qualitative picture of the data.

Voisin et al [19,36,22,23] focused on silver nanoparticles and investigated the coherent vibrational dynamics using femtosecond pump probe spectroscopy. The oscillation dynamics of the silver particles follow the same theoretical underpinnings as the gold oscillations. The heating of the electron gas transfers energy to the lattice which then oscillates in response to the cooling. However, the silver particles were grown and investigate in a glass matrix and prepared via heat treatment. The particles oscillate just

as in the colloidal case , however the oscillations decay much faster (<10ps). Other work by Voisin[22] has investigated the effect of the environment on the oscillation. Using essentially the same experiment as before, they were able to determine that the interaction between the particles and matrix drastically effect the relaxation of the oscillations. This is of particular importance when applied to the array particles since they are unique in the interaction with both air and the glass substrate. This substrate may act by damping the oscillations just as the lead overlayers used by Hodak do.

When the electron gas is thermalized by the laser pulse, the impulse of the heat imparted to the lattice causes an expansion of the lattice coinciding with the lattice breathing mode. The expansion and contraction of the lattice changes the electron density of the particle and thus causes a shift in the plasmon band. The plasmon shifts to the blue and red of the equilibrium value with the oscillation of the particle. Thus if the dynamics of the particle are measured on the blue and red side of the equilibrium plasmon value, the oscillations will be π out of phase with each other. This oscillatory behavior has been studied for both gold and silver particles in colloidal solution and embedded in a glass matrix. In order to be able to detect such phenomenon the particle size dispersity must be extremely small. Otherwise the oscillatory behavior is averaged out by the different breathing mode periods of the different size particles. In order to achieve the highly monodisperse particle solutions necessary for work in colloidal solution, Hodak et al [14-16,30] , have used gamma irradiation to synthesize the nanoparticle. The monodispersity of the solution makes the lattice oscillations easier to detect since almost all of the

particles will share the same oscillation frequency. Since the observation of this behavior is dependent on the size distribution of the sample, the nanosphere lithography method developed by Van Duyne et al.[36-38] offers an effective means to produce highly monodisperse samples. The unique geometry of the particles, truncated octahedral in contrast to the spherical shape of the previously studied particles, also provides an interesting comparison to that of the previously studied particles. The one disadvantage is the fact that the method of preparation can only produce one monolayer. Thus the density of these particles is too small to get strong signal. Here we present some evidence for the presence of these oscillations in the dynamics of the silver and gold nanoparticle arrays.

Experimental

Regular arrays of silver nanoparticles were prepared using nanosphere lithography members of the VanDuyne group.[36-38] In short, an ordered layer of polystyrene nanospheres (Polysciences) was prepared on a glass coverslip (Fisher Scientific. The coverslips were then mounted in a Denton DV-502A Thermal Evaporator to deposit gold in the spaces between the spheres. This gives rise to the triangular shape of the particles in the arrays. The height of the particles is determined by the mass thickness of material deposited and can thus be easily controlled. The thickness of the evaporated gold was monitored by a quartz crystal thickness monitor (Inficon). After evaporation the mask was removed from the substrate by sonicating for 30s in methylene chloride. The arrays were then allowed to dry overnight to allow any residual liquid to

evaporate. The size of the particles was then determined using a Quesant Q-SCOPE atomic force microscope (AFM). The average size of the particles was calculated to be approximately 90 nm wide using the geometric relations determined by Van Duyne *et al* [36] and 50 nm in height when 356 nm polystyrene spheres were used as the mask material. The AFM images are raw images uncorrected for tip convolution effects, and thus the particles appear larger than the calculated value. After removal of the nanosphere mask hexagonal arrays of nanoparticles were present on the coverslip, but did have some defect sites. The 50 nm gold films were prepared by simply evaporating gold onto clean coverslips. The absorption spectra of the arrays and the films were then recorded using a Shimadzu UV-3101-PC spectrophotometer in standard transmission geometry.

The dynamics of the arrays and the films were studied by using femtosecond pump-probe spectroscopy. The setup consisted of regeneratively amplified Ti:Sapphire laser system (Clark-MXR CPA 1000) pumped by the doubled frequency of a Nd:Vanadate laser (Coherent Verdi). The system repition rate was 1 kHz and produced 100 fs (FWHM) duration pulses with energy of 1 mJ centered at 800 nm. A portion of the output beam was split off and focused on a 1 mm thick sapphire plate to generate a white light continuum for use as a probe beam. The remainder of the beam was then doubled by second harmonic generation to produce 400nm light for use as a pump beam.

The pump beam was then sent to a computer controlled variable delay line and then passed through a chopper to modulate the beam at 500 Hz with the same phase. It was then focused onto the sample. The continuum beam was split into probe and reference beams. The probe beam was focused onto the sample and overlapped with the pump beam, and then collected and focused onto a fiber optic cable coupled to a monochromator. The reference beam was focused onto a fiber optic cable that was coupled to the same monochromator. The kinetics measurements were made by monitoring the probe and reference beam signals using two photodiodes at the exit slit of the monochromator. The voltage from the photodiodes was then amplified and fed into a sample and hold system.

Results & Discussion

The absorption spectrum of the 90 nm silver nanoparticles is seen in Figure 1. This spectrum is consistent with spectra of similar particles produced by Van Duyne et al.[36-38] with the center of the plasmon band at 650 nm. Figure 2 shows the dynamics of the silver arrays at different powers. The electron-phonon component decays in 40 ps with a long-lived phonon-phonon component that lasts for >200 ps. Work by Hartland [14-16] has shown that the initial fast absorption is caused by the rapid thermalization of the electron gas causing the absorption. The signal recovers and becomes a bleach which in our setup registers as a change in the phase read by the lock-in amplifier. The oscillations are then overlaid on the phonon-phonon decay curve component. The work

of Vallee et al[17-23] with silver particles embedded in a glass matrix is performed using sample composites containing particles from 2.1 to 15.3 nm radius. This is substantially smaller than the 90 nm diameter particles we use. The differences in particle size will lead to a difference in the frequency of the acoustic breathing mode. Also , the homogeneous damping of the particles we are studying was found to be much stronger than in the case of the colloidal samples. They found that this was due to the larger acoustic mismatch of the particle and the surroundings as well as the increased contribution from the inhomogeneous damping in contrast to the colloidal particles. In contrast, the array samples offer a different environment from either the colloidal case or the composite case. The array particles are inhomogeneously damped since they are attached on one face to the substrate while being surrounded on the other sides by the air atmosphere. Other work by Vallee [22] has found that the simple harmonic description of the acoustic breathing mode of the particles is practically environment independent when the particles are treated as simple elastic spheres embedded in an elastic medium. The same work showed that though this is true, the damping of the oscillation is dependent on the environment particularly the interface between the particle and the medium. This raises the question of the effects of the unique nature of the array particle environment on the damping and oscillatory behavior of the particles.

Perner et al.[34] have investigated the subject of oscillations in particles of non-spherical particles. They studied the oscillations of ellipsoidal silver particles formed by deforming spherical particles grown in a glass matrix. The precursor silver particles had a

mean diameter of 60 nm and the resulting ellipsoidal particles had a diameter of 40 nm and length of 100 nm along the short and long axes respectively. The short and long axis plasmons were probed using parallel and perpendicularly polarized light. The results showed a difference in the periodic oscillation depending on which axis was probed. In the case of the short axis, the oscillation was extremely short, on the order of 22 ps, while the long axis oscillation was found to be considerably longer at 52 ps. The length of the long axis of the particle, and the asymmetry makes it much more comparable to the silver array particles, which are 50 nm high and 90 nm base width. Also of note when comparing the array dynamics to those of the ellipsoidal particles is the behavior of the traces in the early time scale and the quick damping seen when the long axis is excited and when the short axis is excited. In either case after the absorption spike, which is also seen by other groups, the oscillations are very short lived and do not persist to an appreciable extent much beyond one period of the oscillation. However in the cases of particles in colloidal solution, several oscillations are clearly visible in the dynamics. This can be attributed to the previously mentioned differences in damping between matrix embedded particles and those in solution due to the differences in the particle-matrix environment. Perner et al fit their results using both an expression for the change in particle length due to expansion/contraction forces caused by the insertion/dissipation of energy in the lattice, [34,39]

$$\frac{d^2}{dt^2}\Delta x + 2\rho\frac{d}{dt}\Delta x + \omega_0^2\Delta x = \frac{A\sigma}{m} \qquad (3)$$

where ρ is the damping due to the matrix, A is the surface area of the particle, m is the mass of the particle, ω_0 is the vibrational frequency along a particular particle axis, and σ is the stress of the particle, and an expression for stress on the lattice due to this behavior. The foundations of the stress contribution equation are found in the lattice anharmonicity and the thermal effects of the free electrons and give equation,[24,39]

$$\sigma_{L,e} = -\gamma_{L,e} \int_{T_R}^{T_{L,e}} C_{L,e} dT_{L,e} \tag{4}$$

where T_L is the lattice temperature, T_e is the temperature of the electron gas, C_L is the heat capacity of the of the lattice, and C_e is the heat capacity of the electron gas. Thus the conclusion of Perner is similar to that of Valle[17-23] in that the coherent heat impulse from the excitation of the lattice, leads to a coherent expansion and contraction of the lattice. However, in the cases of Valle[17-23] and Hartland[14-16], the spherical symmetry of the particles leads to a long lived oscillatory component in the decay. The array particles studied here do not show such a pronounced oscillation at long times because of the anharmonicity introduced by both the unique geometry and particle-environment interface present. As shown in Figure 2, the dynamics of the particle are similar in form to those obtained by Perner et al. The initial decay is that of the absorption induce by the fast thermalization of the electron gas. As stated previously, our experimental setup does not register this as a negative signal. This is followed by the phonon oscillation that dies out within 50 – 60 ps. This is consistent with the damping of the decay seen in the ellipsoidal particles. The same damping appears in Figure 3

showing the gold array particles. The similarity of the decays is consistent with the theory that the oscillation of the particle itself is independent of the medium considered as elastic spheres. In Figure 2 a) – b) and Figure 3 a) – c) show the power dependence of the silver and gold particles respectively. The gold oscillation is much less pronounced and requires a greater pump power to be used. The fast relaxation dynamics of gold have been explored by many groups, and it has been shown that the electron-phonon relaxation is faster than that of silver. In such a case it might be difficult to transfer the energy to cause the coherent vibration seen much more clearly in silver.

In conclusion, we present evidence of coherent acoustic breathing modes in gold and silver array nanoparticles. We have found that unlike spherical particles, the truncated tetrahedral array particles do not show a persistent oscillation on the long time scale. The oscillation is possibly damped by the anharmonicity caused by the attachment to the substrate and geometry of the particles. The similarity of the oscillation periods of the gold and silver particles is most likely due to the similarity of the particle-environment interface which dominates the damping.

Acknowledgements

The authors would like to thank the NSF for funding this research.

Reference

1) Schmid, G. *Clusters & Colloids: From Theory to Application*; VCH: Weinheim, 1994.

2) Kamat, P. V.; Meisel, D. *Studies in Surface Science and Catalysis, Vol. 103, Semiconductor Nanoclusters - Physical, Chemical, and Catalytic Aspects*; Elsevier: Amsterdam, 1997.

3) Edelstein, A. S.; Cammarata, R. C. *Nanoparticles: Synthesis, Properties and Applications*; Institute of Physics Publishing: Bristol, 1996.

4) Graetzel M. In *Electrochemistry in Colloids and Dispersions*; Mackay, R. A.; Texter, J., Eds.; VCH: Weinheim, 1992.

5) Ahmadi, T. S.; Wang, Z. L.; Green, T. C.; El-Sayed, M. A. *Science* **1996**, *272*, 1924.

6) Henglein, A. *J. Phys. Chem.* **1993**, *97*, 8457

7) Mulvaney, P. *Langmuir* **1996**, *12*, 788.

8) Yguerabide, J.; Yguerabide, E *Anal. Biochem*. **1998**, *262*, 157

9) Nikoobakht, B.; El-Sayed, M. A. *Chem.of Mat*. **2003**, *15*, 1957

10) Nikoobakht, B.; Wang, J.; El-Sayed, M. A. Chem. Phys. Lett. **2002**, *366*, 17

11) Storhoff, J. J.; Mirkin, C. A. *Chem. Rev.* **1999**, *99*, 1849.

12) Link, S.; El-Sayed, M. A. *International Reviews in Physical Chemistry* **2000**, *19*, 409

13) Link, S.; El-Sayed, M. A. *J. Phys. Chem. B* **1999**,*103*, 8410

14) Hodak, J. K.; Henglein, A.; Hartland, G. V. *J. Phys. Chem. B.* **2000**, *104*, 5053

15) Hodak, J. K.; Henglein, A.; Hartland, G. V. *J. Phys. Chem. B.* **2000**, *104*, 9954.

16) Hodak, J. K.; Martini, I.; Hartland, G. V. *J. Phys. Chem. B* **1998**, *102*, 6958.

17) Sun, C.-K.; Vallee, F.; Acioli, L. H.; Ippen, E. P. Fujimoto, J. G. *Phys. Rev. B* **1993**, *48*, 12365

18) Sun, C.-K.; Vallee, F.; Acioli, L. H.; Ippen, E. P.; Fujimoto, J. G. *Phys. Rev. B* **1994**, *50*, 15337

19) Del Fatti, N.; Voisin, C.; Christofilos, D.; Vallee, F.; Flyzantis, C.; *J. Phys. Chem.* A **2000**, *104*, 4321

20) Voisin, C.; Del Fatti, N.; Christofilos, D.; Vallee, F. *J. Phys. Chem. B* **2001**, *105*, 2264

21) Portales, H.; Saviot, L.; Duval, E.; Fujii, M.; Hayashi, S.; Del Fatti, N.; Vallee, F.; *J. Chem. Phys* **2001**, *115*, 3444

22) Voisin, C.; Christofilos, D.; Del Fatti, N.; Vallee, F. *Physica B* **2002**, *316*, 89.

23) Voisin, C.; Christofilos, D.; Del Fatti, N.; Vallee, F. *App. Surf. Sci.* **2000** *164*, 131

24) Anisimov, L.; Kapeliovich, B. L.; Perel'man, T. L. *Sov. Phys. JETP* **1975**, *39*, 375.

25) Maxwell-Garnett, J. C. *Philos. Trans. R. Soc. London* **1904**, *203*, 385.

26) Kerker, M. *The Scattering of Light and Other Electromagnetic Radiation*; Academic Press: New York, 1969.

27) Bohren, C. F.; Huffman, D. R. *Absorption and Scattering of Light by Small Particles*; Wiley: New York, 1983.

28) Roberti, T. W.; Smith, B. A.; Zhang, J. Z. *J. Chem. Phys.* **1995**, *102*, 3860.

29) Ashcroft, N. W.; Mermin, N. D. *Solid State Physics*; Saunders College: Philadelphia, 1976.

30) Hartland, G.; Hu, M.; Sader, J. *J. Phys. Chem. B* **2003**, *107*, 7472

31) Yu, Y.; Chang, S.; Lee, C.; Wang, C. *J. Phys. Chem B* **1997**, *101*, 6661

32) Chang, S.; Shih, C.; Chen, C.; Lai, W.; Wang, C. *Langmuir* **1999**, *15*, 701

33) Hartland, G.; Hu, M.; Wilson, O.; Mulvaney, P.; Sader, J. *J. Phys. Chem* **2002**, *106*, 743

34) Perner, M.; Gresillon, S.; Marz, J.; von Plesson, G.; Feldmann, J.; Porstendorfer, J.; Berg, K.-J.; Berg, G *Phys. Rev. Lett.* **2000**, *85*, 792.

35) Hu, M.; Wang, X.; Hartland, G.; Mulvaney, P.; Juste, J.; Sader, J. *J. Amer. Chem. Soc*. **2003**, *125*, 14925

36) Hulteen, J.C.; Treichel, D.A.; Smith, M.T.; Duval, M.L.; Jensen, T.R.; Van Duyne, R.P. *J. Phys. Chem. B* **1999**, *103*, 3854-3863.

37) Hulteen, J.C.;Van Duyne, R.P. *J. Vac. Sci. Technol. A.* **1995**, *13* **,** 1553-1558.

38) Jensen, T.R.; Schatz, G.C.; Van Duyne, R.P. *J. Phys Chem. B* **1999**, *103*, 2394-2401.

39) Tas, G.; Maris, H.J. *Phys. Rev. B* **1994**, *49*, 15046

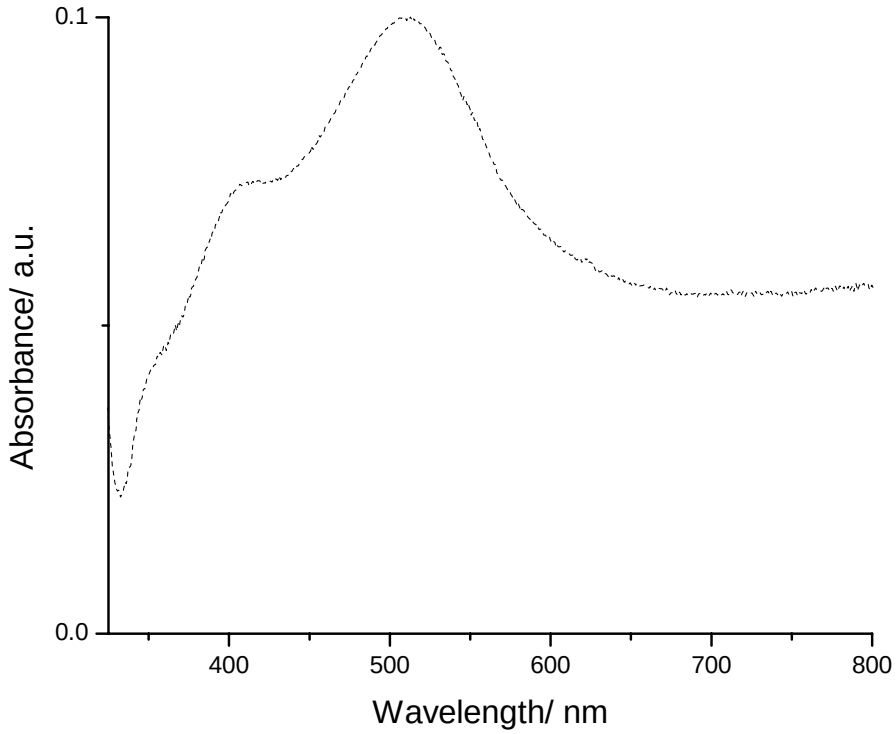

Figure 3-1 UV/Vis absorption spectrum of silver nanoparticle arrays prepared via nanosphere lithography. Plasmon is center around 57 nm

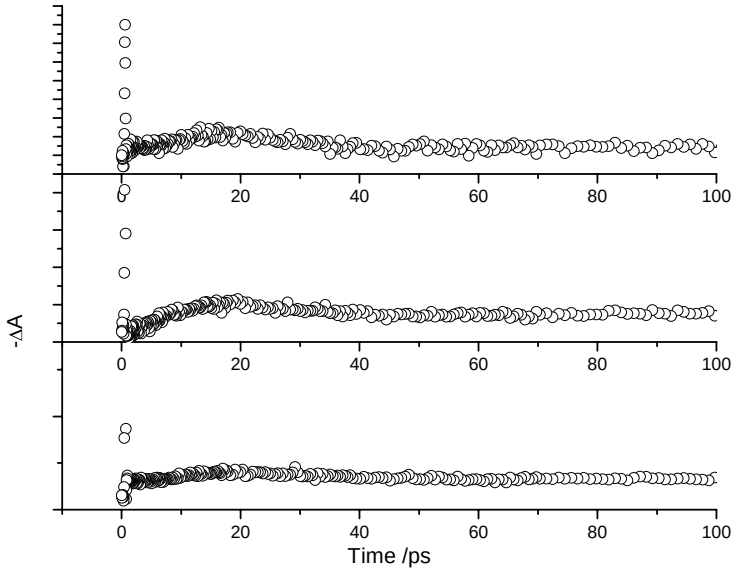

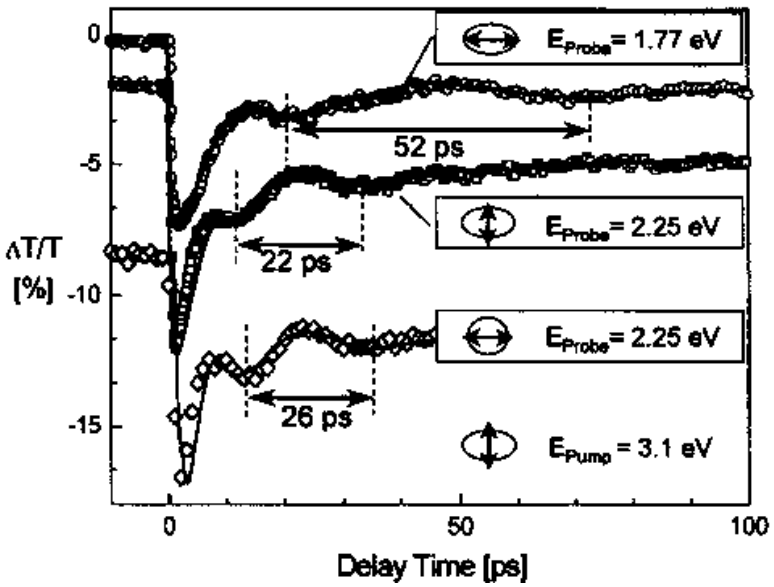

Figure 3-2 Decay dynamics of silver arrays (a)pumped at 400nm and probed at 650 nm. Oscillation can be seen to decay in ~50 ps and intensity varies with power. Oscillations observed by Perner et al using silver nanorods embedded in a glass matrix (b). (Perner, M et al. *Phys. Rev. Lett.* **2000**, *85*, 792.)

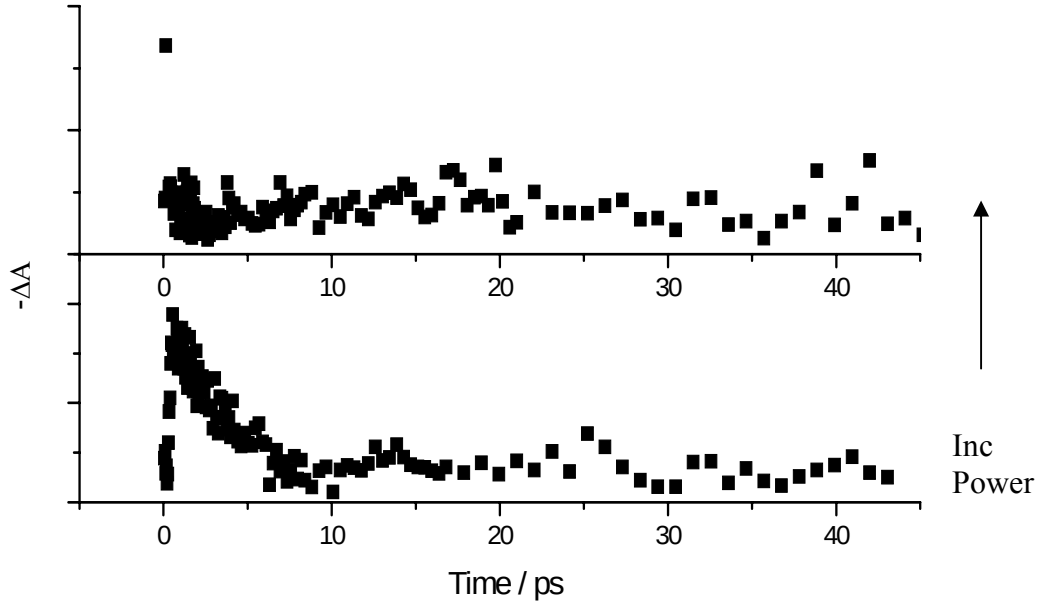

Figure 3-3 Decay dynamics of gold arrays pumped at 400nm and probed at 575 nm. Oscillation can be seen to decay in <50 ps and intensity varies with power. Decay of oscillation is much faster than in silver due to the inherently faster cooling dynamics of gold particles

CHAPTER IV

Medium Effect on the Electron Cooling Dynamics in Gold Nanorods and Truncated Tetrahedra

Abstract

The effect of the medium on the plasmon resonance of metallic nanoparticles has long been known. We present a study of the medium effects on gold nanorods and truncated gold tetrahedra. The increase on electron-phonon relaxation time, and rise of the phonon-phonon component of the gold nanorods is presented. The effects of water, toluene and pyridine on the dynamics of nanlithographcally prepared gold nanoparticle arrays are also studied. It is found that the addition of solvent to the nanoparticle array system quenches the excited particles resulting in a shorter electron-phonon coupling time and the emergence of a phonon-phonon component not seen in the dry samples.

The binding of gold nanoparticles to biological systems and its potential use in diagnostics[1] as well as medical treatment is becoming an active field of nanomaterial research. For example, recently Hamad-Schifferli et al.[2] showed that inductive coupling of a radio-frequency magnetic field to a metal nanoparticle, which is covalently linked to DNA increases the local temperature of the bound DNA, thereby inducing denaturation while leaving the surrounding molecules relatively unaffected. They showed high spatial localization of the denaturation, which might allow in the future controlling portions of proteins or nucleic acids while the rest of the molecule and neighboring species remain relatively unaffected. Due to the strong visible absorption of the surface plasmon absorption of gold nanoparticles and its convenient wavelength, laser photothermal treatment is also expected to be of wide future application. In material applications, laser pulses have shown to be useful in shaping noble metal nanoparticles[3-5] and narrow its size distribution[6]. For these reasons it is important to understand the mechanisms involved in the transfer of the excitation energy from the nanoparticle into the environment. Here we report a study on the electron relaxation dynamics and the thermal cooling of colloidal gold nanorods and truncated tetrahedra in air as well as in water after excitation with femtosecond laser pulses. It is found that that the local energy exchange with the surrounding medium for gold nanoparticles in water occurs on the few picosecond time scale comparable with the electron-phonon relaxation while a slow heat

dissipation by the water ensures that the particles remain heated for hundreds of picoseconds.

Gold, and more generally speaking noble metal nanoparticles larger than a few nanometers, show a strong absorption band in the visible, which is due to the coherent excitation of the conduction band ("free") electrons. This absorption band is known as the surface plasmon resonance and depends on the particle size and even more importantly on the particle shape[3,7]. For nearly spherical particles only one resonance located around 520 nm is seen for gold nanoparticles. For gold nanorods this plasmon absorption splits into two bands, known as the transverse and longitudinal plasmon resonances, which are polarized perpendicular and parallel to the long axis of the rod, respectively. While the transverse mode is relatively insensitive to the nanorod dimensions defined usually by the aspect ratio (length divided by the width), the longitudinal plasmon absorption band redshifts with increasing the aspect ratio[3,7]. Figure 1a (top spectrum, dashed line) shows the absorption spectrum of gold nanorods in aqueous solution having an aspect ratio of 2.9 (length: 35 nm; width: 12 nm).

While the absorption spectrum of nanorods is a rather old problem and had long been solved by Gans[8], the development of preparation methods allowing size selective synthesis of many particle shapes and/or the separation of different particle shapes after the synthesis have allowed the study of the optical properties of other particle shapes recently. Examples of other nonspherical or noncylindrical shapes having also very different absorption spectra are silver nanoprism[9,10] and truncated tetrahedra[11]. The

latter are produced by a nanospehere lithography method developed by Van Duyne and coworkers[12,13]. In this method an ordered array of polystyrene spheres is formed on a glass substrate. A metal vapor is then deposited in the spaces between the polystyrene spheres by thermal evaporation of the metal. The size and shape of the structures can be controlled by the size of the polystyrene spheres, the deposition time[12] as well as the tilt angle[13] between the substrate normal and the deposition beam. In figure 1a an absorption spectrum of a gold particle array consisting of truncated tetrahedra is shown (dotted line). These particles, produced with a mask formed from 356 nm polystyrene spheres, are 90 nm wide at their base and 50 nm high as shown by the AFM image in figure 1b. The absorption band with a maximum around 650 nm is attributed to the plasmon resonance of the particles and was modeled accurately by Schatz and coworkers[11] taking into account the effects of a glass substrate and also the presence of different solvents covering the particle array. In the case of the ordered arrays, the plasmon band observed in the absorption spectrum will be the one polarized perpendicular to the incident light and hence parallel to the substrate surface. In solution, all orientations of the particles are averaged and therefore the two plasmon resonances for the gold nanorods are seen. Figure 1a further shows the effect of the surrounding medium on the plasmon resonance. The plasmon absorption is very sensitive to the dielectric constant of the surrounding medium as it redshifts with increasing its value[7,11]. This is seen when the gold particle arrays are immersed into a thin cell filled with water in figure 1a (solid line).

The electron dynamics in metallic nanoparticles have been followed in numerous studies[3,7,14-16]. In all cases a femtosecond laser pulse excites the electrons in the metal particles which leads to a strong increase in the sample transmission at the maximum of the plasmon resonance for gold nanoparticles. In the difference spectrum (excited sample minus unexcited), a strong bleach feature is therefore observed. Since the bleach is related to the increase in temperature of the electron gas, the bleach recovery then monitors the cooling dynamics of the electrons as they couple to the lattice vibrations. It was found that the electron-phonon coupling constant is independent of particle size or shape for gold nanoparticles[7,15] larger than 5 nm.

The electron-phonon coupling constant is obtained in the low excitation limit, where the rise in the electron temperature is small (100 K) and the rise in the lattice temperature is almost negligible[14]. The plasmon band bleach recovery then follows a monoexponetial behavior with a subpicosecond time constant. As the excitation power and therefore the electron temperature are increased the relaxation times become longer (few picoseconds) which is due to the temperature dependent electronic heat capacity as modeled accurately for thin gold films within the two-temperature model[7,14,15]. While in thin films the heat transport and thermal equilibration can also occur via electronic heat diffusion, this is no longer possible in nanometer confined particles and heat exchange with the surrounding medium has to be considered as well.

Figure 2a shows the bleach recovery dynamics of gold nanorods having an aspect ratio of 2.9 in aqueous solution for different pump intensities. The pump wavelength in

these experiments was set to 400 nm while the probe was 700 nm at the maximum of the longitudinal plasmon absorption. At very low pump intensities the signal decays monoexponetial with a time constant of about 1 ps, corresponding to the electron-phonon relaxation time $\tau_{e\text{-}ph}$. As the pump intensity increases the electron-phonon relaxation time becomes longer and a second decay component is seen. The long decay component could be fit with a time constant between 150 – 200 ps for all excitation powers and was previously ascribed to phonon-phonon relaxation[7,15] between the metal nanoparticles and the surrounding medium. Figure 2b shows a plot of the electron-phonon relaxation times against pump power summarizing the trend from figure 2a. Also shown is the amplitude ratio between the fast and slow decay components. As the particles are heated to higher temperatures the long decay component becomes more important.

While most studies carried out so far have focused on the intrinsic electron-phonon coupling in the metallic nanoparticles, the question of energy exchange with the surrounding medium has only been addressed recently[17-21]. This is a problem directly related to the photothermal reshaping of metallic nanoparticles with laser light. It has already been shown that gold nanorods can be transformed into spherical particles by exposure to laser light through a thermal reshaping (melting) process[3-6]. By using pulsed laser light with different pulse durations[5], it was found that the time scales of energy loss by the nanorod should not be faster than the rate of heating in order to induce such a photothermal reshaping process. The rate of cooling of the metallic nanoparticles is

influenced by the strength of the coupling to and the thermal properties of their environment.

In a recent study by Hu et al.[17], it was shown that the phonon-phonon relaxation time is proportional to the square of the particle radius for spherical gold nanoparticles in aqueous solution. The effect of changing the surrounding medium was studied by El-Sayed and coworkers[18,19] who found that both of the two decay components of the plasmon bleach recovery (electron-phonon and phonon-phonon) are influenced by the surrounding medium when the medium is changed from an organic solution to $MgSO_4$ powder[18] or from aqueous solution to a series of polymer gels[19] (hydrogel and different organic gels). The recovery times become slower when the thermal conductivity of the medium is decreased (as for hydrogel compared to the organic gels) or when the thermal contact between the particles and the matrix is decreased (as in the $MgSO_4$ powder system). These results strongly suggest that the thermal properties of the surrounding medium and the surface properties of the metallic nanoparticles play important roles in the cooling dynamics of the hot carriers in metallic nanoparticles. Similar results have been obtained by Bigot et al.[20] who measured the relaxation dynamics of 6.5 nm silver nanoparticles embedded in two different types of transparent glasses (alumina and glass). An increase of the electron-phonon relaxation time from 0.77 to 1.4 ps was found when comparing the alumina and glass matrices, respectively. This was explained by the better heat conductivity of the alumina. An interesting study was also recently reported by Westcott et al.[21] who showed that the chemical nature of surface adsorbed molecules has

an effect on the electron dynamics of gold core-shell nanoparticles. They found a direct correlation between the electron dynamics and the dipole moment of the absorbed molecule. The study showed that molecules providing the strongest change in the dynamics (decreasing the electron relaxation lifetime from 2.7 ps to 1.7 ps) have the largest induced dipole moments near the metal surface.

In order to test the influence of the surrounding medium and especially the role of water in the studies on aqueous solutions of metallic nanoparticles we measured the electron dynamics of gold particle arrays. Their plasmon absorption is in a similar spectral range compared to the gold nanorods. Furthermore those particles are deposited on a glass substrate, but otherwise surrounded by air leaving only the base in thermal contact with another solid or liquid medium. The bleach recovery dynamics for these particles (shown in figure 3a) are probed close to the plasmon maximum at 650 nm after 400 nm excitation. The excitation power was about 70 nJ. The plasmon band bleach recovers with a monoexponential time constant of 4.1 ps with no evidence of a long component. The absence of a long relaxation time on the 200 ps time scale is especially surprising given that the fast relaxation component is much slower than the corresponding value for the colloidal gold nanorods in the limit of low excitation powers (about 1 ps, see figure 2). Since the initially deposited energy has to be dissipated, the glass substrate, which is a good heat conductor and better than water, could serve as an energy sink. Evaporation of atoms by which the particles cool off could also be a relaxation mechanism, which we cannot rule out at this point. However, we do not

observe a permanent bleaching of the signal in successive laser scans suggesting that only a few atoms overall would take part in this cooling process.

The relaxation dynamics change drastically when the gold particle arrays are immersed into water as shown in figure 3b. The fast relaxation time deceases to 2.6 ps and a longer relaxation time is now observed similar to the dynamics of the gold nanorod solution. This suggests that the addition of water quenches the heat of the gold arrays very rapidly, on the same time scale as the pure electron-phonon relaxation. Since the particles are in this case mainly covered by water on all sides, except for the base, a rapid local heating of the water must have occurred. The long relaxation component can then be attributed to the heat diffusion in water, which is consistent with the fact that a solid like the glass substrate is a much better heat conductor compared to water. This change in relaxation dynamics is reversed when the particle arrays are dried indicating that no permanent chemical change/reaction has taken place.

In order to further demonstrate the interaction principles toluene and pyridine were also used to cover the arrays. In the case of toluene no detectable second component was observed. However, when the arrays are covered with pyridine, a phonon-phonon component comparable to that observed when the arrays were covered with water. The toluene has an extensive and tightly bound pi system that has limited interaction with the thermally excited particles. The heat diffusion away from the particles into the surrounding medium is therefore limited by this lack of interaction.

VanDuyne et al. have demonstrated the almost irreversible binding of pyridine to gold array particles. The thermal properties of pyridine are also very similar to those of toluene and thus facilitate the comparison of the pyridine interaction with that of toluene or water. The similarity of the thermal properties with toluene and the presence of lone pair electrons as in water allow for information on the importance of each interaction to be probed. As shown in Figure 4 , when pyridine is added the phonon-phonon component becomes extremely pronounced. This is indicative of the quenching that was seen in the case of water. This leads to the conclusion that the quenching of the heated gold arrays must be dependent on the amount of interaction of the solvent with the particles. If this quenching was dependent solely on the thermal properties of the solvent, then the relaxation times of the pyridine and toluene would be very similar, as the thermal conductivities of the two are 0.165 W/m K and 0.131 W/m K respectively. However, as noted earlier, both the initial relaxation times and the phonon-phonon component are drastically different.

In summary, we have shown the role of the surrounding medium, and in particular water, on the electron cooling dynamics of metallic nanoparticles. At higher excitation powers, local heat exchange close to the surface of the nanoparticles appears to take place on a time scale comparable to that of electron-phonon processes. The slow relaxation (~200 ps) observed in water and pyridine is therefore assigned to mainly the heat diffusion through the water solvent away from the thermally excited nanoparticles.

Acknowledgements:

We would like to thank Lynn Peyser for help with the AFM characterization. This work was supported by the Materials Research Division of the National Science Foundation (grant # 0138391).

Experimental:

Colloidal gold nanorods with an aspect ratio of 2.9 (width 12 nm ±2) were synthesized by a modified version of the seed-growth method[22] developed by Jana et al.[23]. The seed solution consisted of 5 ml of 0.2 M CTAB solution mixed with 5 ml of 0.0005 M $HAuCl_4$. To the stirred solution, 0.6 ml of ice-cold 0.01 M $NaBH_4$ was added. Vigorous stirring of the seed solution was continued for 2 minutes. After stirring, the solution was kept at 25 °C. The growth solution was prepared with 5 ml of 0.2 M CTAB added to 0.1 ml of 0.004 M $AgNO_3$ solution. To this solution 5 ml of 0.001 M $HAuCl_4$ was added and after gentle mixing of the solution, 70 μl of 0.0788 M ascorbic acid was added. In the final step 12 μl of the seed solution was added to the growth solution. The size of the gold nanorods were determined using TEM.

Regular arrays of gold nanoparticles were prepared using nanosphere lithography following the method developed by van Duyne and coworkers[12,13]. An ordered layer of 356 nm polystyrene nanospheres (Polysciences) was prepared on a glass coverslip (Fisher Scientific). The coverslips were mounted in a Denton DV-502A Thermal Evaporator to deposit gold in the spaces between the spheres. The thickness of the evaporated gold was monitored by a quartz crystal thickness monitor (Inficon). After evaporation the mask was removed from the substrate by sonicating for 30s in methylene chloride. The size of the particles is determined by the polystyrene mask and was 90 nm wide at its base and 50 nm in height in these studies as verified using a Quesant Q-SCOPE atomic force microscope (AFM).

Absorption spectra were recorded using a Shimadzu UV-3101-PC spectrophotometer. Transient absorption studies[18,19] were performed using an amplified Ti:Sapphire laser system (Clark CPA 100). The second harmonic of the 800 nm fundamental was used as excitation and a white light continuum probe beam was generated by focusing a small part of the fundamental beam into a saphhire window. The pump beam was mechanically chopped and the differential transmission signal was recorded using a pair of Si photodiodes (Thorlab) and a lock-in amplifier (Stanford Research Systems).

References:

[1] J. Yguerabide, E. E. Yguerabide, *Anal. Biochem*. **1998**, *262*, 137; **1998**, *262*, 157.

[2] K. Hamad-Schifferli, J. J. Schwartz, A. T. Santos, S. Zhang, J. M. Jacobson, *Nature* **2002**, *415*, 152.

[3] M. A. El-Sayed, *Acc. Chem. Res.* **2001**, *34*, 257.

[4] S. Link, C. Burda, M. B. Mohamed, B. Nikoobakht, M. A. El-Sayed, *J. Phys. Chem. A* **1999**, *103*, 1165.

[5] H. Kurita, A. Takami, S. Koda, *Appl. Phys. Lett.* **1998**, *72*, 789.

[6] F. Mafune, J. Kohno, Y. Takeda, T. Kondow, *J. Phys. Chem. B* **2002**, *106*, 7575.

[7] S. Link, M. A. El-Sayed, *J. Phys. Chem. B* **1999**, *103*, 8410.

[8] R. Gans, *Ann. Physik* **1915**, *47*, 270.

[9] M. Maillard, S. Giorgio, M. P. Pileni, *Adv. Mater.* **2002**, *14*, 1084.

[10] R. Jin, Y. W. Cao, C. A. Mirkin, K. L. Kelly, G. C. Schatz, J. G. Zheng, *Science* **2001**, *294*, 1901.

[11] T. R. Jensen, G. C. Schatz, R. P. Van Duyne, *J. Phys Chem. B* **1999**, *103*, 2394.

[12] C. L. Haynes, R. P. Van Duyne, *J. Phys. Chem. B* **2001**, *105*, 5599.

[13] C. L. Haynes, A. D. McFarland, M. T. Smith, J. C. Hulteen, R. P. Van Duyne,. *J.* C.

[14] Voisin, N. Del Fatti. D. Christofilos, F. Vallee, *J. Phys. Chem. B* **2001**, *105*, 2264.

[15] J. H. Hodak, A. Henglein, G. V. Hartland, *J. Phys. Chem. B* **2000**, *104*, 9954.

Phys. Chem. B **2002**, *106*, 1898.

[16] M. Perner, P. Bost, G. v. Plessen, J. Feldmann, U. Becker, M. Mennig, H. Schmidt, *Phys. Rev. Lett.* **1997**, *78*, 2192.

[17] M. Hu, G. V. Hartland, *J. Phys. Chem. B* **2002**, *106*, 7029.

[18] S. Link, A. Furube, M. B. Mohamed, T. Asahi, H. Masuhara, M. A. El-Sayed, *J. Phys. Chem. B* **2002**, *106*,945.

[19] M. B. Mohamed, T. S. Ahmadi, S. Link, M. Braun, M. A. El-Sayed, *Chem. Phys. Lett.* **2001**, *343*, 55.

[20] V. Halte, J.-Y. Bigot, B. Palpant, M. Broyer, B. Prevel, A. Perez, *Appl. Phys. Lett.* **1999**, *75*, 3799.

[21] S. L. Westcott, R. D. Averitt, J. A. Wolfgang, P. Nordlander, N. J. Halas, *J. Phys. Chem. B* **2001**, *105*, 9913.

[22] B. Nikoobakht, M. A. El-Sayed, *Chem. Mater.*, submitted.

[23] N. R. Jana, L. Gearheart, C. J. Murphy, *J. Phys. Chem.* B **2001**, *105*, 4065.

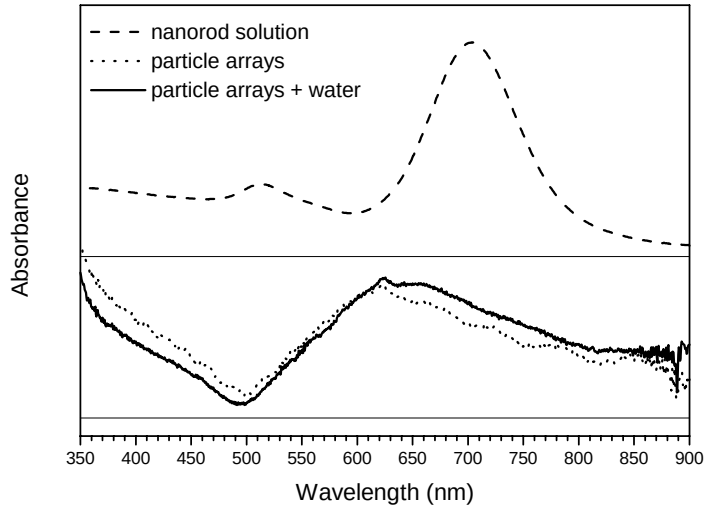

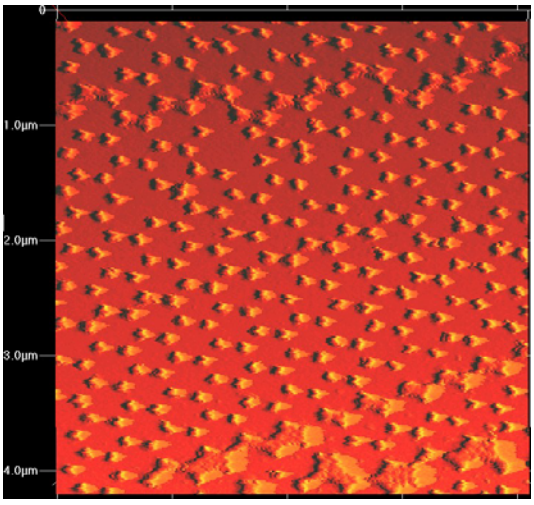

Figure 4-1: (A) UV-vis absorption spectra of a colloidal gold nanorod solution with an aspect ratio of 2.9 (dashed line) and gold arrays of truncated tetrahedra produced by nanosphere lithography in air (dotted line) and after immersing them in water (solid line). (B) AFM image of 4 µm x 4 µm area of nanolithographically prepared gold particle arrays. Particles are 50 nm in height and approximately 90 nm in width at the base

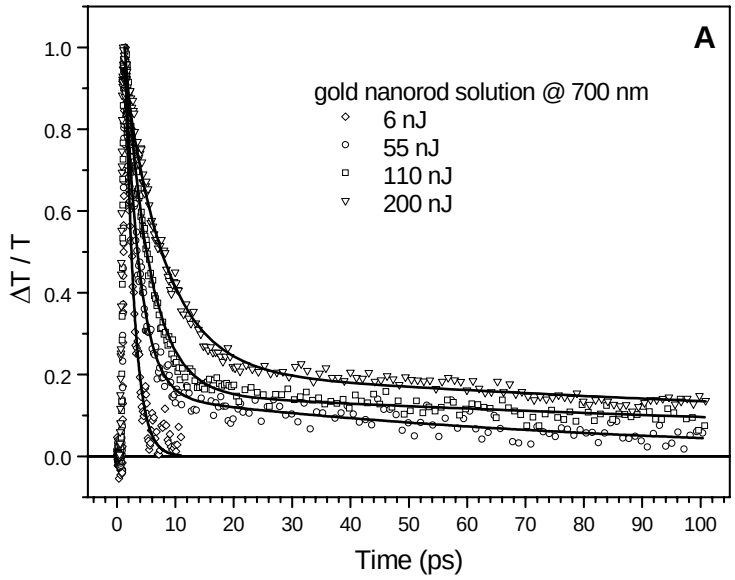
A
gold nanorod solution @ 700 nm
6 nJ
55 nJ
110 nJ
200 nJ
ΔT / T
Time (ps)

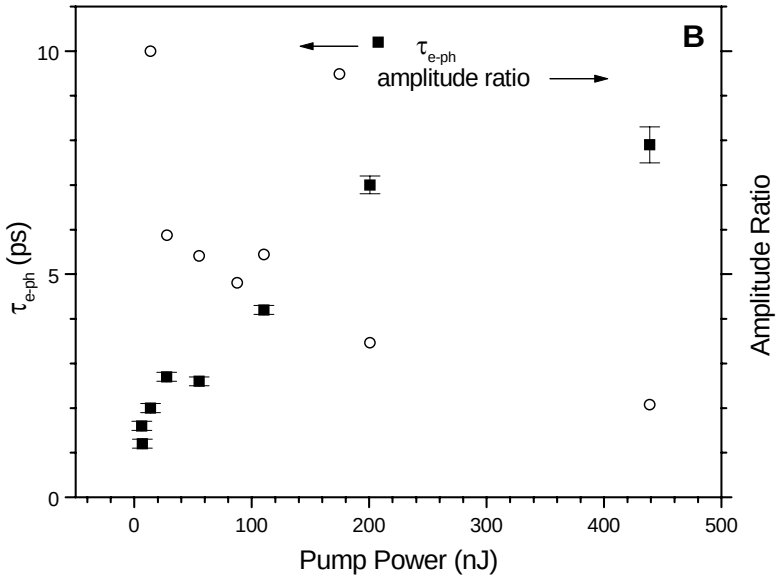
B
τe-ph
amplitude ratio
τe-ph (ps)
Amplitude Ratio
Pump Power (nJ)

Figure 4-2: (A) Pump power dependence of the bleaching of the longitudinal surface plasmon band of colloidal gold nanorods observed at 700 nm after excitation with 400 nm femtosecond laser pulses. (B) Plot of the fast relaxation time (solid squares) and the amplitude ratio (open circles) as a function of excitation power.

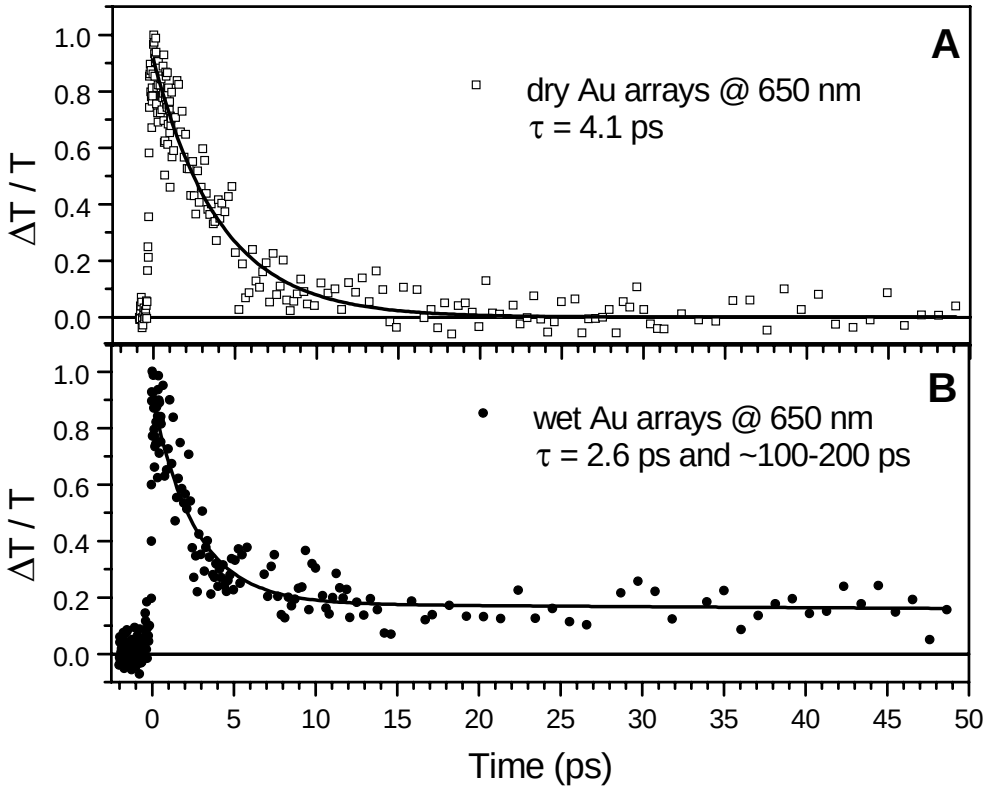

Figure 4-3: Plasmon band bleach dynamics of gold arrays observed at 650 nm after excitation at 400 nm for particles in air (A) and immersed in water (B).

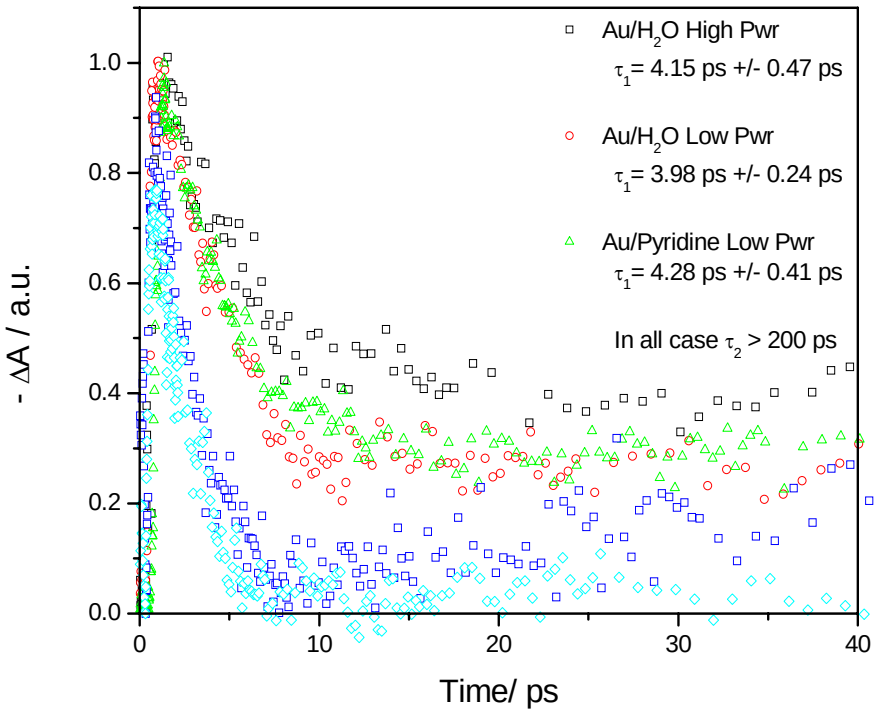

Figure 4-4 Dynamics of Au arrays in different solvents. Dramatic increase in phonon-phonon component is seen as the availability of lone pair electrons to interact with the particle surface.

CHAPTER V

Effect of Pt, Pd, and Rh Nanoparticles on the Peak Power of Polymer Electrolyte Fuel Cells

Abstract

The effects on the power output of polymer electrolyte membrane fuel cells with Pt, Pd, or Rh, doped proton exchange membranes were studied. The studies show a significant increase in the peak power with the addition of the nanoparticles over that of the unmodified membrane. In this study we have determined that the modification of Nafion membranes with Pt, Pd, or Rh nanoparticles increase the peak output power of the fuel cells by varying amounts. It has been determined that Pt enhances the power output more effectively than either Pd or Rh. This increase is 40 % to 50 % over the power output of the unmodified cells. The effect of the addition of the nanoparticles on the oxygen reduction reaction is found to be more than when it is placed on the H_2 side. This together with the observation that Pt nanoparticles are more effective than Pd nanoparticles is consistent with the mechanism in which the electron density of the metal is donated to the empty anti-bonding molecular orbital of the oxygen molecule leading to its dissociation.

Introduction

Though the study of single crystals under ultra-high vacuum [1] has done much to elucidate the catalytic process, since the early 1940s the potential use of transition metal nanoparticles in catalysis have attracted a great deal of interest[4]. These particles have been the subject of study in solution [1,2], in polymers [3], and immobilized on supports [4-6]. The wide variety of media in which these particles can exist in have facilitated their use in exploring their catalytic properties in a wide variety of reactions including, but not limited to, hydrogenation [5], CO oxidation[4], Suzuki coupling reactions [3], and isomerization [4].

Particles within this size range exhibit interesting properties that are unique to their small size. As the number of atoms in the particle decreases, the fraction of the number of atoms on the surface to the total increases. This increases the surface to volume ratio of the particles and thus increases the number of atoms per gram of the catalyst that can be involved in the catalysis process. Furthermore, as the size of the particle decreases, the chemical activity of the surface atoms is expected to change due to an increase in the surface tension of the particle with decreasing size and increasing curvature.

Rampino et al[1] studied the effect of size on rate of hydrogenation using platinum and palladium particles capped with polyvinyl alcohol, methyl methacrylate , and polyacrylic acid methyl ester. They compared the rates of hydrogen uptake of the Pd-

PVA catalyst with the uptake rates of several commercially available catalysts of known activity. Their test shows that the uptake rate of the Pd-PVA catalyst is almost 5 times larger than the uptake of the Pd-C catalyst. These early results set the context for investigations of metallic nanoparticle catalysis showing the much greater efficiency of the nanoparticles over standard catalysts.

More recently, groundbreaking work by Schmid[4,5] and Bonnemann[4,6,8] has shown the effect and uses of nanoparticles in heterogeneous catalysis process such as hydrogenation and hydroformylation reactions. In Schmid's early work he found that, in order for the catalyst to survive the reaction and maintain its effectiveness, it was necessary to support the particles on substrates such as TiO_2 or Al_2O_3 [9]. In these studies the ability of small rhodium and palladium particles to catalyze the hydroformylation of ethene was explored. These particles were supported on TiO_2 and a Na-Y zeolite. These catalysts are produced by chemisorption of the particles onto the support surface via addition of the support to a solution containing the particles. This results in loading of 5% and 1.5 % by weight for the zeolite and the TiO_2 respectively. The catalytic effect of the particles was tested heterogeneously on the hydroformylation reaction of ethene, however the deactivation of the surface due to by-products formation led to the study of these species using an aqueous suspension of the particles. The limited solubility of the by-products in the aqueous media decreases the chances of catalyst deactivation. The studies of ethene hydroformylation, using 1 % loading , achieved a turnover frequency of 140 mol mol^{-1} min^{-1} while similar studies using propene led to turnover frequencies of 400-

600 mol mol^{-1} min^{-1}. These turnover frequencies are much higher than those found using homogeneous catalysts, but show decreased selectivity.

The hydrogenation of 1-hexene[5] was investigated using small Pd particles on TiO2. In these studies the difference in effectiveness between the supported particles and commercially available catalysts is truly remarkable, with 100% conversion to the alkane by the supported particles and only 29.7% conversion by the commercial catalyst. Similarly impressive results are achieved with diverse compounds such as dicyclopentadiene (100%), 1-hexyne (97.5%), and crotonaldehyde (95.1%). These catalysts not only show an increased effectiveness over traditional catalysts, but in contrast to the rhodium particles, show no deactivation even after many cycles.

Studies by Bonnemann[6] using rhodium nanoparticles have also shown vastly increased activities. The hydrogenation of butyronitrile was performed using a commercially available 5% Rh on charcoal catalyst and a 5% Rh on charcoal nanoparticle catalyst. The difference in activity is astounding, with the nanoparticle catalyst having essentially double the activity of the commercially available catalyst at the same loading. The colloidal Pd nanoparticle catalyst also shows an increased lifetime over conventional catalysts, lasting approximately 2.5 times longer than the conventional catalyst. These studies eloquently show the enhanced activity of transition metal colloid based catalysts in relation to the activity of comparable commercially available catalysts.

In our lab we have shown in a Science report [10] that polymer stabilized platinum and palladium nanoparticles of different shapes can be synthesized using a

hydrogen gas reduction in an aqueous solution[10]. This relatively simple method allows us to produce nanoparticles of tetrahedral, cubic, and truncated octahedral shapes. Each shape has its own characteristic crystal facets that can catalyze surface reactions. It has been shown from work on single crystals that certain reactions are sensitive to the surface structure of the crystal. This sensitivity can take the form of enantioselective reactions, and or simple selectivity towards product formation only using a certain facet[11]. In the case of our particles different shapes have different facets. The cubes only have (100) facets, while the tetrahedral have only (111) facets. Recent work by our group has already shown that these catalysts are effective in the catalytic hydrogenation of propylene[7]. Others have also shown that platinum/gold alloys can be used to catalyze the reaction of H_2 and O_2 up to 50 times the normal rate[12].

B. Fuel Cells

Fuel cells have long been of interest as an alternative energy source in a wide variety of applications ranging from the space program[13] to more terrestrial concerns such as a replacement for the aging internal combustion engine[13]. While some applications have been realized, such as the use of fuel cells in some bus systems and cellular phone batteries, there are still many areas that could benefit from the use of fuel cells as an energy source. The auto industry is one of the most promising sectors for growth, primarily because of the higher efficiency and lower emissions of a fuel cell system relative to the conventional internal combustion energy. While conventional combustion engines reach only ~30% efficiency, low temperature fuel cells could

routinely reach efficiencies of 40% - 50% with emissions of only water vapor. Using such technology in only a fraction of the cars produced in the next decade could significantly reduce the amount of greenhouse gases for which the US is responsible, as well as increase energy security by reducing the dependence of the US on oil imports.

Larger scale fuel cells using a variety of different fuels also hold promise as a cleaner replacement for present day fossil fuel based power plants[13]. Running on renewable resources and emitting almost no waste gases, these plants generate power not only by conversion in the fuel cell but also by utilizing the waste heat for power generation increasing the efficiency of the process further.

Fuel cells can generally be broken down into four different types: polymer electrolyte membrane/phosphoric acid , molten carbonate, solid oxide, and alkaline fuel cells each with its own unique advantages and disadvantages.

Alkaline fuel cells have already found uses in a variety of capacities including power generation on the space shuttles. Alkaline fuel cells operate using the following reactions[13]:

$$\text{Anode : } 2H_2 + 4OH^- \rightarrow 4H_2O + 4e^-$$

$$\text{Cathode : } O_2 + 2H_2O + 4e^- \rightarrow 4OH^-$$

$$\text{Overall: } 2H_2 + O_2 \rightarrow 2H_2O + \text{energy}$$

These cells often run at temperatures ranging from 100^{o}C to 250 ^{o}C, and use highly corrosive concentrated KOH as the electrolyte. These cells are extremely sensitive to CO and must be fed only the purest gases in order to operate at peak performance. This combination of high temperature and highly corrosive electrolyte makes these cells dangerous to use outside of a tightly controlled environment.

Molten carbonate fuel cells work at even higher temperatures,600^{o}C- 800^{o}C but is much more tolerant of feed gas impurities. These cells are often fed with commercial natural gas and steam. Molten carbonate fuel cells work by the following reactions[13]:

$$\text{Anode : } CO_3^{2-} + H_2 \rightarrow H_2O + CO_2 + 2e^-$$

$$\text{Cathode : } CO_2 + 1/2O_2 + 2e^- \rightarrow CO_3^{2-}$$

$$\text{Overall: } H_2 + ½\ O_2 \rightarrow H_2O + \text{energy}$$

These react at the anode with the carbonate ions generated at the cathode by the reduction of oxygen and CO_2. These cells have already been tested as stationary power and co-generation systems.

The heart of the solid oxide fuel cell is a solid electrolyte element. In these cells, the operating temperatures are between 600 ^{o}C – 1000 ^{o}C in order to make the solid

electrolyte sufficiently conductive to ions. The following reactions generate the flow of electrons necessary for cell operation[13]:

$$\text{Anode: } H_2 + O_2^- \rightarrow H_2O + 2\,e^-$$

$$CO + O_2^- \rightarrow CO_2 + 2e^-$$

$$\text{Cathode: } O_2 + 4e^- \rightarrow 2O_2^-$$

$$\text{Overall: } H_2 + CO + O_2 \rightarrow H_2O + CO_2 + \text{energy}$$

One of the main advantages to this type of fuel cell is the lack of catalyst. This drastically decreases the cost of such cells for large-scale implementation in generation or back-up systems.

The direct methanol fuel cell has also shown considerable promise as a low temperature system to deliver limited amounts of power. This type of fuel cell, however, does require more catalyst than other fuel cells. However, these cells do offer the advantage of using a liquid fuel that is abundant and does not have the flammability or toxicity problems associated with some of the other fuel cell types. Electricity is generated by the following reactions[13]:

$$\text{Anode: } CH_3OH + H_2O \rightarrow CO_2 + 6H^+ + 6e^-$$

$$\text{Cathode: } 3/2O_2 + 6H^+ + 6e^- \rightarrow 3H_2O$$

$$\text{Overall: } CH_3OH + 3/2O_2 \rightarrow CO_2 + 2H_2O$$

This technology[14] has already been applied to several consumer electronics markets with moderate success.

Many previous studies[19-30] and patents[15-18] have focused on enhancing the porous carbon electrode or the catalyst layer using supported catalysts. Theses methods vary from sputtering a thin layer of Pt on to the gas diffusion electrode [19] to reduction of organometallic precursors onto supports for use in the catalyst layer [6,8]. The effect of sputtering Pt on to the carbon electrodes on the oxygen reduction reaction kinetics was recently studied by Mukerjee et. al [19]. The sputtered layer electrodes had Pt nanocrystallite with an average size of 25-30 Å on the surface. The loading of the catalyst layer was held constant at 20% Pt/C in the carbon cloth catalyst layer. They found that the addition of the small Pt nanocrystallites caused a 4-fold improvement in the oxygen reduction reaction at 0.9V and a 3.6-fold improvement in the exchange current densities. This study illustrates how the accessibility of the oxygen to the Pt nanocrystallites vastly increases the efficacy of the process.

Recent work by Bonnemann et al[8] has explored the idea of using a bimetallic colloidal precursor on polymer electrolyte fuel cell anode to improve the CO tolerance. Pure platinum catalysts suffer from poisoning problem resulting from CO adsorption on the surface. However, this problem has been addressed by the development of alloy catalysts that are much more resistant to poisoning than the pure metals. Bonnemann et al seek to take advantage of not only the increase in activity shown with nanoparticles, but also the CO resistance introduced by alloying with other metals. The platinum precursor

colloids were produced by coreduction of platinum and ruthenium chloride using tetractylammonium-triethylhydroborate in THF. The platinum-ruthenium and platinum-tin particles are produced via a multi-step borate reduction mechanism. The platinum-ruthenium particles are also synthesized via a trialkylaluminum reduction. The particles were then deposited on a Vulcan XC72 substrate. The capping layer was then removed by reactively annealing at 300^{o}C in a 10% O_2 in N_2 atmosphere and then at 300^{o}C in pure H_2. The particles were then deposited onto a glassy carbon electrode and then fixed with Nafion solution. These catalysts show a slightly higher activity towards the reduction of H_2 than commercial catalysts as well as having essentially the same activity even when 2% CO is added to the reaction mixture.

Obviously, to realize these goals much more basic research needs to be done to increase the amount of energy the cells can produce so that one day they may become as ubiquitous as standard flashlight batteries. One method by which this can achieved is by increasing the efficiency of the conversion of the cell. The most interesting way to achieve this is to use the advantages afforded by novel nanomaterials, specifically, transition metal nanoparticles.

Our primary interest is in the polymer electrolyte fuel cell, and more specifically in the proton conducting membrane sandwiched between the electrodes. In the polymer electrolyte fuel cell, a feed stream of hydrogen is fed to the anode and there split into individual protons giving up two electrons. The electrode often has a thin layer of platinum either on it or adjacent to it in a carbon support matrix. The electrons travel

through the external circuit, while the protons are conducted through the polymer electrolyte to the cathode where the oxygen is reduced and combines with hydrogen to give of water and energy as shown here[13]:

$$\text{Anode: } 2H_2 \rightarrow 4H^+ + 4e^-$$

$$\text{Cathode: } O_2 + 4H^+ + 4e^- \rightarrow 2H_2O$$

$$\text{Overall: } 2H_2 + O_2 \rightarrow 2H_2O + \text{energy}$$

These cells hold the advantage of their low operating temperature (<80 ^oC) and their relatively high efficiencies of ~ 50%. Unfortunately, the catalyst is very sensitive to the purity of the feed gases and thus easily poisoned. Our proposed research focuses on the modification of the polymer membrane with the addition of shape controlled Pt nanoparticles. We shall use our hydrogen reduction technique[10] to synthesize shape controlled alloy nanoparticles designed for poisoning resistance and to increase catalytic activity.

Watanabe and co-workers have recently reported data [14] on the incorporation of platinum nanoparticles into the membranes of polymer electrolyte fuel cells. They used membranes containing Pt, TiO_2, and Pt-TiO_2 particles. The primary focus of their work was the suppression of gas crossover and to introduce a method to control self-humidification of the membranes. The platinum particles were produced by soaking the membranes in a precursor solution consisting of $[Pt(NH_3)_4]Cl_2$ overnight. The ions were reduced to the metal by reacting with excess neutral hydrazine overnight. TEM images of

the particles confirmed the size range of 1-2 nm. The terminal voltage and power density measurements show a substantial increase in the performance of the modified membranes versus the unmodified ones. While they conclude that many of these effects are due to the better water distribution achieved with their particles, they make no mention of the catalytic enhancement of the oxidation of the hydrogen or reduction of the oxygen.

We have modified the commercially available fuel cell (H-Tec) and studied the effect of depositing platinum nanoparticles within the membrane on its performance. Figure 5-1 shows the effect of the deposited Pt in the membrane on the relative power of the cell. Indeed, there is over 60% enhancement of the relative power at a cell potential of 0.4 V when platinum nanoparticles are grown within the membranes. This has encouraged us to move our research in this direction.

Experimental

The synthesis of transition metal nanoparticles has been reported by our labs with the ability to control the size and shape distribution of the nanoparticles[10]. We propose to use a modified version of this method to synthesize transition metal and composite nanoparticles inside the Nafion membranes. First, a section of Nafion membrane is added to a three-neck flask containing a $1x10^{-4}$ M solution of the salt of the metal of interest. The solution is degassed by bubbling Ar through it for approximately 30 min. The metal ion is then reduced by bubbling H_2 through the solution for 5-10 minutes. In order to have as clean a particle surface as possible, the polymer capping material that is normally

used to stabilize the particles is not used. The pores of the membrane essentially become the stabilizing capping system for the particles. Synthesizing different solutions and then removing the membranes at different intervals can enable us to monitor the progress of the growth.

The electrical measurements are made using a fuel cell setup purchased from Solar Hydrogen Systems as shown in Figure 5-2. The cell consists of two Lucite outer blocks with H_2 inlet and outlet on one side and O_2 inlet and outlet on the other. Inside is a typical PEM fuel cell layout containing an ion conducting membrane sandwiched between two conductive carbon sheets, which are in turn pressed between the electrodes. The entire system is kept pressed tightly together by tightening two screws. The build up of water vapor from the reaction is limited and any that is noticeable is reabsorbed by the membrane.

The fuel cell is attached to a homemade load box consisting of a variable resistor as well as a multimeter and a Pine Instrument Bipotentiostat. The current and voltage are then read out to compare the properties of the different membranes to that of an unmodified membrane from the same film casting.

-Effect of Pt, Pd, Rh

As shown in previous studies [1-3,31], the efficacy of transition metal nanoparticles for catalyzing reactions has been proven. As shown in Figure 5-1, the peak power generation capacity of the transition nanoparticle modified Nafion™ is increased

with respect to that of the cell using the standard membrane. The addition of the nanoparticles catalyzes the oxygen reduction reaction, as will be discussed later. This in turn increases the overall measured potential from the fuel cell reaction. In standard fuel cells the catalyst resides in the carbon paper sandwiched between the electrode and the membrane. The catalyst grown on and in the membrane acts as a second catalytic layer on which the catalytic reduction of oxygen can take place. It is well documented for gas phase systems that the presence of atomic scale kinks and defects can lower the activation energy for reactions on that surface. In this case the transition metal nanoparticles present act as secondary catalyst for both the oxidation of hydrogen on the anode side of the cell and the reduction of oxygen on the cathode side of the cell.

Several groups have seen an increase in power by using nanomaterials and clusters on carbon and TiO_2 supports in Nafion on rotating disk electrodes. By modifying the membrane directly for use in operating fuel cells we endeavor to test these materials in a real world environment. As proof of concept we first attempted modification of the membrane with platinum particles. As shown in Figure 5-1, the addition of Pt particles on the surface increases the peak power from 19 mV to 29 mV using a dry membrane in the synthesis. As shown the dry membrane, when added after the Pt salt has been added, absorbs the Pt ion more readily and enhances the growth of the particles. Work by Watanabe and co-workers have shown that the addition of carbon supported Pt particles assists in the continued hydration of the Nafion membrane, which must remain moist to function as a proton conductor. In this case the platinum is inside the membrane as

opposed to located on the surface, as is the case in our method. In order to determine the effect of the nanoparticle impregnation, we studied the concentration, pH , and composition dependence as discussed in latter sections.

The membranes were also impregnated with Pd and Rh nanoparticles. Rhodium has shown catalytic activity in many organic and gas phase reactions [11]. The membranes were impregnated using the same method as for Pt. As shown in Figure 5-3 (a) the Rh membranes also show an increase from 26 mV to 29 mV over the power output of the standard membranes. Though the increase is not as much as that of the Pt membrane it is an important increase. Though rhodium is a less potent catalyst than platinum for this type of reaction, it fulfills the same role as the platinum particles, assisting in the oxidation of hydrogen and the reduction of oxygen. The effect of pH and concentration are discussed in following sections.

Palladium particles were also synthesized in the membranes and showed an increase in power output, though still not as large as the increase seen with the addition of platinum nanoparticles. As shown in Figure 5-3 (b) , the modified membranes show an increase from 26 mV for the unmodified membrane to 28 mV. As previously discussed, the Pd particles offer enhanced surface area on which the oxidation and reduction reactions can take place. Alloy, pH, and precursor concentration were also investigated to determine their effect on the power output.

-Effect of different synthesis pH and precursor concentration on film power

The effects of different pH and precursor concentration on the power output of the final membranes were investigated. In the cases of the pH studies the pH was adjusted using either 0.1 M NaOH or 1M HCL with the pH being adjusted after the introduction of the membrane. It has already been shown that the shape of transition metal nanoparticles can be affected by the pH of the synthesis solution. Thus the pH would have an effect on the particles synthesized with the membrane. As shown in Figure 5-4 (a), the increase from 19 mV to 30 mV across the pH range from 8.50 to 7 can be illustrated most dramatically with rhodium particles. This is in agreement with previous work from our group which shows the dependence of rhodium nanoparticle shape on the solution pH. This can directly affect the size and shape of the nanoparticles. The rhodium particles synthesized at pH 7 show the largest increase in the overall power output. This is also the pH most used in solution measurements, and has been shown to produce extremely small particles of a mostly tetrahedral shape. Both the platinum and palladium particles have also been shown to have a dependence of shape on the synthesis conditions, so the effects of different pHs were studied as well.

Platinum also shows dependence of output power on pH. As shown in Figure 5-4 (b) , the power output is at the maximum at pH 7. This pH is also where best results have been obtained for the colloidal synthesis of both types of particles. The pH sensitive nature of the polymer membrane itself may also affect the power output by indirectly influencing the proton conductivity of the membrane. At pH 7, after the adjustment with

HCl and NaOH, the membrane is in a protonated state and can easily conduct the protons when in operation. However, at the basic pH, the protons in the membrane may be depleted which leads to diminished proton conduction as well as affecting the particle nucleation and growth. This can lead directly to a decrease in the output power of the fuel cell at operation. At acidic pH, there would not be much change in the membrane, only an increase in the protonation of some sites in the membrane. This would only slightly increase the proton conductivity and would have a much larger effect on the particle shape and thus influence the output power in that manner.

The effect of concentration was also investigated to determine if the production of more particles would lead to increased output. While there were some runs where the output was greater than that of the blank membrane, in general the increase of concentration had very little effect as shown in Figures 5-5 (a), (b), and (c). The additional particles disrupt the polymer structure to the point that proton conduction is affected.

-Alloy Effects

The effects of alloying two metals, platinum and palladium, were of interest to increase catalytic effect. Both metals are catalytically active, though the addition of palladium adds an increased resistance to carbon monoxide poisoning, a source of performance degradation and deactivation. The alloys were synthesized by varying the precursor composition from 100 mol % Pt to 100 mol% Pd as shown in 6-1 and 6-3 (b).

The performance of both the 100 % Pt and 100 % Pd membranes were as previously evaluated with the peak powers being significantly higher than those of the blank unmodified membranes. Due to the method of synthesis, these particles are most likely of homogenous composition with respect to the platinum and palladium. As shown on Figure 5-6, the alloy particles show less activity (lower output power) than the pure metal particles. The increased palladium in the alloy dilutes the platinum surface sites available for reaction. Though the palladium does catalyze the reaction, it does so with far less affinity than platinum. Though various other metal alloys have shown promise as catalysts, specifically Pt/Au catalysts for the H_2/O_2 reaaction, many other alloys have proven to be significantly less effective.

-Oxygen Reduction Studies W/ Pt, Pd

Many studies[32,33] have focused on the oxygen reduction reaction mechanism and catalysis for fuel cells. In order to determine whether the platinum and palladium catalyst catalyzed either the reduction or oxidation reaction more favorably, the power output was measured with the catalyst on different sides. The modified membrane was placed in the fuel cell assembly along with an unmodified membrane. By switching the side the catalyst was on, the effect on each reaction could be measured. As shown in Figure 5-7, the output power of the reaction was higher when the catalyst is on the oxygen reduction side. When the catalyst is on the oxidation side, little difference is seen. This leads to the conclusion that the catalyst is enhancing the reduction of the oxygen. In

Figure 5-7 (b), it can be seen that there is also a difference using the palladium particles. The difference is smaller than with the platinum particles, but this is because of the smaller catalytic effect of the palladium in general when used in this system. In both cases the mechanism is most likely similar to that of the bulk, with the metal catalyzing the breaking of the molecular oxygen bonds, thus accelerating the uptake of the electron from the oxidized hydrogen. The higher electron density of the metallic platinum makes it easier for the oxygen to bind and stabilizes the intermediate structure. The lower electron density of the palladium decreases the amount of density that can be donated to the oxygen as well as decreasing the stabilizing effect that can take place. The platinum therefore increases the power output when catalyzing the oxygen side of the cell more than palladium in the corresponding position.

Conclusions

Our work with Pt, Pd, and Rh nanoparticle modified fuel cell membranes has led to number of observations. First, the wet chemical synthesis method used by our group to produce shaped transition metal nanoparticles can be used to produce capping material free particles in and on the surface of polymer electrolyte membranes. This allows the use of particles with minimum surface contamination as well as not needing a support and they can be used with pre-cast films that are available in bulk. Secondly, platinum , as was expected, proved to enhance the power output of the fuel cells by up to 60 % by catalyzing the oxygen reduction reaction. The higher electron density of Pt makes it a better catalyst as well as enhances the O_2 reduction. Palladium has also been shown to

significantly increase the output, while rhodium only slightly increases the output of the cells. The effect of pH and concentration has been determined for platinum, palladium and rhodium modified membranes, and the overall determination that the addition of transition metal nanoparticles to the polymer membrane does in fact enhance power generating capabilities of the fuel cells.

Acknowledgments

We wish to thank the Savannah River Site for providing exploratory funding for this project and Dr. Thomas Walters of the Savannah River Site for many helpful discussions.

References

1) Rampino, L.D., Nord, F.F. *J. Am. Chem. Soc*., **1942**, *63*, 2745

2) Li, Y., Petroski, J., El-Sayed, M.; *J. Phys. Chem*., **2000**, *104*, 10956.

3) Li, Y., Hong, X., Collard, D., El-Sayed, M.; *Organic Le*tters, **2000**, *2*, 2385.

4) Aiken III, J.D., Finke, R.G.; *J. Mol. Catalysis A: Chemical*, **1999**, *145*, 1 and references therein

5) Scmid, G. ; *Chem. Rev*. **1992**, *92*, 1709 and therein

6) Bonnemann, H., Braun, G., Brijouz, W., Brinkmann, R., Schulze Tilling, A., Seevogel, K., Siepen, K.; *J. Organometallic Chem.* **1996**,*520*, 143

7) J.W. Yoo, D.J. Hathcock, M.A. El-Sayed J. Catalysis, **2003**,*1*,214

8) Bonnemann, H. Brinkmann, R., Britz, P., Endruschat, U., Mortel, R., Paulus, U.A.,

Feldmeyer, G.J., Schmidt, T.J., Gasteiger, H.A., Behm, R.J.; *J. New Mat. Electrochem. Systems*, **2000**, *3*, 199

9) Bonnemann, H., Brinkmann, R., Britz, P., Endruschat, U., Mortel, R., Paulus, U.A., Feldmeyer, G.J., Schmidt, T.J., Gasteiger, H.A., Behm, R.J., *J. New Mat. Electrochem. Systems*, **2000**, *3*, 199

10) Ahmadi, T.S., Wang, Z.L., Green, T.C., Henglein, A., El-Sayed, M.A. *Science*, **1996**, *272*, 1924

11) Somorjai, G. Introduction to Surface Chemistry and Catalysis **1994**, John Wiley & Sons; New York

12) Lam, Y.L., Criado, J., Boudart, M.; *Nouv. J. Chem*., **1977**, *1*, 461

13) www.fuelcelltoday.com

14) Watanabe, M., Uchida, H., Emori, M.; *J. Phys. Chem. B*, **1998**, *102*, 3129

15) U.S. Patent #5767036

16) U.S. Patent #5489563

17) U.S. Patent #6287717

18) U.S. Patent #5861222

19) Mukerjee, S.,Srinivasan, S., Appleby, A.J.; *Electrochimica Acta*, **1993**, *38*, 1661

20) Steigerwalt, E.S., Deluga, G., Cliffel, D., Lukehart, C., *J. Phys. Chem. B*, **2001**, *105*, 8097

21) Lasch, K., Jorissen, L., Garche, J., *Journal of Power Sources*, **1999**, *84*, 225

22) Starz, K., Auer, E., Lehmann, Th., Zuber, R., *Journal of Power Sources*, **1999**, *84*, 167

23) Rohlans, B., Plzak, V., *Journal of Power Sources*, **1999**, *84*, 183

24) Gupta, S., Tryk, D., Zecevik, S., Aldred, W., Guo, D., Savinell, R.F., *J.Appl. Electrochem*., **1998**, *28*, 673

25))Ticianelli, E.A., Derouin, C.R., Srinivasan, S.; *J. Electroanal. Chem.*, **1988**, *251*, 275

26) Dalmia, A., Linken, C.L., Savinelli, R.F.; *J. Coll. Interface Sci.* , **1998**, *205*, 535

27) Gottesfeld, S., Wilson, M.S.; *J. Appl. Electrochem*, **1992**, *22*, 1

28) Gottesfeld, S., Wilson, M.S.; *J. Electrochem Soc.* , **1992**, *139*, L28

29) Taylor, E.J., Anderson, E.G., Vilambi, N.R.K.; *J. Electrochem. Soc.* **1992**, *139*, L45

30) Faubert, G., Guay, D.,Dodelet, J.P.; *J. Electrochem. Soc.* **1998**, *145*, 2985

31) Petroski, J.M. Green, T.C., El-Sayed, M.A. *J. Phys. Chem. A* **2001**, *105*, 5542

32) Hilgendorff, M.; Bogdanoff, P.; Bron, M.; Dorbandt, I. *Schriften des Forschungszentrums Juelich, Reihe Energietechnik* **2003**, *26*, 227

33) Lefevre, M.; Dodelet, J. *Electrochimica Acta* **2003**, *48*, 2749

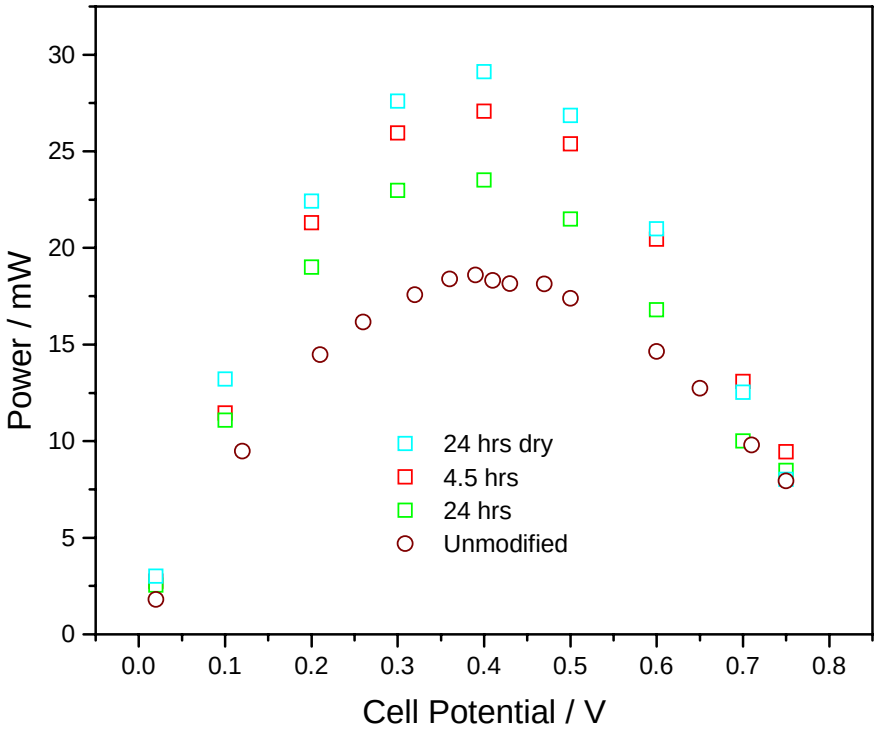

Figure 5-1 Comparison of platinum modified, unmodified, and different time increments of membrane exposure to growth medium.

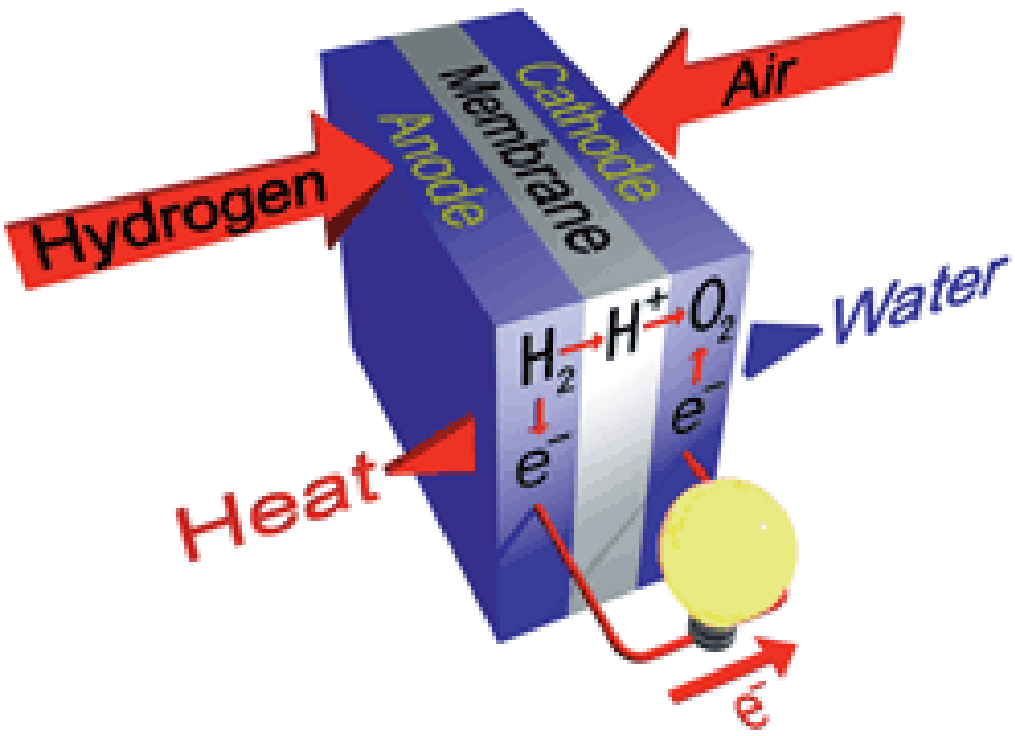

Figure 5-2 Schematic representation of standard PEM fuel cell.(www.fuelcelltoday.com)

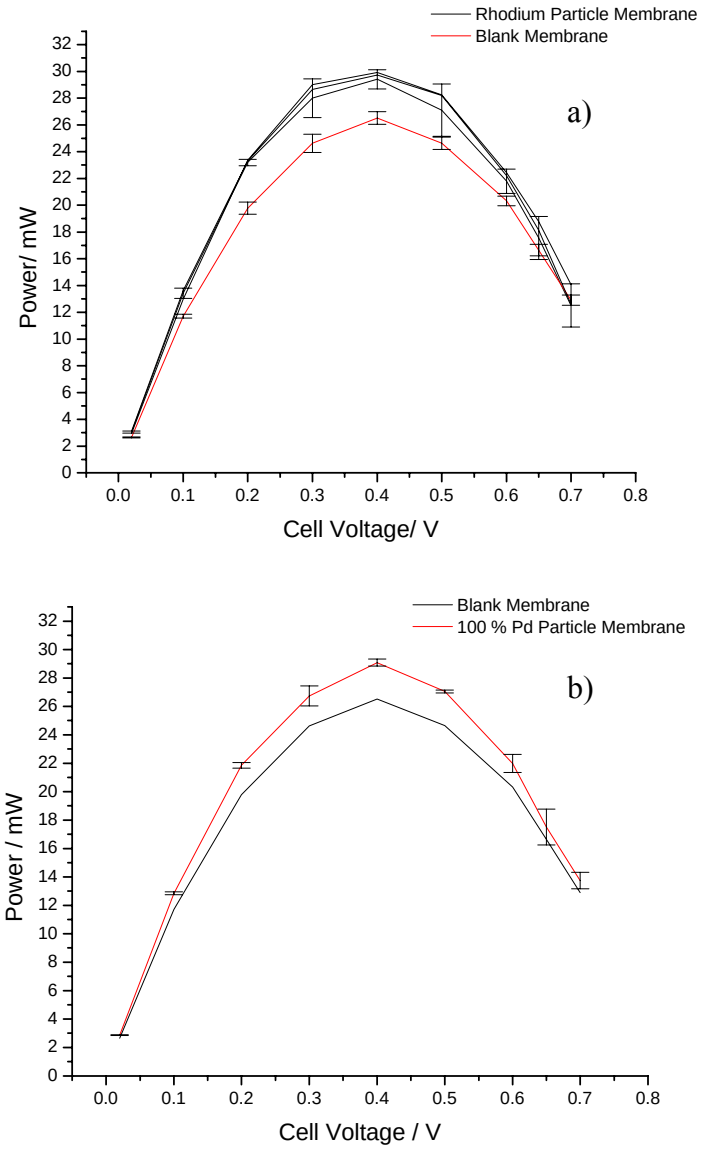

Figure 5-3 Power comparison of both regular and rhodium modified membranes (a). Power curve of fuel cell modified with palladium particle impregnated membrane (b).

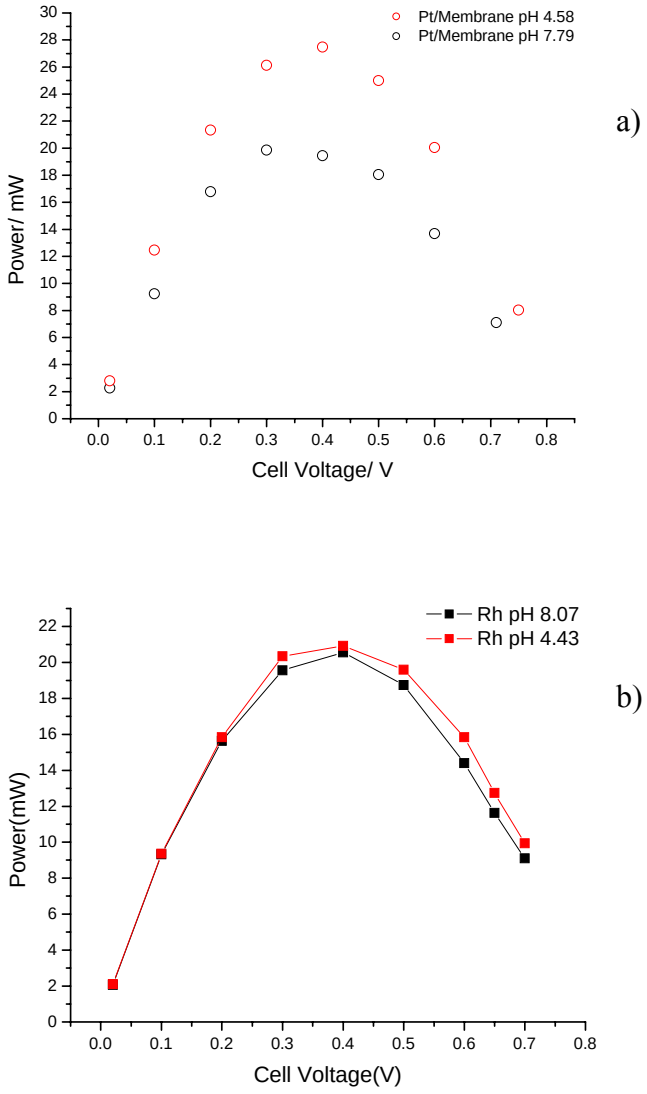

Figure 5-4 Dependence of power on platinum (a) and rhodium (b) on particle synthesis

pH.

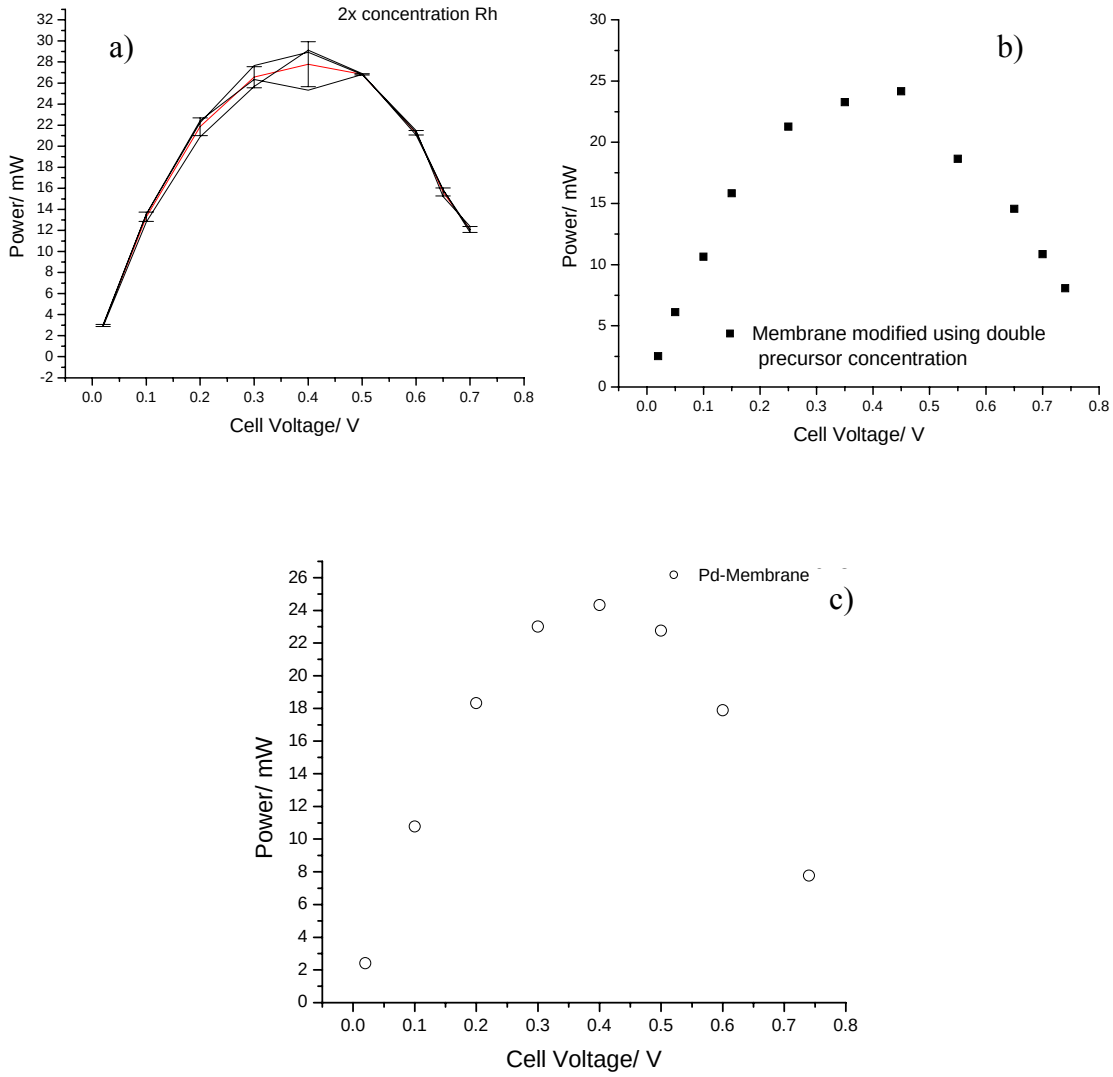

Figure 5-5 Dependence of fuel cell power on rhodium (a), Pt (b), and Pd (c) salt concentration

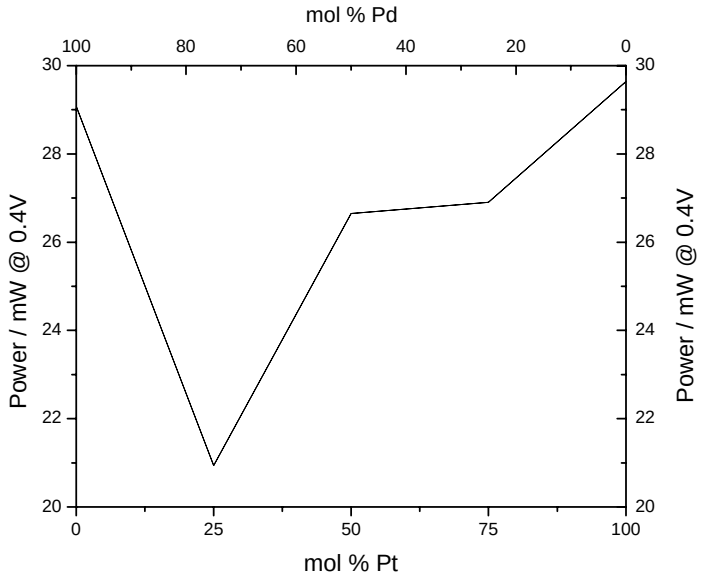

Figure 5-6 Dependence of peak power on mole fraction of the platinum and palladium initial salts used for the synthesis of the nanoparticles.

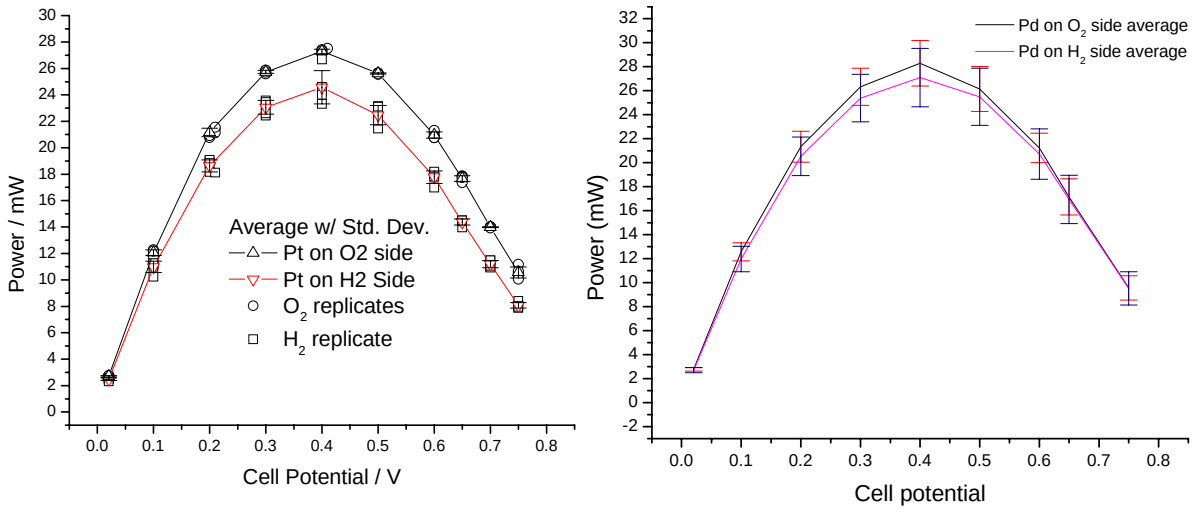

a) b)

Figure 5-7 Power dependence of platinum (a) and palladium (b) catalyst membranes on oxygen or hydrogen side

CHAPTER VI

PROPENE HYDROGENATION OVER TRUNCATED OCTAHEDRAL PT NANOPARTICLES SUPPORTED ON ALUMINA

Abstract

Colloidal Pt nanoparticles synthesized by a 1:5 concentration ratio of K_2PtCl_4 to polyacrylate were loaded on nanoporous alumina using the impregnation method at room temperature. The deposited Pt particles, present on the external surfaces of the support, were characterized by transmission electron microscopy, which indicated predominantly truncated octahedral (TO) shapes with a mean diameter of 10 nm. Their catalytic performance in the hydrogenation of propene at 30-80 C was studied as a test reaction. The initial rate, reaction order, rate constant, activation energy, and turnover frequency were determined. The activation energy was found to be 8.4 ± 0.2 kcal/mol, which is slightly lower than results reported for other platinum systems (10-14 kcal/mol). The TO

platinum nanoparticles have atom-high surface steps, ledges and kinks and these atomic-scale fine structures are expected to decrease the activation energy. The reactivity of the surface atoms in this nanoparticle is so high that above 50 C side reactions leading to complete surface poisoning take place within a few minutes. The effect of the polymer concentration of the polyacrylate-capped TO Pt/Al_2O_3 on the hydrogenation catalytic activity was also investigated.

1. Introduction

Transition metals have long been used in the catalysis field(1-15). The field of catalysis on transition metal surfaces is rich in activity and has been carried out as early as 1823 (14,15). However, active studies on catalysis with nanoparticle surfaces is a very young field but is increasing in activity almost exponentially.(16)

Nanometer-sized colloidal metal particles are of great interest in modern chemical research, where they find application in such diverse fields as photochemistry (17), electrochemistry (17-19), optics (17-21), and catalysis (16, 17, 22). The chemical and physical properties of these particles are distinct from those of the bulk phase and those

of isolated atoms and molecules. In relation to catalysis, this difference was noted very early and has been the subject of early studies.(23,24) The specific properties of nano-sized metal particles in catalysis are usually associated with a change in their electronic properties relative to the bulk samples. This change is a result of size effects giving rise to an increase in the surface energy and a characteristic high surface-to-volume ratio. These lead to an enhancement of their catalytic properties (25) as large fractions of the active metal atoms are on the surface and thus are accessible to reactant molecules and available for catalysis (26). For these reasons, many workers have synthesized platinum nanoparticles deposited on inorganic materials as used in heterogeneous catalysis for use in various reactions (27-30). These catalysts are typically prepared without capping materials by impregnation/ion-exchange methods using various Pt precursors such as H_2PtCl_6 (27), $Pt(NH_3)_4(NO_3)_2$ (28), $Pt(AcAc)_2$ (28), $Pt(NH_3)_4Cl_2$ (29), $Pt(NH_3)_4(OH)_2$ (12) and $Pt(allyl)_2$ (30) which, give mainly amorphous (no shaped) nanoparticles.

Generally, the particle sizes and the dispersion states of metal nanoparticles are important factors in explaining their catalytic property. A relationship between the size of copper nanoparticles and the catalytic activity evaluated by hydration of unsaturated

nitriles was reported by Hirai et al. (31). They attributed the increase in the catalytic activity to an increase in the surface area of the nanoparticles due to the decrease of the particle size. However, the opposite result was also reported (32). An enhancement of both the specific activity and the turnover-frequency on the large silver particles in the hydrogenation of crotonaldehyde was observed compared with the small silver particles. In addition, the selectivity to the unsaturated alcohol is found to increase with increasing silver particle size (32). This catalyst gave a higher selectivity to crotyl alcohol (53 %) than the ultradispersed small silver particles that produced crotyl alcohol with a selectivity of only 28 %. These results indicate that the rate-determining step depends critically not on the surface areas and dispersion states but on the silver particle size and surface structure. As described by these workers (32), the activity and selectivity of some reactions depend on the nature of the surface sites on the nanoparticles. Factors which determine the coordination of surface metal atoms depend on size, shape, exposed facets and surface roughness (33).

The dependence of the selectivity and activity on the substrate surface has been well known for many years. A variety of different surface reactions have shown a large

dependence not only on the surface roughness of the catalyst but also on the crystal lattice. This has been shown for single crystal platinum samples under UHV conditions by a variety of groups and in several early works for dispersions of colloidal transition metals.

Capping material (e.g. polymer) is added to the suspension in order to prevent coagulation and precipitation of the metal nanoparticles. A part of the added polymer exhibits a protective function by the adsorption of the polymer onto the metal nanoparticles and the other part of the polymer dissolves freely in the suspension of the metal nanoparticles. Both the amount of the polymer adsorbed on metal nanoparticles and the concentration of free polymer are important for the application of the metal nanoparticles. However, there have been no reports on correlation of the catalytic activity with either the amount of the polymer adsorbed on metal nanoparticles or the concentration of free polymer in catalysts.

In the present study, truncated octahedral (TO) platinum nanoparticles are synthesized using K_2PtCl_4 solution and polyacrylate as the capping material and impregnated on alumina support. The particle size/shape are characterized by

transmission electron microscopy (TEM). The catalytic activity is measured by the values of the activation energy and the turnover frequency as studied for the heterogeneous hydrogenation of propene. Quantities of the polyacrylate on TO platinum deposited on alumina are determined by FT-IR and are qualitatively correlated to the catalytic activity of the hydrogenation.

2. Experimental

2.1. Chemicals

K_2PtCl_4 (99.99 %), sodium polyacrylate (average MW 2100), and alumina (neutral, surface area 155 m^2/g, pore size 5.8 nm) were obtained from Aldrich. All solutions were prepared using doubly deionized water. Propene (99.9995 %) and hydrogen (99.995 %) were purchased from Matheson and were used without further purification. The purity of the propene was checked by mass spectrometry.

2.2. Catalyst Preparation

The platinum deposited on alumina (Pt/Al_2O_3) catalyst was prepared as follows. The

platinum nanoparticles were synthesized in aqueous solution by using the methods reported by Rampino and Nord (23) and Henglein et al. (34). 1 ml of 0.1 M sodium polyacrylate as a capping polymer was added to 250 ml containing 8.0 x 10^{-5} M K_2PtCl_4 solution. The initial concentration ratio of K_2PtCl_4 to polyacrylate was 1:5. The pH of the solution was adjusted to 7 with 0.1 M HCl and purged with Ar for 20 min. The platinum complexes were reduced by bubbling H_2 for 5 min. The solution was left for 12 h in the dark. 5 g alumina was added to this solution and impregnated using rotary evaporation at room temperature under reduced pressure. Finally, it was dried at 110 C for 12 h.

2.3. TEM and FT-IR measurements

TEM was used to determine the particle size and shape of the platinum nanoparticles supported on alumina. For TEM sample preparation of the Pt/Al_2O_3 catalyst, it was suspended in deionized water by ultrasonification for 1 h after grinding of the Pt/Al_2O_3 and subsequently left for several hours. The suspended sample was deposited on a carbon grid and was left to dry slowly at room temperature. TEM images were taken by using a JEM 100C operated at an acceleration voltage of 100 kV at a magnification of

100,000-190,000 at room temperature. The particle size and shape were determined from an enlarged TEM images.

FT-IR spectra are recorded from pellets of the sample using a Bruker IFS 66/S FT-IR spectrometer. Typically, 100 scans were accumulated for each spectrum with a resolution of 2 cm^{-1} using Bruker's OPUS 2.0 software. FT-IR spectra were recorded in the range of 2300-1000 cm^{-1}. Static pressure was applied to the powder sample until the pellet made a clear disk.

3. Results and discussion

3.1. TEM images of platinum nanoparticles-deposited on alumina

In general, structure characterization of real catalysts by electron microscopy is complicated by the strong contrast features originating from the support material, by the random orientation of metal particles and by superposition of particle images due to the nonplanar morphology of the catalyst (35). Where the support is thick, it is not possible to see the metal particles at all through the support. It is difficult, therefore, to determine clear structural features such as particle size and shape. Figure 6-1 shows TEM pictures

of Pt/Al_2O_3 in which the platinum particles were synthesized with 1:5 concentration ratio of K_2PtCl_4 to polyacrylate followed by impregnating alumina with the platinum solution at room temperature under atmospheric pressure. The platinum particles in aqueous solution at 60-80 C are observed to aggregate during impregnation. As can be observed in the TEM pictures, the platinum particles that are supported on alumina show clear images even in the presence of alumina. The nanoparticles are randomly distributed on the support and 90% of them are found to have TO shape with a size range of 8-10 nm. This result is in good agreement with those obtained in the absence of alumina and reported by our group (36). The particle size of the TO platinum is larger than the alumina pore aperture (5.8 nm) from which it can be concluded that the nanoparticles are located on the external surfaces of the alumina support.

3.2. Catalysis of propene hydrogenation

To evaluate the catalytic activity of the nanoparticles, the hydrogenation of gaseous propene was selected as a test reaction. The propene hydrogenation was carried out in a batch reactor. Prior to the reaction, the catalyst was preheated to 210 C for 2 h under an

Ar flow and then evacuated under high vacuum at this temperature for 10 min. This treatment is carried out in order to remove the capping material, water and volatile impurities (37).

The hydrogenation experiments were typically run in the presence of 0.12 g of TO Pt/Al_2O_3 mixture which is 0.078 % by wt of platinum. Propene (24 torr), and hydrogen (165 torr) were then added and the mixture was heated to the specified temperature in the 30-80 C range. An aliquot of the reaction mixture was taken out at different reaction times and were analyzed by mass spectrometry (VG Analytical, 70-SE). The relative intensities of propane to propene mass peaks in the hydrogenation reaction were calibrated from known standard propene/propane gas mixtures. The relative mass peak intensities of propene to propane, observed at each time during the catalyzed reaction, were converted to concentration by use of a predetermined calibration curve.

The kinetic studies were carried out in following manner. First, propane concentration *vs* time is plotted at each temperature studied (Figure 6-2). The reaction rates as a function of time are determined from the tangent of the slopes of the plots at different reaction times. These rates *vs* time are then plotted to determine the initial rates

for each temperature by extrapolating to zero time (Figure 6-3). The reaction order for each of the reactants (the propene and hydrogen) and thus the rate law is obtained from the dependence of the initial rates on the concentration of H_2 and propene at 40 C. The rate constant (k) at different temperatures is then calculated from the initial reaction rate, the rate law, the corrected initial H_2, and propene concentrations at each temperature. An Arrhenius plot is then used to determine the value of the activation energy (Figure 6-4).

The hydrogenation reaction on platinum catalyst is well studied in terms of specific catalytic activity, kinetic reaction law, and activation energy (38, 39). However, effects of platinum nanoparticle shape and capping material on the value of the activation energy in the propene hydrogenation have not been studied. Under our mild reaction conditions, propane is the only reaction product detected by the mass spectrometer. These observations are in agreement with the work of Bond et al. (40) who has shown that platinum metal is an effective catalyst to selectively convert propene to propane.

Figure 6-2 shows a plot of propane concentration *vs* reaction time in the propene hydrogenation over TO Pt-deposited on alumina in the temperature range of 30-80 C. The propane concentration is found to increase almost linearly with time in the range of 30-50

C but in the 60-80 C range, the concentration tends to level off slowly and almost reaches constant value within 8 min. The slope (tangent) of these curves at any time gives the instantaneous rate of the reaction at this time. In order to determine the initial rate, these slopes are plotted as a function of time and extrapolated to zero time at each temperature. The results are shown in Figure 6-3 and the calculated initial rates at different temperatures are given in Table 6-1. From Figure 6-3 it is obvious that above 50 C , the apparent rate of production of propene drops to almost zero in ~8 minutes. The apparent constancy of the product could be due to reaching equilibrium in which the rate of the dehydrogenation of propane becomes equal to the forward hydrogenation reaction. It could also result from poisoning of the catalyst surface. The fact that we did not observe any dehydrogenation of propane on this catalyst at these temperatures suggests that the surface gets poisoned due to secondary reactions that become fast at temperatures higher than 50 C. It is well known that Pt single crystal catalysts involved in hydrogenation reactions can build up carbonaceous deposits on the surface leading to deactivation(41,42). UHV studies by Somorjai et al have found that these layers build up on the surface and can interfere with the hydrogenation of organic molecules(42).

Because of the similarities between the hydrogenation of propene and the hydrogenation reaction of ethylene, such a process could conceivably occur at the surface of the nanoparticles. In the case of small nanoparticles, the highly active nature of the surface could make them more susceptible to this type of poisoning.

The reaction is assumed to follow the reaction rate law:

$$\text{Initial Reaction Rate} = k\,[C_3H_6]^{\alpha}\,[H_2]^{\beta}$$

Where α and β are the order of the reaction with respect to C_3H_6 and H_2, respectively. By determining the initial rates at different reactant concentrations, the α and β are found to be 0.13 and 0.58 respectively. These values are quite similar to those reported by Cocco et al. (43) for the catalysis using Pt on SiO_2 and TiO_2, suggesting a similar mechanism.

The specific rate constant *k* at different temperatures is calculated from these initial reaction rates, the reaction order, and the corrected initial H_2 and propene concentrations at the different temperatures. This is shown in Table 1. Figure 6-4 gives the Arrhenius plot of the natural logarithm of the rate constant *vs* 1/T for the reaction catalyzed by TO

Pt/Al_2O_3. As shown, normal Arrhenius behavior is observed in the temperature range of 30-80 C. The activation energy of the reaction is calculated to be 8.4 ± 0.2 kcal/mol from the observed slope of the linear part of the Arrhenius plot. The fact that all the points fall on the same straight line, even the ones above 50 C, suggest that the initial rates represent the hydrogenation reaction. The secondary reactions, leading to surface poisoning, build up at slightly longer times than zero time.

Other groups (43, 44) have reported the activation energy and reaction orders with respect to propene and hydrogen in the propene hydrogenation catalyzed by platinum supported on silica and titania. The supported platinum particles have been prepared by impregnation/ion-exchange methods by immersing the calcined supports in an aqueous or organic solution of platinum precursors such as H_2PtCl_6 (44) and $Pt(allyl)_2$ (43), without the addition of capping material. The platinum catalysts are reduced in flowing of hydrogen at about 450 C. These methods typically give amorphous nanoclusters although there is no detailed description about the particle shapes. From reviewing the work on the propene hydrogenation reported, it is found that the reaction orders for propene and hydrogen converge to 0 and 0.5 respectively and the activation energy ranges from 10 to

14 kcal/mol (43,44). The activation energies were found to be dependent upon the type of support (silica, titania) and the structure (anatase, rutile) due to the different interactions between the platinum and the support giving different electronic effects (43, 44). Otero-Schipper et al. (44) showed that the activity increases as the percentage of platinum exposed increases. The fact that the activation energy is independent of the percentage of platinum exposed while the overall activities vary suggests an activity compensation in which variations in the activity are due to variations in the preexponential factor. Thus they correlated the activity measured by the turnover frequency to the fraction of atoms on edges and corners of the exposed crystallite. They found that the turnover frequency increases linearly as the ratio of edge and corner atoms to total exposed atoms increases. It is believed that, in general, the chemical activities of platinum particles with different shapes are sensitive not only to the surface facets but also on the atomic structures, such as steps, ledges and defects (45). The TO platinum nanoparticles are mainly defined by the {100}, {111}, and {110} facets, on which numerous atom-high surface steps, ledges and kinks have been observed (45). These atomic-scale fine structures of the surfaces of the TO platinum nanoparticles are expected to have lower activation energy than those

reported by others.

The turnover frequency was calculated by determining the moles of surface atoms per particle. This was done using the TEM measurements of the particles size and the geometric relationship shown by Benfield et al (46) since the particles are of a cubic close packed cuboctahedra. The cuboctahedra are made up of complete shells of atoms, the number of which can be calculated from known equations (46) and the TEM data. Using this geometric relationship, the number of total surface atoms per particle and therefore, the moles of surface atom available for reaction, can be calculated. However, it was assumed that all of the surface atoms are available for reaction. Similar methodology has been followed to correlate the particle size and geometric structure in electrocatalysis(47) and organic reactions.(48)

For quantitative understanding, the catalytic activity in terms of turnover frequency (TOF) is calculated and compared to that reported by others. Our catalyst shows TOF of 0.62 mol_{C3H8}/mol_{Pt}, s at 70 C. Although some workers have published papers about the hydrogenation of propene over platinum nanoparticles supported on inorganic materials, they did not give the catalytic activities in terms of TOF. Therefore, we compare our TOF

to that obtained for similar reaction conditions using the same group metal, palladium. Ciebien et al. (49) synthesized palladium nanoclusters within diblock copolymer films and applied to the hydrogenation of propene. Maximum TOF of 0.021 mol_{C3H8}/mol_{Pt}, s was obtained at 120 C in a concentration ratio of 2:1 hydrogen to propene pressure. Our catalyst shows much higher activity. Although the deposited active metals are different, the reason might be ascribed to the surface irregularities, steps, ledges, and kinks of the TO platinum deposited. Of course, this high catalytic activity of our TO Pt particles is the reason for the rapid poisoning of the surface during the reaction.

Capping materials such as polyacrylate (36, 50) and poly(N-vinyl-2-pyrrolidone) (51,52) have been typically used as stabilizers for protecting these nanoparticles against aggregation and as a controller of the platinum nanoparticle shapes (TO, cubic, and tetrahedral). This is controlled by changing the ratio of the concentration of the capping material to that of the platinum precursor. Although the capping material has advantages like those described above, it is expected that they have a negative effect due to the partial covering of the active sites of the nano-sized metal particles. Nevertheless many studies have been carried out on the hydrogenation reaction over nanometal particles

capped with polymers (51-53).

Polyacrylate-capped TO Pt/Al_2O_3 samples were studied by FT-IR before and after thermal treatment at 210 C or 310 C under the flow of argon to investigate the influence of the polymer quantity on the catalytic activity of the propene hydrogenation. The results are shown in Figure 6-5. Polyacrylate (Figure 6-5a) has strong absorption bands at 1570 and 1406 cm^{-1} assigned to the asymmetric and symmetric stretching vibrations of the COO^- moiety, respectively. The peak at 1456 cm^{-1} is assigned to the CH_3 rocking vibration (54). Characteristic bands of alumina (Figure 6-5b) are observed at 1643 and 1400 cm^{-1}, which are clearly resolved from the polymer bands. As-synthesized TO Pt/Al_2O_3 exhibits physisorbed and chemisorbed bands at 1570 and 1561 cm^{-1}, respectively as shown in Figure 6-5c. From this observation, some polymers act as stabilizer to protect against aggregation through the chemical attachment of COO^- of the polyacrylate onto platinum nanoparticle surfaces. The others are physically adsorbed on the TO Pt/Al_2O_3. Figure 6-5d, shows the FT-IR of the sample that was heated at 210 C for 2 h with flowing of argon gas followed by pumping under vacuum (10^{-3}-10^{-4} torr) for 10 min. This shows the chemisorbed polymer bands with reduced intensity when compared

to those of as-synthesized TO Pt/Al_2O_3. On the other hand, the physisorbed polymer is almost completely eliminated. The polyacrylate used for preparation of TO shaped platinum nanoparticles was reported to be removed at 180 C and the particle shape is not transformed until 350 C (37). This result is in contrast with that concluded from our FT-IR. The reason might be that the TEM experiment was detecting the physisorbed polymer and could not detect the chemisorbed component. Furthermore, the high vacuum used (10^{-9} – 10^{-11} torr) might have been effective in removing a large fraction of the polymer. Temperature treatment was increased up to 310 C. The polymer is found to remain due to the strongly bound chemisorbed polymer. As an alternative method, the sample was calcined under air atmosphere at 310 C for 2 h. The polymer bands were completely removed as indicated in Figure 6-5f.

The TO Pt/Al_2O_3 catalysts were treated under different conditions present different TOF (indicated at 30 C) depending on the quantity of the polymer (Figure 6-6) The TOF obtained after thermal treatment at 210 C is found to increase by about 80 % as compared to that of the as-synthesized catalyst. This is attributed to the complete removal of the physisorbed polyacrylate which covered the surface of the active site of platinum

nanoparticles. The TO Pt/Al_2O_3 heated at 310 C shows ~11 % enhancement over that heated at 210 C. This is due to an increase in the exposed surface resulting from the dissociation of the chemisorbed polymer as suggested by the FT-IR results. The polymer-removed TO Pt/Al_2O_3 by air calcination exhibits a 30 % reduction in the catalytic activity compared to that treated in argon gas atmosphere. The reason for this could be due to the possible oxidation of the platinum surfaces in the air calcinated catalyst

4. Conclusions

The platinum nanoparticles were synthesized by using K_2PtCl_4 in the presence of polyacrylate as capping material and deposited on nanoporous alumina by impregnation at room temperature. TEM images showed that the nanoparticles are mainly TO shape with size range of 8-10 nm. These are randomly dispersed on the external surface of alumina, since the particle size is larger than the alumina pore aperture (5.8 nm).

The TO Pt/Al_2O_3 catalyst was used for the propene hydrogenation to evaluate its catalytic activity as measured by the value of its activation energy and TOF. The

activation energy is found to be 8.4 ± 0.2 kcal/mol, which is lower than those values reported by others on other platinum particles (10-14 kcal/mol). However, for experiments above 50 C, the activity of the particles degraded to zero after only a few minutes, suggesting a poisoning process on the surface of the particles. Both the lower activation energy and the rapid poisoning of the catalyst surface at ≥50 C suggest that Pt atoms on the surface of the TO nanocatalyst are very active (reactive) . They might be due to the facets, edges, corner and defects present in the TO nanoparticles.

Polyacrylate-capped TO Pt/Al_2O_3 samples, before and after thermal treatment, are characterized by FT-IR with and without thermal treatment in order to investigate the influence of the polymer quantity on the catalytic activity of the hydrogenation reaction. Even under high vacuum at 310 C, the chemisorbed polymer is found to be strongly bound to the surface of the particles. The catalytic activity increases as the amount of capping polymer is removed.

Acknowledgements

Financial support of this work was from the Julius Brown Chair Research Fund at

Georgia Tech. We wish to thank Colin Heyes for proofreading the manuscript.

References

1.Somorjai, G.A. *in* "Introduction to Surface Chemistry and Catalysis", John Wiley & Sons, Inc., New York, 1994, and references therein.

2. Langmuir, I., *J. Am. Chem. Soc*. **40**, 1361 (1918)

3. Donnelly, R. P., Hinshelwood, C.N., *J. Chem. Soc*. 1727 (1929)

4. Hinshelwood, C. N., Burk, R. E. J. Chem. Soc. **127,** 2896 (1925)

5. Breakspere, R. J.,Eley, D. D., Norton, P. R., *J. Catal*. **27** , 215 (1972)

6. Eley, D. D., *Catalysis: Hydrogenation and Dehydrogenation* **3** , 49 (1955)

7 Mikovsky, R. J., Boudart, M., Taylor, H.S., *J. Am. Chem. Soc*. **76**, 3814 (1954)

8. Hayes, K. E., Taylor, H. S., *Z. physik. Chem. (Frankfurt)* **15,** 127 (1958)

9. Woodman, J. F., Taylor, H. S., Turkevich, J. *J. Am. Chem. Soc*. **62**, 1397 (1940)

10. Tucholski, T.; Rideal, E. K.. *J. Chem. Soc*. 1701 (1935)

11. Rideal, E. K.. *Chem. Soc.* **121,** 309 (1922)

12. Addy, J.; Bond, G. C.. *Trans. Faraday Soc*. **53**, 388 (1957)

13. Bond, G. C. *Trans. Faraday Soc.* **52**, 1235 (1956)

14. J.W. Döbereiner, *J. Chem. (Schweiger)* **38**, 321 (1823)

15. J.W. Döbereiner, Ann. Phys.(Gilbert) **74**, 269 (1823)

16. Aiken III, J. D., and Finke, R. G., *J. Mol. Catal. A: Chem.* **145**, 1 (1999).

17. *In* "Clusters and Colloids" (Ed; G. Schmid). VCH, Weinheim 1994.

18. Rao, C. N. R., Kulkarni, G. U., Thomas, P. J., and Edwards, P. P., *Chem. Soc. Rev.* **29**, 27 (2000).

19. Schmid, G., and Chi, L. F., *Adv. Mater.* **10**, 515 (1998).

20. Henglein, A., *Chem. Rev.* **89**, 1861 (1989).

21. Schmid, G., *Chem. Rev.* **92**, 1709 (1992).

22. Lewis, L. N., *Chem. Rev.* **93**, 2693 (1993).

23. Rampino, L. D., and Nord, F. F., *J. Am. Chem. Soc.* **63**, 2745 (1942).

24. Bond, G. C., *Trans. Faraday Soc*. **52,** 1235 (1956)

25. Hwang, C.-B., Fu, Y.-S., Lu, Y.-L., Jang, S.-W., Chou, P.-T., Wang, C.R., and Yu, S.J., *J. Catal*. **195**, 336 (2000).

26. Chen, C-W., Serizawa, T., and Akashi, M., *Chem. Mater.* **11**, 1381 (1999).

27. Jackson, S. D., McLellan, G. D., Webb, G., Conyers, L., Keegan, M. B. T.,

Mather, S., Simpson, S., Wells, P. B., Whan, D. A., and Whyman, R., *J. Catal*. **162**, 10 (1996).

28. Jacobs, G., Ghadiali, F., Pisanu, A., Borgna, A., Alvarez, W. E., and Resasco, D. E., *Appl. Catal. A* **188**, 79 (1999).

29. Englisch, M., Jentys, A., and Lercher, J. A., *J. Catal*. **166**, 25 (1997).

30. Cocco, G., Campostrini, R., Cabras, M. A., and Carturan, G., *J. Mol. Catal*. **94**, 299 (1994).

31. Hirai, H., Wakabayashi, H., and Komiyama, M., *Bull. Chem. Soc. Jpn*. **59**, 545 (1986).

32. Claus, P., and Hofmeister, H., *J. Phys. Chem. B* **103**, 2766 (1999).

33. van Hardeveld, R., and Hartog, F., *Surf. Sci*. **15**, 189 (1969).

34. Henglein, A., Ershov, B. G., and Malow, M., *J. Phys. Chem.* **99**, 14129 (1995).

35. Gai, P. L., Goringe, M. J., and Barry, J. C., *J. Microscopy* **142**, 9 (1986).

36. Li, Y., Petroski, J., and El-Sayed, M. A., *J. Phys. Chem*. **104**, 10956 (2000).

37. Wang, Z. L., Petroski, J. M., Green, T. C., and El-Sayed, M. A., *J. Phys. Chem. B* **102**, 6145 (1998).

38. Segal, E., Madon, R. J., and Boudard, M., *J. Catal*. **52**, 45 (1978).

39. Zaera, F., and Somorjai, G. A., *J. Am. Chem. Soc*. **106**, 228 (1984).

40. Bond, G. C., *in* "Catalysis by Metals,"Academic Press, New York, 1962.

41. Somorjai, G.A. and Zaera, F., *J. Phys. Chem*. **86**, 3070 (1982).

42. Salermon, M. and Somorjai, G.A., *J. Phys. Chem*. **86**, 341 (1982)

43. Cocco, G., Campostrini, R., Cabras, M. A., and Carturan, G., *J. Mol. Catal*. **94**, 299 (1994).

44. Otero-Schipper, P. H., Wachter, W. A., Butt, J. B., Burwell, R. L., and Cohen, J. B., *J. Catal*. **50**, 494 (1977).

45. Wang, Z. L., Ahmad, T. S., and El-Sayed, M. A., *Surf. Sci*. **380**, 302 (1997).

46. Benfield, R. E. *J. Chem. Soc., Faraday Trans.* **1992**, *88*, 1107

47. Mukerjee, S.; McBreen, J. *J. Electroanal. Chem.* **1998**, *448*, 163

48. Le Bars, J.; Specht, U.; Bradley, J. S.; Blackmond, D.G. *Langmuir* **1999**, *15*, 7621

49. Ciebien, J. F., Cohen R. E., and Duran, A., *Supramolecular Science* **5**, 31 (1998).

50. Ahmadi, T. S., Wang, Z. L., Green, T. C., Henglein, A., and El-Sayed, M. A., *Science* **272**, 1924 (1996).

51. Liu, M., Yu, W., Liu, H., and Zheng, J., *J. Colloids Int. Sci*. **214**, 231 (1999).

52. Shiraishi, Y., Nakayama, M., Takagi, E., Tominaga, T., and Toshima, N., *Inorg. Chim. Acta*, **300**, 964 (2000).

53. Lu, P., and Toshima, N., *Bull. Chem. Soc. Jpn* **73**, 751 (2000).

54. Zinola, C. F., Gomis-Bas, C., Estiu, G. L., Castro, E. A., and Arvia, A. J., *Langmuir* **14**, 3091 (1998).

Table 6-1. Initial rates and rate constants of propene hydrogenation over truncated octahedral Pt/Al_2O_3 thermally pretreated at 210 ^oC at different temperatures.

T (K)	Initial rate ($/10^{-6}$ mol L^{-1} s^{-1})	$[C_3H_6]_{Initial}$ ($/10^{-3}$ M)	$[H_2]_{Initial}$ ($/10^{-3}$ M)	Rate constant ($k/10^{-4}$)
	1.18	1.27		0.44
303	1.76	1.23	8.73	0.67
313	2.58	1.19	8.45	1.0
323	3.56	1.16	8.19	1.42
333	5.46	1.12	7.95	2.22
343			7.71	

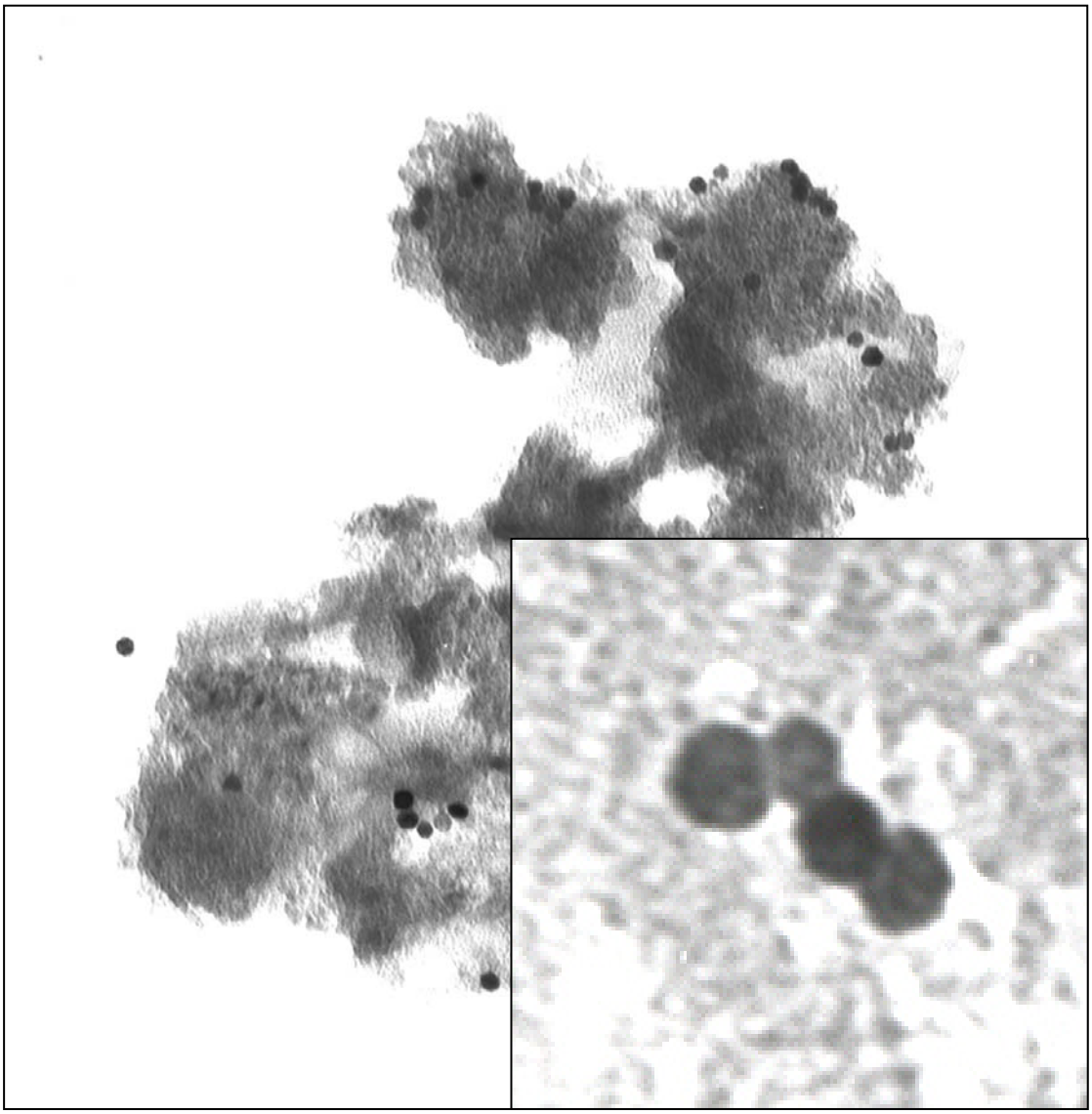

Figure 6-1. TEM images of (a) TO Pt/Al_2O_3, synthesized with a concentration ratio of 1:5 platinum complex to polyacrylate following impregnation on alumina, (b) enlargement of TO Pt/Al_2O_3.

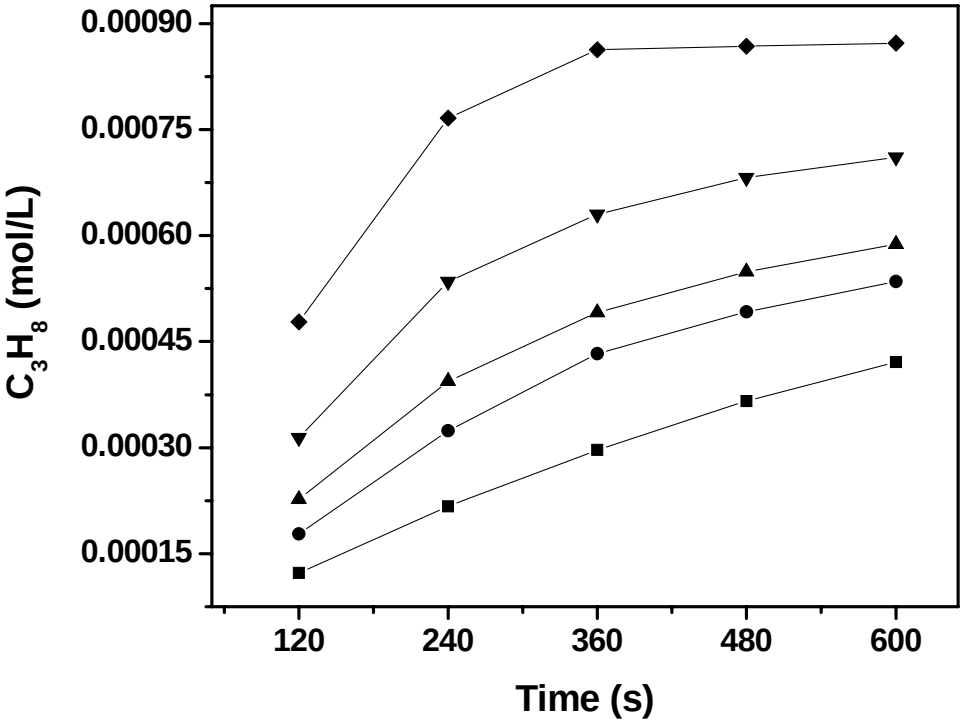

Figure 6-2. Propane concentration for temperature-dependant propene hydrogenation over TO Pt/Al_2O_3 catalyst as a function of reaction time: (a) at 30 ^oC, (b) at 40 ^oC, (c) at 50 ^oC, (d) at 60 ^oC, and (e) at 70 ^oC.

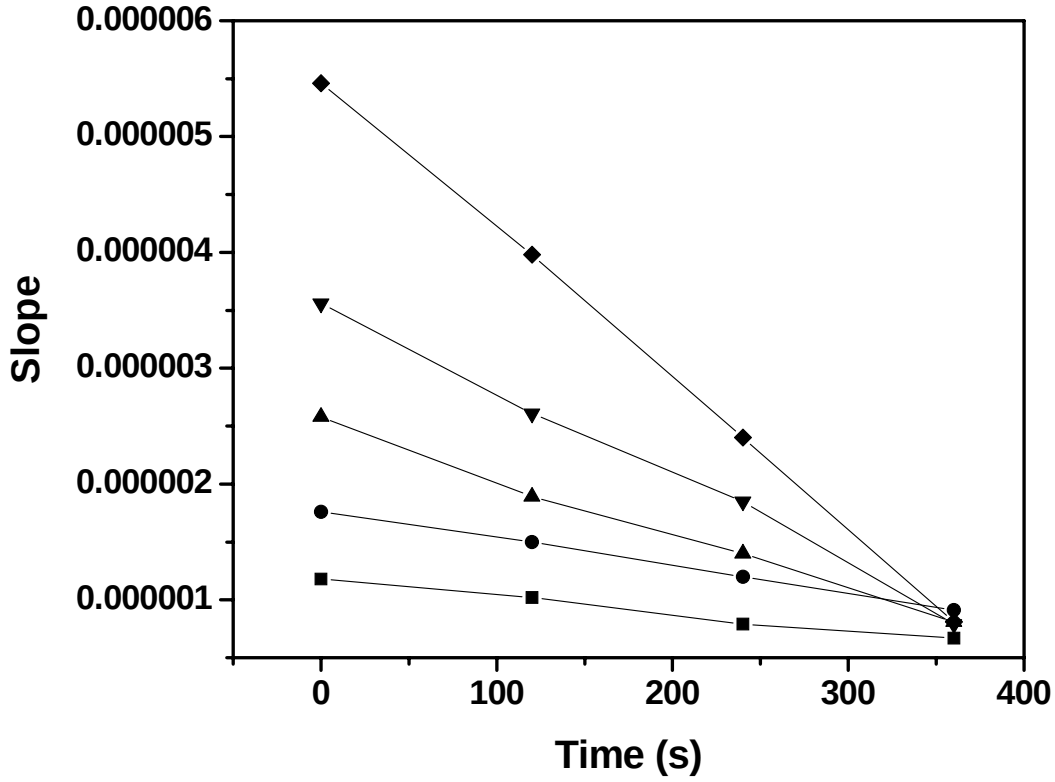

Figure 6-3. Slope of propane concentration for temperature-dependant propene hydrogenation over TO Pt/Al_2O_3 catalyst as a function of reaction time: (a) at 30 ^oC, (b) at 40 ^oC, (c) at 50 ^oC, (d) at 60 ^oC, and (e) at 70 ^oC.

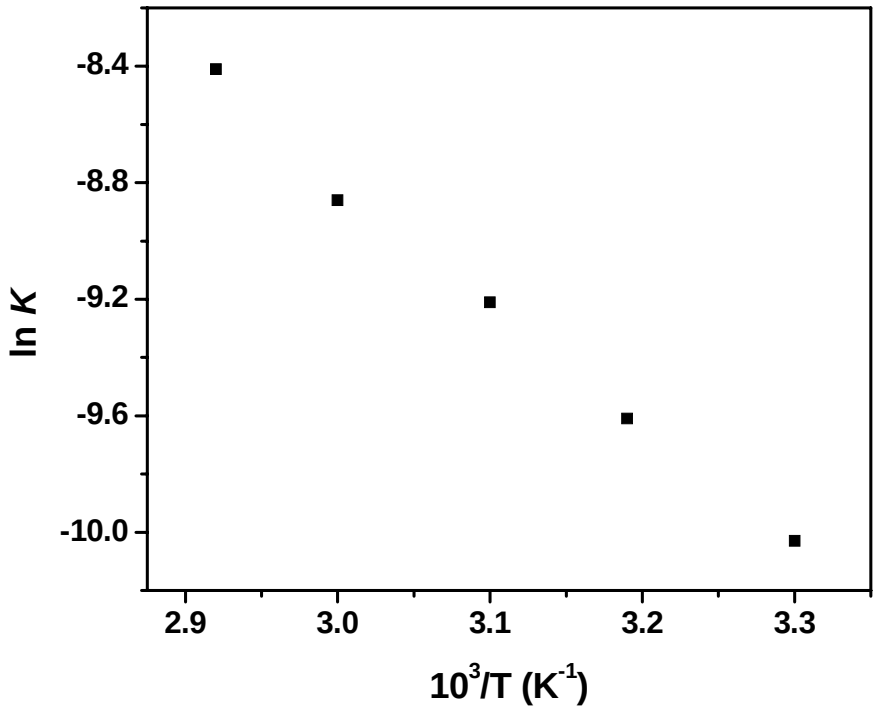

Figure 6-4. Arrhenius plots of the propene hydrogenation over TO Pt/Al_2O_3 catalyst.

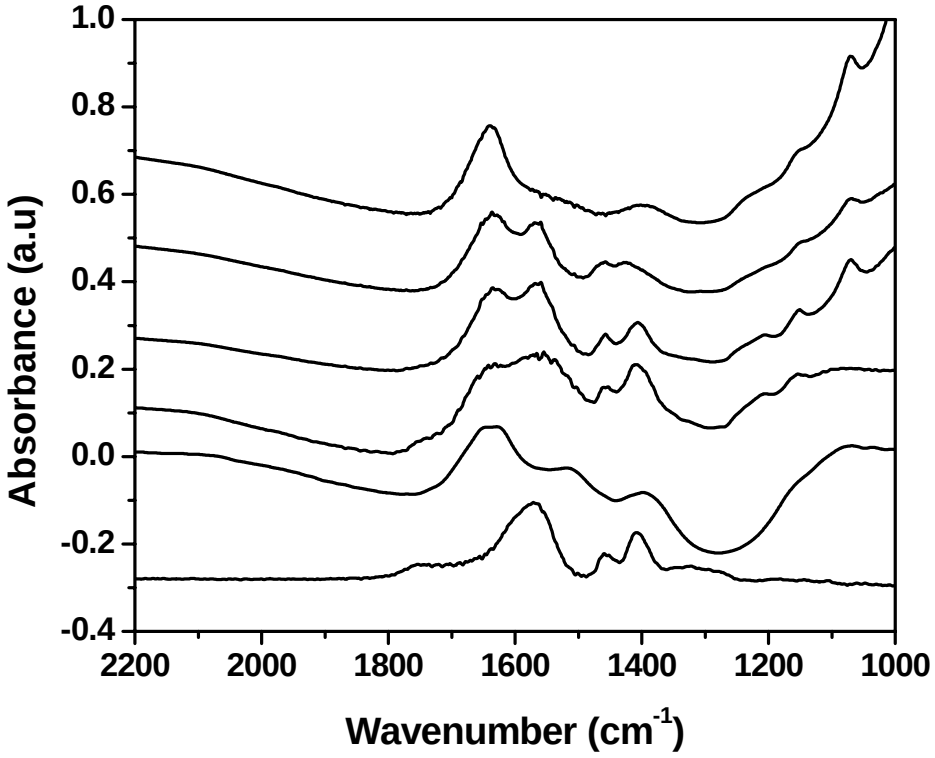

Figure 6-5. FT-IR spectra of (a) polyacrylate, (b) alumina, (c) as-synthesized TO Pt/Al_2O_3, (d) heated (c) sample at 210 ^oC for 2 h under flowing argon and evacuated at same temperature for 10 min., (e) thermally treated (c) sample at same conditions as (d) sample except at 310 ^oC, (f) thermally oxidized (c) sample at 310 ^oC for 2 h.

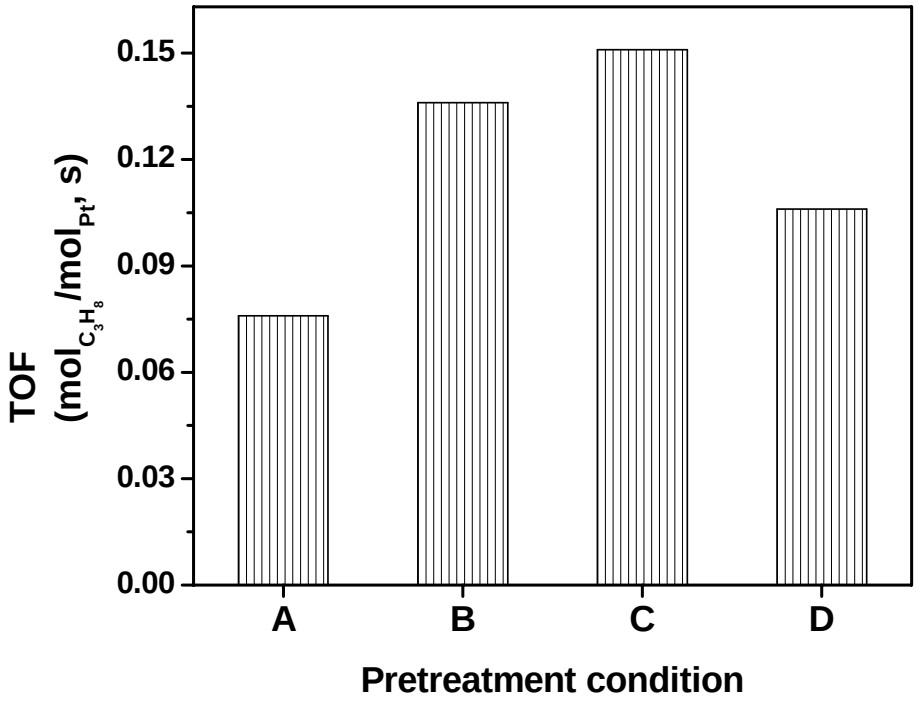

Figure 6-6. Effect of catalyst pretreatment on catalytic activity (indicated at 30 ^{o}C for 4 min.) over TO Pt/Al_2O_3; (a) as-synthesized TO Pt/Al_2O_3, (b) heated (a) sample at 210 ^{o}C for 2 h under flowing argon and evacuated at same temperature for 10 min., (c) thermally treated (a) sample at same conditions as (b) sample except at 310 ^{o}C, (d) thermally oxidized (c) sample at 310 ^{o}C for 2 h.

Chapter VII

Characterization of Pt Nanoparticles Encapsulated in Al_2O_3 and Their Catalytic Efficiency in Propene Hydrogenation

Abstract

Pt nanoparticles supported in nanoporous Al_2O_3 catalyst are prepared by reduction of K_2PtCl_4 solution using H_2 in the presence of Al_2o_3 and poly(acrylic acid) as capping material. After thorough washing with water to remove Pt nanoparticles located on the external surface of the Al_2O_3 and drying at 70^oC for 12 h, they were used in propene hydrogenation to evaluate catalytic activity as measured by the value of the activation energy in the temperature range between 30 and 90 ^oC. The Pt nanoparticles are characterized by using transmission electron microscopy (TEM). The particles in Pt/Al_2O_3 are found to be encapsulated and uniformly dispersed inside the Al_2O3; however, the size and shapes are not clearly seen. After extraction of the Pt nanoparticles from the Al_2O3 channels by using as ethanol-diluted HF solution, various shapes such as truncated octahedral, cubic, tetrahedral, and spherical with a size around 5 nm are observed. The encapsulated particles have various but are smaller in size than those prepared in K_2PtCl_4 solution with the polyacrylate in the absence of Al_2O_3. Using FT-IR studies, the capping material initially used in Pt/Al_2O_3 is not found in the Al_2O_3 channels. This might be due to the fact that the polymer (average MW 2100) is too large to be

accommodated within the Al_2O_3 pored. The nanopores of Al_2O_3 have several roles in the synthesis of these nanoparticles. It allows for the uniform dispersion and encapsulation of Pt nanoparticles. It controls the Pt sizes with narrow distribution that is determined by the pore dimension (5.8 nm). It protects against metal particle aggregation and produces various shapes even in the absence of the capping material. Using these Pt nanoparticles, the catalysis of the hydrogenation of propene was studied. The initial rates, reaction order, rate constants, and activation energy for the hydrogenation are determined by use of mass spectrometric techniques. The activation energy is found to be 5.7 kcal/mol, which is about one-half that previously reported for catalysis by Pt metal deposited in SiO_2 and TiO_2 synthesized by using H_2PtCl_4 and $Pt(allyl)_2$ by impregnation method

Introduction

Metal nanoparticles are of considerable interest because they can exhibit physical and chemical properties, due to quantum size effects, that differ from those of bulk metals. They possess unique electronic, optical, and catalytic properties that are different from bulk macrocrystallites.[1-4] These nanoparticles are presently under intensive study for applications in optoelectronic devices,[5] ultrasensitive chemical biological sensors,[6-8] and as catalysts in chemical and photochemical reactions.[9,10] In particular, they have a characteristic high surface-to-volume ratio, and consequently large fractions of the metal atoms are on the surface and thus are accessible to reactant molecules and available for

catalysis.[11] They have been used as catalysts[12,13] in hydrogenation, hydroformylation, hydration, and various other reactions.

Heterogeneous catalysts, in particular, porous materials such as alumina, silica, and zeolites, have many advantages as supports because of their high surface areas, shape/size selectivity, and easy separation from the reaction mixtures. For these reasons, the use of Pt nanoparticles deposited on such porous materials has been increased recently.[14-17] These catalysts have typically been prepared by impregnation/ion-exchange methods by immersing the calcined porous materials in an aqueous solution of various Pt precursors such as H_2PtCl_4, [14] $Pt(NH_3)_4(NO_3)_2$,[15] $Pt(AcAc)_2$,[15] $Pt(NH_3)_4(OH)_2$,[16] and $Pt(allyl)_2$.[17] The dried Pt catalysts are calcined in flowing air and reduced in flowing H_2 around 450^{o}C. These methods are very complex, take a long time, and give mainly amorphous nanoparticles. These Pt nanoparticles have been used in the catalysis of unsaturated hydrocarbon hydrogenation and aromatization to understand the dependence of the catalytic propertied on the particle size.[18]

Another method to make metal nanoparticles has used capping materials, polyacrylate and poly(N-vinyl-pyrrolidone)(PVP), in the precursor solution.[19,20] The capping material has roles not only to prevent particle aggregation, but also to control shape and size.[19] Relatively speaking, the latter method is simple and can obtain good shaped particles.

The hydrogenation of various hydrocarbon compounds has been employed from time to time as a convenient probe reaction for evaluating the catalytic properties of

support Pt metals. Platinum is a superior catalyst for a variety of hydrocarbon conversion reactions.[21] Under suitable conditions (reactant composition, pressure, and reaction temperature) platinum is active for hydrogenation. Propene hydrogenation has also been used for this purpose.[17,22]

In the present study, Pt nanoparticles deposited in nanoporous Al_2O_3 are synthesized using K_2PtCl_4 solution and poly(acrylic acid) as the capping material in the presence of Al_2O_3. The particle size/shape and capping material are clearly characterized by transmission electron microscopy (TEM) and FT-IR. The catalytic activity, as measured by the value of the activation energy, is studied for the heterogeneous hydrogenation of propene and compared with literature values of others synthesized by different methods and on different support material. The observed difference is discussed.

Experimental section

Chemicals. K_2PtCl_4 (99.99%) sodium polyacrylate (average MW 2100) and Al_2O_3 (neutral, surface area 155m^2/g, pore size 5.8 nm) were obtained from Aldrich. All solutions were prepared using doubly deionized water. Propene (99.9995%) and hydrogen (99.995%) were purchase from Matheson Company and used without further purification. The purity of the propene was checked by mass spectrometry.

Catalyst Preparation. The preparation method of the Pt/Al_2O_3 catalyst is similar to that used by Rampino and Nord[23] and Henglein et al.[24] except for the addition of Al_2O_3. A 5 g sample of Al2O3 was added to 250 mL of solution made by adding 1 mL of 0.1 M

sodium polyacrylate (capping material) to 249 mL of 8.0 x 10^{-5} M K_2PtCl_4. The initial concentration ratio of the K_2PtCl_4 to polyacrylate was 1:5. The pH of the solution was then adjusted to 7 with 0.1 M HCl and purged with Ar for 20 min. Pt complexes were reduced by bubbling H_2 for 5 min. The solution was left for 12 h in the dark. Subsequently, it was filtered, washed with 5 L of water, and dried at 70^{o}C for 12 h.

For comparison, Pt/Al_2O_3 catalyst without the addition of the poly(acrylic acid) was prepared under the same condition as that used in the presence of the polymer.

TEM and FT-IR Measurements. TEM was used to determine the particle size/shapes of Pt nanoparticles supported in Al_2O_3. For making a TEM sample of supported Pt on Al_2O_3 catalyst dried and washed after separation from the Pt/Al_2O_3 solution, it was suspended on ethanol (99.9 wt%) by ultrasonification for 1 h after grinding the Pt/Al_2O_3 and subsequently left in the Pt/Al_2O_3 solution for several hours. The suspended sample was deposited on a carbon grid by slow evaporation at room temperature. To clearly image the particles encapsulated in Al_2O_3, the particles must be extracted from the Al_2O_3 channels. A small amount of Pt/Al_2O_3 was added to a 20 wt. % HF solution diluted with ethanol. The Al2O3 gradually dissolved after stirring this solution. The Pt nanoparticles, in 20 wt. % HF solution, were separated and washed with ethanol several times via centrifuge. TEM images were taken using a JEM 100C operated at an acceleration voltage of 100kV at a magnification of 100K – 190K at room temperature. The particle size/shapes were determined from the enlarged TEM images.

FT-IR spectra are recorded on pellets made of the sample with a Bruker IFS 66/S FT-IR spectrometer. Typically, 100 scans were accumulated for each spectrum with 2 cm^{-1} resolution by OPUS 2.0 software. FT-IR spectra were recorded in the range of 2300 – 1000 cm^{-1}. Pressure was applied to the powder sample until the pellet made a clear disk.

Results and Discussion

A. Particle Characterization. Figure 7-1a shows a TEM image of the Pt/Al_2O_3 prepared from a 1:5 concentration ratio of K_2PtCl_4 to polyacrylate. In this figure, the Pt nanoparticles are shown as small black dots that are homogenously dispersed within the Al_2O_3 support. The Pt nanoparticles appear to be located within the Al_2O_3 channels (Al_2O_3 pore size is 5.8 nm) since the diameter of the Pt nanoparticles observed is less than 5 nm. No Pt particles are observed on the external surfaces. As indirect evidence, the diameter of Pt nanoparticles in solution prepared under the same conditions is about 8 nm,[25] which is larger in size than that of the Pt/Al_2O_3 pore aperture. Actually, the Pt/Al_2O_3 solution in the presence of the polymer as after the H_2 reduction for 12 h is colorless, which is quite different from those of Pt nanoparticles synthesized in solution in the absence of Al_2O_3 or SiO_3, otherwise, under the same synthetic conditions. The solution of the particles prepared in solution with no alumina or with silica gives a bright golden color; these observations can be explained as follows. Pt salt dissolved in water diffuses into the Al_2O_3 channel and strongly interacts and absorbs on Al_2O_3 channel walls.[26] Reduced Pt atoms begin nucleation and growth uniformly within the Al_2O_3 channel. In the case of Pt/SiO_2, however, though Pt precursor diffuses into the SiO_2

channels (pore size is 6 nm), there might not be any interaction between the precursor and the support and the growth takes place in solution with the polymer capping. Therefore, the color of the resultant solution is bright golden, which is the same as the solution of Pt nanoparticles with the capped polymer.

Encapsulated Pt particles were extracted from Al_2O_3 channels by dissolving the support with an HF solution. Figure 7-1b clearly shows Pt size and shapes, indicating various shapes such as truncated octahedral, tetrahedral, cubic, and spherical with a considerably narrow distribution of 4-5 nm size. The variety in shapes is quite different from that observed for samples prepared in solution with only capping polymer under the same conditions. In such a case, more than 90% of truncated octahedral Pt nanoparticles were normally observed.[25] This difference in particle shape distribution can likely be attributed to the influence of the Al_2O_3 channel used for the growth of Pt particles with different shapes.

To compare size/shapes of Pt nanoparticles formed by the encapsulation method and those prepared in solution, the Pt encapsulated in Al_2O3 was impregnated with Pt nanoparticle solution which was prepared from a 1:5 concentration ratio of K_2PtCl_4 to polyacrylate. The TEM images of the Pt particles extracted from the sample are shown in Figure 7-1c. First of all, a large difference in the size is clearly shown. Larger particles formed in the solution are in the range of 8 – 10 nm and are primarily truncated octahedral. On the other hand, encapsulated Pt particles show 4 -5 nm in size. This

suggests that in the encapsulated method, the particles grom in the pores. This limits their growth to be smaller than the pore size (5.8 nm).

Capping materials such as poly(acrylic acid)[19,25] and poly(N-vinyl-2-pyrrolidone)[27,28] have been typically used as stabilizer in making mono- or bimetallic nanoparticles for protecting aggregation of the metal itself. Specifically, poly(acrylic acid) can be used to control the shapes (tetrahedral, cubic, icosahedral) and sizes of Pt nanoparticles by changing the ratio of the concentration of the capping material to that of the Pt cations in aqueous solution.[19] Though the capping material has advantages such as described above, from a viewpoint of its application to catalysis, it is expected not to have a positive effect due to it partially covering active sites of the nanosized metal particle. Nevertheless many works have done the various hydrogenation reactions over nonmetal particles containing polymer. [27-29]

Our Pt/Al_2O_3, prepared using poly(acrylic acid) is characterized by FT-IR to investigate the influence of the polymer on the catalytic activity (shown in Figure 7-2). Poly(acrylic acid) (Figure 7-2a) has strong absorption bands at 1570 and 1406 cm^{-1} assigned to the asymmetric and symmetric stretching of the CO_2^- moiety, respectively , and at 1456 cm^{-1} due to the CH_3 rocking.[30] Characteristic bands of Al_2O_3 are observed at 1643 and 2400 cm^{-1}, which are clearly resolved from the polymer bands. Surprisingly, no polymer bands in our as-synthesized Pt/Al_2O_3 are detected. Since only Al_2O_3 characteristic bands are observed in the spectrum shown in Figure 7-2d. This does not look like the FT-IR spectrum of a mixture of the polymer and the Al_2O_3 shown in Figure

7-2c. It looks more like that of Pt/Al2O3 prepared in the absence of the polymer (shown in Figure 7-2f). It seems that the length of the polymer (average MW 2100) is too long to be accommodated into the Al2O3 channel. From the above results, it can be concluded that the nanoporous Al2O3 support fulfills four roles; (1) it gives uniform dispersion and encapsulation of Pt nanoparticles through strong interaction with the Pt salt, (2) it controls the Pt particles size and gives it narrow distribution as determined by the Al2O3 channel dimensions, (3) it prevents particle aggregation and allows the formation of various shapes such as truncated octahedral, tetrahedral, cubic, and spherical with a narrow distribution even in the absence of the capping material, (4) it provides a larger surface area for the deposition.

B. Catalytic Hydrogenation of Propene. To evaluate the catalytic activity, hydrogrnation of gaseous propene is selected as a test reaction. The propene hydrogenation was carried out in a batch reactor. Prior to the reaction, the catalyst was first preheated at 155^{o}C for 2 h under flowing Ar and then the reactor was evacuated and held at low pressure (and at the same temperature) for 10 minutes. This treatment was carried out in order to remove water and volatile impurities.

The hydrogenation experiments were typically run in the presence of 0.5 g of Pt/Al_2O_3, propene (24 torr), and hydrogen (165 torr) at 30 – 90 ^{o}C. The gaseous reaction mixtures were analyzed my mass spectrometry (VG Analytical, 70-SE). The mass spectrum is shown in Figure 7-3a. The peak at mass number 44.1 is assigned to propane, while the peak at 42.1 is assigned to propene with a small contribution of propane using a

known propane/propene gas mixture as a standard. The relative mass peak intensities of propene to propane, observed at any time during the catalyzed reaction, were converted to concentration ratios by using a calibration curve (shown in Figure 7-3b).

The kinetic studies were carried out in the following manner. First, a plot of propane concentration vs. time is constructed at each temperature studied. The reaction rates as a function of time are determined from the tangent of this plot at different times. These rates v time are then plotted to determine the initial rates at different temperatures by extrapolating these lines to zero time. The reaction orders for the propene and hydrogen reaction are obtained from the dependence of the initial rates on the concentration of H2 and propene at 40^{o}C. The rate constant (*k*) at different temperatures is then calculated from the initial reaction rate, the rate equation, the corrected initial H2, and propene concentrations at each temperature. An Arrhenius plot is then used to determine the value of the activation energy.

The hydrogenation reaction on Pt is quite well studied in terms of specific catalytic activity, kinetic law, and activation energy.[31,32] Under our mild conditions, propane is the only reaction product detected and no deactivation processes are observed during the reaction. These observations are in agreement with the work of Bond et al.[33] who has shown that Pt metal is an effective catalyst to convert propene to propane selectively. The C-C bond cracking/recombination of propene and propane over Pt/Al2O3 catalyst under out reaction conditions does not occur. Less than 1% of propane is found to dehydrogenate to produce propene at high temperatures in our reaction. The

Pt/Al2O3 catalyst gives the propene conversion of 16 – 39 % with 100% selectivity of propane in the reaction times of 9 min at 30 – 90 ^{o}C.

Figure 7-4 shows a plot of propane concentration vs reaction time in the propene hydrogenation over Pt encapsulation in Al_2O_3 in the temperature range of 30 – 90 ^{o}C. The propane concentration is found increase almost linearly with time in the range of 30 – 60 ^{o}C but in the 70 – 90 ^{o}C range, the concentration tends to level off slowly and almost reaches steady-state within 9 minutes. The slope (tangent) of these curves at any time gives the instantaneous rate of the reaction at this time. To determine the initial rate, these tangents (slopes) are plotted as a function of time and extrapolated to zero at different times to give the initial rates. The results are shown in Figure 7-5 and the calculated rates at different temperatures are given in Table 1.

The reaction is assumed to follow the reaction rate law:

$$\text{Initial reaction rate} = k[C_3H_6]^{\alpha}[H_2]^{\beta}$$

where α and β are the order of the reaction with respect to C_3H_6 and H_2 respectively. By determining the initial rates at different reactant concentrations, the α and β are found to be 0.03 and 0.75, respectively. These values are found to be quite similar to those reported by Otero-Schipper et al.[22] for the catalysis over Pd on SiO_2 and TiO_2, suggesting a similar mechanism. The specific rate constant k at different temperatures is calculated from these initial reaction rates, the reaction order, and the corrected initial H_2 and propene concentrations at the different temperatures shown in Table 7-1. Figure 7-6 gives the Arrhenius plots of the natural logarithm of the rate constant vs 1/T for the reaction

observed in the temperature range 30 – 90 ^{o}C. The activation energy of the reaction is calculated to be 5.7 kcal/mol from the observed slope of the linear part of the Arrhenius plot. The reaction was repeated twice, and the reproducibility is found to be satisfactory. The variance in the value of the activation energy is found to be less than 5%.

Until now, systematic studies to clarify the understanding of the effects of Pt nanoparticle size, shape and capping material (which is usually used in the preparation of shaped particles and to prevent aggregation) on the activation energy of propene hydrogenation have not been done. Several studies[17,22,34] have simply reported the activation energy for propene hydrogenation catalyzed by Pt on SiO_2 and TiO_2. Cocco et al.[17] prepared Pt particles supported on SiO_2 and on different TiO_2 structures, such as anatase and rutile, using $Pt(allyl)_2$ precursors reduced be H_2 in organic solution. The activation energies reported for this reaction are in the range of 12.2 – 14.9 kcal/mol. TiO_2 support shows a lower activation energy than those of SiO_2 and rutile TiO_2 indicates a lower value of 2.3 kcal/mol compared to that for anatase TiO_2 while the reaction orders for hydrogen and propene are almost the same. From the reported results, the activation energy appears to be dependent upon the support type and structure. Otero-Schipper et al.[22] reported 10.4 kcal/mol for the activation energy over Pt particles deposited on SiO_2 prepared using H_2PtCl_4 by impregnation. They suggested that the values of the activation energy and turnover number are proportional to the fraction of the metal exposed to reactants for similar hydrocarbon hydrogenation. The lowest value for the activation energy is 7.4 kcal/mol and was obtained by using 1 wt% Pt nanoparticles deposited on

external surfaces of SiO2 with an average particle diameter of 6.5 nm.34 The reaction orders for the hydrogen and propene were 0.5 and 0, respectively. These activation energies, except 7.4 kcal/mol, are about twice as large as our value.

There are three possible reasons for the lower activation energy observed in our system. The effect of support on the activation energy could be one. Another reason is the fact that we are using a batch reactor at a relatively high pressure. Mass transport effects could lead to lower activation energy. However, in the reaction of butane hydrogenation using Pt single crystals, it was found that the activation energy is ~10kcal/mol when using up to 500 Torr pressure.[35] The third reason for the lower activation energy in our Pt/Al_2O_3 studies could be the higher uniform dispersion of small, shaped, particles (less than 5 nm) in the Al_2O_3 channels due to strong interaction between the Pt precursor and the Al_2O_3 support. Small particles with specific shapes have edges, corners, epices, and their surfaces are expected to have many defects. Atoms places at the corners, edges, or at defect sites are expected to be highly catalytically active. In addition, having these particles in close contact with the Al_2O_3 support could add greatly to their catalytic activity.

Conclusions

Pt nanoparticles were encapsulated in an AL_2O_3 channel by reducing its $(PtCl_4)^{-2}$ with H2 in the presence of poly(acrylic acid). TEM images showed that the nanoparticles are mainly located inside the Al_2O_3 channel and are highly dispersed. After extraction of the Pt particles from the Al_2O_3 channel to observe clear images of the sizes and shapes,

various shapes such as truncated octahedral, cubic, tetrahedral, and spherical with narrow size distribution of around 5 nm are observed. Comparing to size/shapes of the Pt nanoparticles prepared in K_2PtCl_4 solution with polyacrylate (without Al_2O_3), the particles formed are found to have doubled in size with most truncated octahedral in shape. FT-IR results show that the capping material is not present upon the formation of Pt nanoparticles in the Al_2O_3 channel. It seems that the polymer length is too long to be accommodated by the Al_2O_3 channel. The nanoporous Al_2O_3 has four important roles in the synthesis of Pt nanoparticles; (1) it gives uniform dispersion and encapsulates them inside the channel due to the strong interaction with the Pt precursor, (2) it controls the Pt size distribution as the growth is limited by the narrow Al_2O3 channels, (3) it protects the particles against aggregation and allows for the formation of various shapes such as truncated octahedral, tetrahedral, cubic, and spherical even in the absence of capping material, (4) it provides larger surface for deposition.

The Pt/Al_2O_3 catalyst was used for the propene hydrogenation to evaluate its catalytic activity as measured by the value of its activation energy and compare it with other studies that used different supports. The activation energy is found to be 5.7 kcal/mol. This is about one-half the value of the activation energy reported by others. This may be attributed to the fact the particles are small and have shapes. Small nanoparticles with shapes have many active atoms present on edges, corners, and defective sites. This gives them highly catalytic properties. The use of Al_2O_3 support in close interaction with these particles could also account for the observed activity.

Acknowledgements. Financial support by the National Science Foundation (Grant No. CHE-9727633) is gratefully acknowledged. We also thank the staff of the mass spectrometry lab and the TEM Microscopy Center for providing the training necessary to carry out this research.

References

1) Schmidt, G. in *Clusters and Colloids*; VCH: Weinheim, 1994.
2) Lewis, L.N. *Chem. Rev.* **1993**, *93*, 2693.
3) Alivisatos, A.P. *Science* **1996**, *271*, 993.
4) Henglein, A. *Chem. Rev.* **1989**, *89*, 1861.
5) Colvin, V.L.; Schlamp, M.C.; Alivisatos,A.P. *Nature* **1994**, *370*, 354.
6) Emory, S.R.; Nie, S. *J. Phys. Chem. B* **1998**, *102*, 493.
7) Bruchez, M. Jr.; Moronne, M.; Gin, P.; Weiss, S.; Alivisatos, A.P. *Science* **1998**, *281*, 2013.
8) Chan, W.C.W.; Nie, S. *Science* **1998**, *281*, 2016.
9) Toshima, N.; Nakata, K.; Kitoh, H. *Inorg. Chim. Acta* **1997**, *265*, 149.

10) Schmidt, T.J.; Noeske, M.; Gasteiger, H.A.; Behm, R.J. *Electrochem. Soc.* **1998**, *145*, 925.

11) Chen, C.-W.; Serizawa, T.; Akashi, M. *Chem. Mater.* **1999**, *11*, 1381.

12) Weller, H. *Angew. Chem., Int. Ed. Engl.* **1993**, *32*, 41.

13) Henglein, A. *J. Phys. Chem* **199**, *97*, 5457.

14) Jackson, S.D.; McLellan, G.D.; Webb, G.; Conyers, L.; Keegan, M.B.T.; Mathers, S.; Simpson, S.; Wells, P.B.; Whan, D.A.; Whyman, R. *J. Catal.* **1996**, *162*, 10.

15) Jacobs, G.; Ghadiali, F.; Pisanu, A.; Borgna, A.; Alvarez, W.E.; Resasco, W.E. *Appl. Catal. A* **1999**, *188*, 79.

16) Englisch, M.; Jentys, A.; Lercher, J.A. *J. Catal.* **1998**, *166*, 35.

17) Cocco, G.; Campostrini, R.; Cabras, M.A.; Carturan, G. *J. Mol. Catal.* **1994**, *94*, 299.

18) Arai, M.; Takada, Y.; Nishiyama, Y. *J. Phys. Chem B* **1998**, *102*, 1968.

19) Ahmadi, T.S.; Wang, Z.L.; Green, T.C.; Henglein, A.; El-Sayed, M.A. *Science* **1996**, *272*, 1924.

20) Toshima, N.; Yonezawa, T.; Kushihashi, K. *J. Chem. Soc. Faraday Trans.* **1993**, *89*(14), 2537.

21) Somorjai, G.A. *In Introduction to Surface Chemistry and Catalysis*, Wiley: New York, 1994.

22) Otero-Schipper, P.H.; Wachter, W.A.; Butt, J.B.; Burwell, R.L.; Cohen, J.B. *J. Catal.* **1977**, *50*, 494.

23) Rampino, L.D.; Nord, F.F. *J. Am. Chem. Soc.* **1942**, *63*, 2745.

24) Henglein, A.; Ershov, B.G.; Malow, M. *J. Phys. Chem.* **1995**, *99*, 14129.

25) Li, Y.; Petroski, J.; El-Sayed, M.A. *J. Phys. Chem.* **2000**, *104*, 10956.

26) Tauster, S.J. *J. Acc. Chem. Res.* **1987**, *20*, 389.

27) Liu, M.; Yu, W.; Liu, H.; Zheng, J. J. *Colloids Int. Sci*. **1999**, *214*, 231.

28) Shiraishi, Y.; Nakayama, M.; Takagi, E.; Tominaga, T.; Toshima, N. *Inorg. Chim. Acta* **2000**, *300*, 964.

29) Lu, P.; Toshima, N. Bull. Chem. Soc. Jpn. **2000**, 73, 751.

30) Zinola, C.F.; Gomis-Bas, C.; Estiu, G.L.; Castro, E.A.; Arvia, A.J. *Langmuir* **1998**, *14*, 3091.

31) Segal, E.; Madon, R.; *Boudard, M. J. Catal.* **1978**, *52*, 45.

32) Zaera, F.; Somorjai, G.A. *J. Am. Chem. Soc*. **1984**, *106*, 228.

33) Bond, G.C.; In *Catalysis by Metals; Academic Press*: New York, 1962; Chapter 11.

34) Campostrini, R.; Carturan, G.; Baraka, R.M. *J. Mol. Catal.* **1993**, *78*, 169.

35) Yoon, C.;Yang, M.X.; Somorjai, G.A. *J. Catal*. **1998**, *176*, 35.

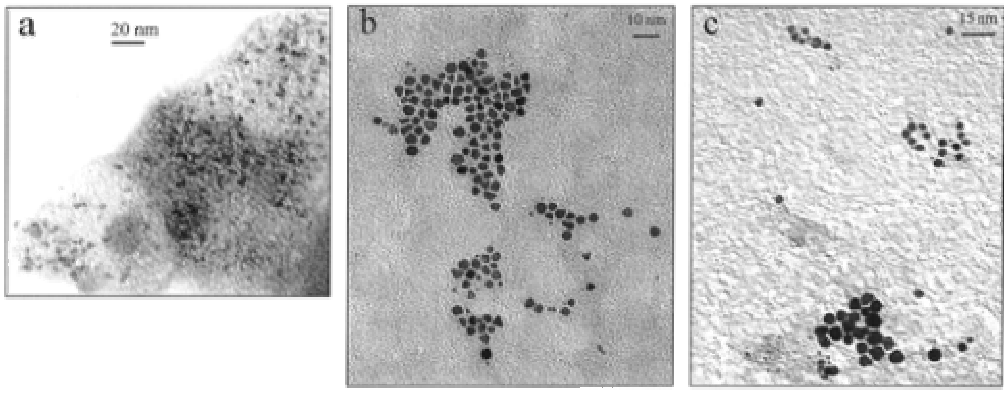

Figure 7-1. TEM images of (a) Pt nanoparticles synthesized in the presence of Al2O3 and polyacrylate with a concentration ratio of 1:% Pt to polyacrylate. (b) Pt nanoparticles extracted from (a) using 20 wt % HF solution, and (c) Pt particles extracted from sample, prepared by impregnation of (a) with Pt Particle solution synthesized with 1:5 concentration ratio of K_2PtCl_4 to polyacrylate.

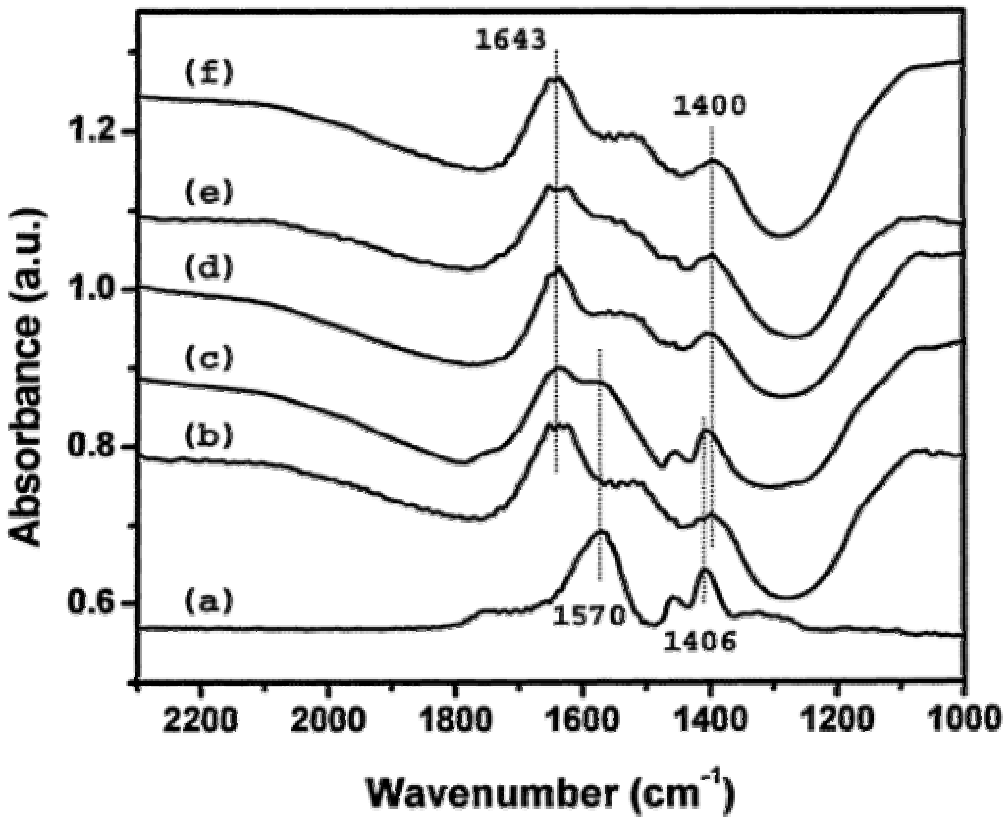

Figure 7-2. FT-IR spectra of (a) polyacrylate, (b) alumina, (c) mixture of polyacrylate and alumina, (d) as-synthesized Pt/Al_2O_3 with polyacrylate, (e) thermal treated (d) at 155^oC, and (f) as-synthesized Pt/Al_2O_3 prepared without polyacrylate.

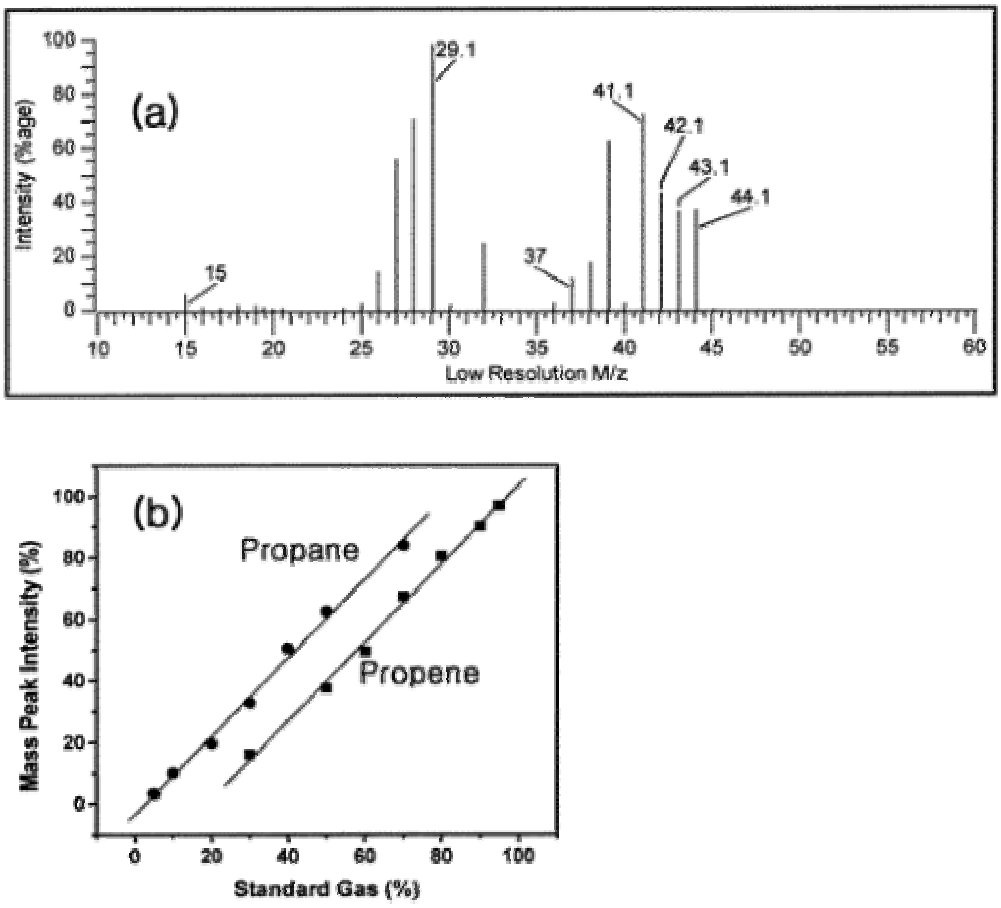

Figure 7-3. Mass spectrum of propene hydrogenation over Pt/Al_2O_3 catalyst (a) and calibration curve between propene and propane (b).

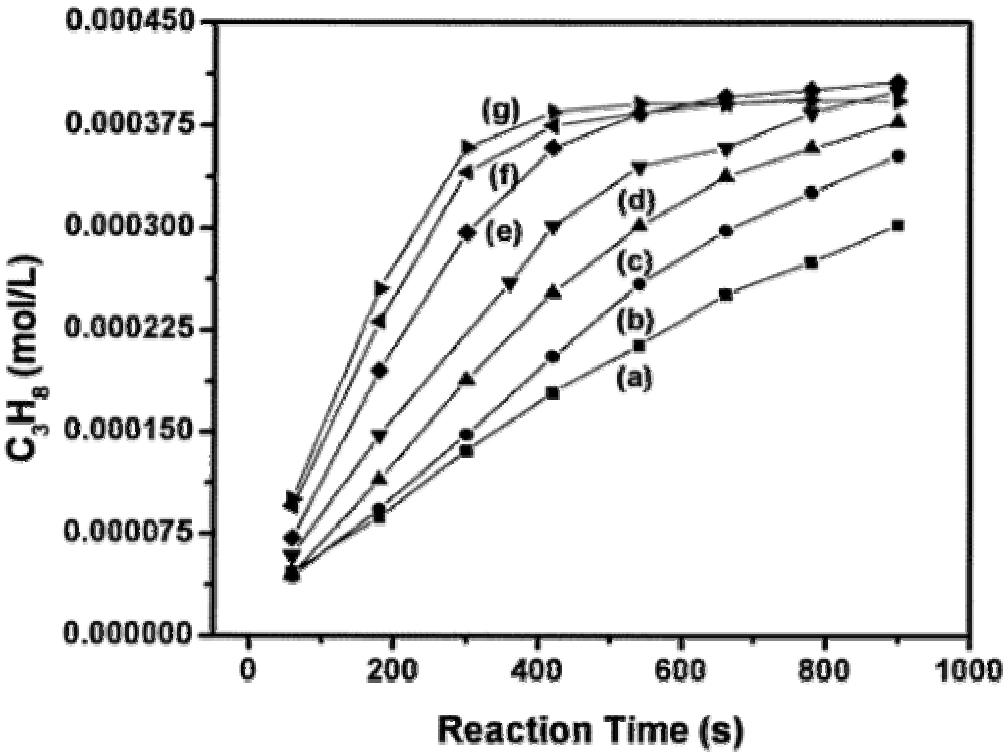

Figure 7-4. Propane concentration for temperature-dependent propene hydrogenation over Pt/Al2O3 catalyst as a function of reaction over time: (a) at 30 ^{o}C, (b) at 40 ^{o}C, (c) at 50 ^{o}C, (d) at 60 ^{o}C, (e) at 70 ^{o}C, (f) at 80 ^{o}C, and (g) at 90 ^{o}C.

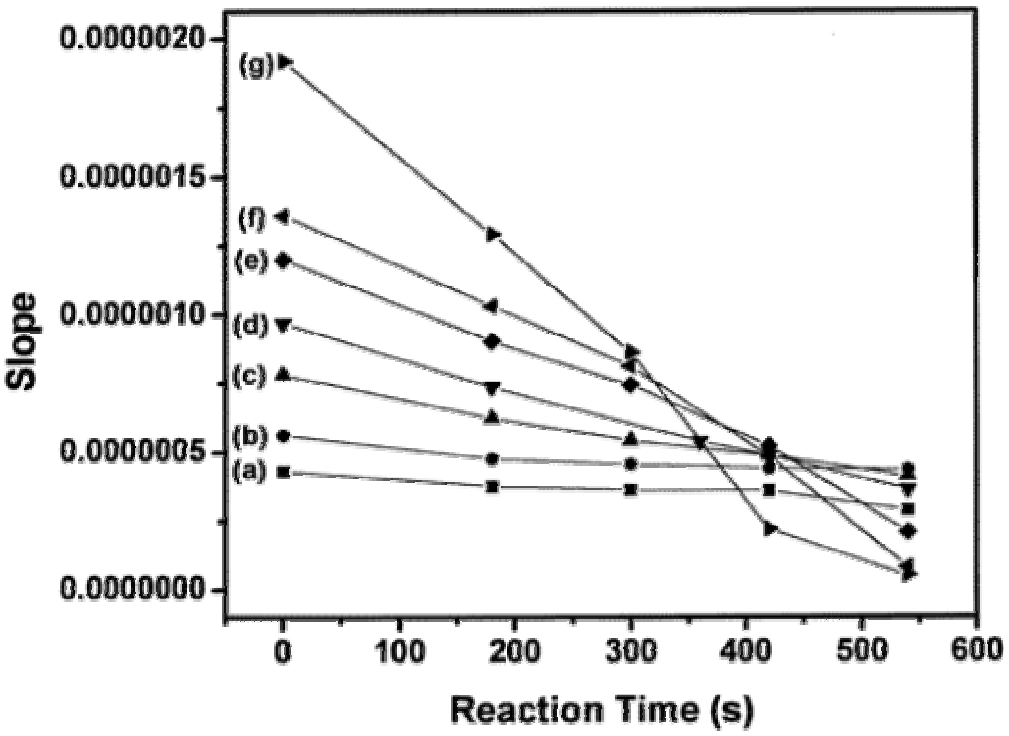

Figure 7-5. Slope, of propane concentration for temperature-dependent propene hydrogenation over Pt/Al2O3 catalyst as a function of reaction time: (a) at 30 ^{o}C, (b) at 40 ^{o}C, (c) at 50 ^{o}C, (d) at 60 ^{o}C, (e) at 70 ^{o}C, (f) at 80 ^{o}C, and (g) at 90 ^{o}C.

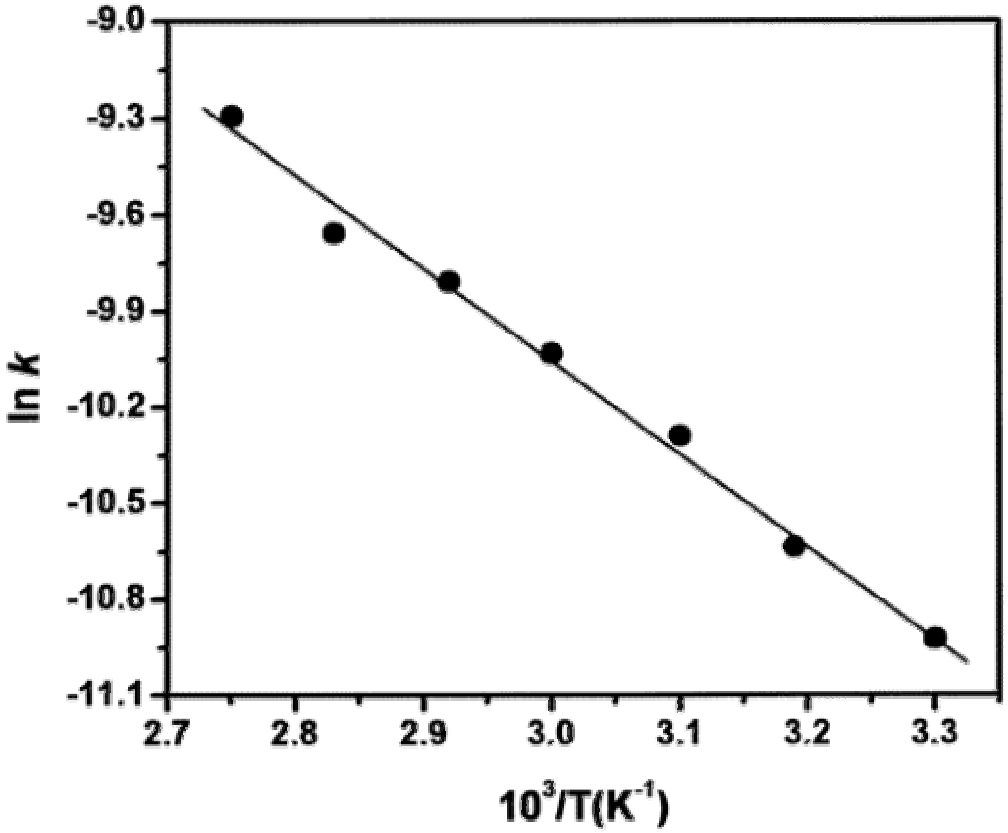

Figure 7-6. Arrhenius plots of the natural logarithm of rate constant vs 1/T for propene hydrogenation over Pt/Al_2O_3.

Table 7-1: Initial Rates and Rate Constants of Propene Hydrogenation over Pt/Al_2O_3 at Different Temperatures

T (K)	initial rate ($/10^{-7}$ mol L^{-1} s^{-1})	$[C_3H_6]$ initial ($/10^{-3}$ M)	$[H_2]$ initial ($/10^{-3}$ M)	rate constant ($k/10^{-5}$)
303	4.3	1.27	8.73	1.8
313	5.6	1.23	8.45	2.4
323	7.8	1.19	8.19	3.4
333	9.7	1.16	7.95	4.4
343	12.0	1.12	7.71	5.5
353	13.6	1.09	7.50	6.4
363	19.2	1.06	7.29	9.2

David J. Hathcock

2205 Peachtree Park Drive
Atlanta, GA 30309
Work: (404) 894-4009
Home: (404) 483-0743
david.hathcock@chemistry.gatech.edu

Education

Ph.D. in Analytical Chemistry
Georgia Institute of Technology, Atlanta, Georgia
Thesis Advisor: Dr. Mostafa A. El-Sayed
Thesis Title: Dynamic and Catalytic Properties of Some Metallic Nanoparticles

B.S. in Chemistry, (American Chemical Society Certified), June 1998
State University of West Georgia, Carrollton, Georgia

Research Experience

Georgia Institute of Technology, School of Chemistry and Biochemistry
Atlanta, Georgia **September 1998 to Present**
Graduate Research Assistant to Dr. Mostafa A. El-Sayed

- Characterization of the catalysis of the hydrogenation of ethylene gas by platinum nanoparticles of different shapes
- Investigation of the ultra-fast relaxation dynamics of the fullerenes
- Investigation of the electron cooling dynamics of nanolithographically prepared gold and silver nanoparticle arrays on a variety of substrates
- Characterization of the catalytic properties of platinum, palladium, and rhodium nanoparticle/composite polymer electrolyte membrane fuel cells for the enhancement of efficiency and power
- Performed characterization of nanomaterials using atomic force microscopy (AFM), transmission electron microscopy (TEM), femtosecond spectroscopy, mass spectrometry (EI-MS), ultra-violet/visible spectroscopy (UV/VIS), fluorescence spectroscopy, scanning electron microscopy (SEM)
- Prepared funding proposal to the National Science Foundation

State University of West Georgia, Department of Chemistry
Carrollton, Georgia **June 1996- June 1998**
Undergraduate Research Assistant to Dr. Spencer Slattery

- Studies related to the magnetic properties and spin state tuning of iron and cobalt complexes
- Synthesis and characterization of novel iron and cobalt terpyridine complexes

- Synthesis of novel bipyridine and terpyridine derivatives for pH dependent redox studies
- Utilized ^{1}H NMR, cyclic voltammetry, thin layer chromatography, and ab initio computational techniques

Awards

1998	Georgia Institute of Technology, School of Chemistry and Biochemistry, Dean's Professional Development Grant
1998	State University of West Georgia, School of Chemistry, James E. Boyd Research Award in Chemistry
1997	State University of West Georgia, School of Chemistry, James E. Boyd Research Award in Chemistry
1996	State University of West Georgia, College of Arts & Sciences, Sigma Xi Research Society Student Research Presentation Award

Publications

J.W. Yoo, D.J. Hathcock, M.A. El-Sayed, "Propene Hydrogentation over Truncated Octahedral Pt Nanoparticles Supported on Alumina" J. Catalysis, 214,1,(2003)

S.Link, D.J Hathcock, B. Nikoobakht, M.A. El-Sayed, "Medium Effect on the Electron Cooling Dynamics in Gold Nanorods and Truncated Tetrahedra" Adv. Mater., 15(5), 393, (2003)

Burda, C.; Samia, A. C. S.; Hathcock, D. J.; Huang, H.; Yang, S., "Experimental Evidence for the Photoisomerization of Higher Fullerenes" J. Am. Chem. Soc.,; 124(42), 12400, (2002)

J.W. Yoo, D.J. Hathcock, M.A. El-Sayed, "Characterization of Pt Nanoparticles Encapsulated in Al_2O_3 and their Catalytic Efficiency in Propene Hydrogenation" J. Phys. Chem. A, 106, 2049, (2002)

C.D. Lane, D.J. Hathcock, A.J. Leavitt, F.A. Khan, J.E. Hansen, " Measurement of Bulk Modulus of a Liquid using a Pump-Probe Laser Technique" Chemical Educator, 6, 235, (2001)

T. Ayers, S. Scott, J. Goins, N. Caylor, D.J. Hathcock, S.J. Slattery, D.J. Jameson "Redox and Spin State Control of N-Heterocyclic Complexes", Inorganica Chimica Acta, 307, 7, (2000)

D.J. Hathcock, K. Stone, J. Madden, and S.J. Slattery, "Electron Donating Substituent Effects on Redox and Spin State Properties of Fe(II) Bis-terpyridyl Complexes", Inorganica Chimica Acta, 282, 131 (1998)

D.J. Hathcock, J. Morris, J. Madden, and S.J. Slattery, "Ligand Substituent Effects on Ru(III/II) Redox Properties: An Advanced Inorganic Laboratory Experiment", The Chemical Educator, 2, 3, (1997)

Publications in preparation

D.J. Hathcock, S. Link, M.A. El-Sayed, "Hot Electron Cooling Dynamics of Lithographically Prepared Au Nano-arrays"

D.J. Hathcock, M.A. El-Sayed, " Phonon Oscillations in Gold and Silver Nano-Arrays"

D.J. Hathcock, M.A. El-Sayed " Effect of Transition Metal Nanoparticles on the Output of Polymer Electrolyte Membrane Fuel Cells"